PLASMA NANOCOATINGS

ON COBALT CHROMIUM L605 ALLOY

FOR CARDIOVASCULAR STENT APPLICATIONS

A Dissertation

presented to

the Faculty of the Graduate School

at the University of Missouri-Columbia

In Partial Fulfillment

of the Requirements for the Degree

Doctor of Philosophy

---

by

ThiThuHa Phan

Dr. Qingsong Yu, Dissertation Supervisor

JULY 2022

The undersigned, appointed by the dean of the Graduate School, have examined the dissertation entitled

PLASMA NANOCOATINGS ON COBALT CHROMIUM L605 ALLOY

FOR CARDIOVASCULAR STENT APPLICATIONS

presented by ThiThuHa Phan, a candidate for the degree of Doctor of Philosophy,

and hereby certify that, in their opinion, it is worthy of acceptance.

_____

Professor Qingsong Yu

_____

Professor Jian Lin

_____

Professor Zheng Yan

_____

Professor William Fay

_____

Professor Doug Bowles

ACKNOWLEDGEMENTS

There are many people who have helped me along the way on this journey. I would like to take this moment to express my gratitude to them.

First, I would like to express my sincere thanks to my advisor, Dr. Qingsong Yu, whose valuable guidance, keen interest, and kind supervision given to me at every stage of this research. I would like to extend my gratitude to my distinguished Ph.D. committee members: Dr. Jian Lin, Dr. Zheng Yan, Dr. William Fay, and Dr. Bowles. Especially, Dr. Lin and Dr. Yan gave brilliant comments and suggestions. Additionally, Dr. Bowles and Dr. Fay provided valuable feedback and recommended helpful advises for advancing the plasma nanocoating project in biological aspects.

I would like to give special thanks to Dr. John Jones and Dr. Meng Chen for guiding and assisting me in biological experiments and plasma techniques. I would like to further thank my research colleagues, including Hekmat Khoukaz, David Stalla, Yan Ji, Jingyao Zhang, and Yixuan Liao. Gratitude is extended to my friends Thao Phan, Ngan Le and Lan Uong for their gracious support.

Finally, to my parents, my husband and my son, I thank for your love, understanding, and encouragement helping me through all the difficulties.

TABLE OF CONTENTS

LIST OF ILLUSTRATIONS

LIST OF TABLES

ABSTRACT

Coronary stents have been essential devices in treating blocked coronary arteries, Unfortunately, they face in-stent restenosis and thrombosis complications. Drug eluting stents (DES) have been developed to minimize restenosis, but could cause late-thrombosis and poor endothelialization. Furthermore, DES require dual-antiplatelet therapy (DAPT) to prevent thrombosis. DAPT usage is problematic for patients with high bleeding risk, and minimal DAPT duration less than one month is desired.

Bioactive stent coatings, which do not elute drugs, may be an alternative to DES. In this study, cobalt chromium (CoCr) L605 coronary artery stents and coupons were coated with Trimethysilane (TMS) plasma nanocoatings of 20-25 nm in thickness. Direct current (DC) glow discharges were utilized for TMS plasma coatings and additional NH_3/O_2 plasma surface modification. Effects of plasma nanocoatings on CoCr L605 alloy surfaces were studied in terms of: 1) Surface properties, 2) In vitro biological responses, and 3) corrosion behavior.

The plasma nanocoating surfaces were characterized by contact angle measurement, Fourier-transform infrared spectroscopy (FTIR), X-ray photoelectron spectroscopy (XPS), and scanning electron microscope (SEM). Mechanical stability of the plasma nanocoating was evaluated using a tape adhesion test (coupon) and SEM (stent). Chemical stability of the plasma nanocoatings were studied by contact angle measurements, FTIR, and XPS spectroscopy up to 2 years. A series of in vitro experiments were conducted to find out the effect of plasma nanocoatings in improving cell proliferation selectively toward endothelial cells (ECs), while inhibiting smooth muscle cells (SMCs) proliferation and platelet adhesion and activation. These in vitro experiments include cell culture, cell migration, cell co-culture, protein adsorption, platelet adhesion

and activation under static and flow conditions. Corrosion behavior of plasma nanocoatings was assessed by immersion test, electrochemical tests, ion releasing, and cytotoxicity test.

Results show that NH_3/O_2 modified TMS plasma nanocoating is hydrophilic. Though aging occurs gradually, NH3/O2 modified plasma nanocoating surface is more hydrophilic (48.5° after 2-year aging) than the uncoated counterpart. NH_3/O_2 modified TMS plasma coatings mostly contain O–, Si– and C–rich functionalities (39.39 at.%, 31.92 at.%, and 24.12 at.%, respectively) and a very small but essential amount of N (2.77 at.%). Modified plasma nanocoatings contain nitric oxide (NO)-like functionalities which play an essential role in their biological responses.

Plasma nanocoatings with NH_3/O_2 plasma modification maintained similar level of porcine coronary artery endothelial cell (PCAEC) proliferation while porcine coronary artery smooth muscle cell (PCASMC) viability decreased by 73% after 7-day incubation compared to those on uncoated bare L605 surfaces. PCAEC and PCASMC cell co-culture and migration were also conducted. In cell co-culture, the cell ratio of PCAEC/PCASMC on NH_3/O_2 modified TMS plasma nanocoatings was 1.5-fold higher than that of uncoated bare L605. Migration test showed comparable PCAEC migration distance for uncoated L605 and NH_3/O_2 modified TMS plasma nanocoatings. In contrast, PCASMC migration distance reduced 6-fold for TMS plasma nanocoatings without the NH_3/O_2 plasma modification. Lower adhered platelets distribution (70% decrease) and less platelet activation were observed on NH_3/O_2 modified TMS plasma nanocoated surfaces compared to uncoated L605.

Corrosion resistance was improved with TMS plasma nanocoatings by decreasing corrosion rates and increasing corrosion potential, no pitting corrosion, and no mineral adsorption layer. Ion releasing test by inductively coupled plasma mass spectrometry

(ICP-MS) revealed that Co, Cr, Ni ion concentrations reduced 57-72% for plasma nanocoatings compared to uncoated L605. TMS plasma nanocoatings showed no sign of cytotoxicity.

In vitro tests provide strong evidence that TMS plasma nanocoatings with NH_3/O_2 plasma surface modification may be a promising approach for preventing both restenosis and thrombosis in stent applications.

Chapter 1

INTRODUCTION

Biomaterials need to possess good mechanical properties in order to function properly in biological environment, and assure biocompatibility and hemo-compatibility so that do not induce any chronic inflammatory responses. A good way to achieve those requirements is surface treatment techniques such as thin film deposition and surface modification due to maintaining intact bulk materials and gaining desired surface characteristics.

Plasma glow discharge is a surface treatment technique that has been applied to many biomaterials due to its ability to alter surface properties, including surface energy and surface chemistry, without affecting their mechanical properties. Plasma is composed of highly excited atomic, molecular, ionic and free radicals. Various gas species excited by radio frequency (RF), direct current (DC), or microwave can either deposit an overlay thin film onto host substrates or treat the surface for specific purposes. Some main advantages of plasma techniques can be listed: 1) Reliable, reproducible, relatively non-expensive; 2) Different samples geometries, different materials; 3) Changes in variety of surface characteristics, and 4) sterile surfaces can be provided by plasma processing. Plasmas are effective and economical techniques for surface modification such a plasma sputtering and etching, plasma spray, plasma implantation, plasm deposition, and so on.

Coronary artery disease (CAD) resulting from plaque build-up is one of the major causes of death in developed countries. Stent deployment inside obstructed arteries can combat and ideally alleviate the blockage and finally restore blood flow. The primary problem of stenting is the fact that stent surfaces are poorly recognized by blood. In-stent

restenosis and thrombosis are two common complications of artery stenting. When a stent is expanded, it exerts a pressure on the vascular intima, leading to injured endothelial cell (EC) layers and exposure of smooth muscles (SMC) layers. Endothelial cell layers can inhibit thrombus adhesion and suppress excessive SMC proliferation. Thus, while stenting restores blood flow to the heart, complications can follow including incomplete endothelialization, resulting in in-stent restenosis and thrombus complications.

In the era of drug eluting stents, both in-stent restenosis and thrombosis events are substantially reduced. However, long-term clinical issues have been raised concerning allergic and inflammatory reactions as well as incomplete endothelialization. Modified bare metal stents (BMSs) with plasma nanocoatings is believed to be biocompatible and hemo-compatible in order to adapt with human environment.

The aim of this research is to evaluate plasma techniques for the modification of coronary stent surface properties. In vitro tests are conducted to understand surface bioactivities with respect to the coronary vasculature. Engineering tests are performed to evaluate nanocoating stability against shearing stresses.

Chapter 2 focuses on current research and development of surface modification for cobalt chromium (CoCr) cardiovascular stents. Coating is an essential method to suppress in-stent restenosis and enhance endothelialization. Also, in chapter 2, fundamental theory of plasma glow discharge is reviewed.

In Chapter 3, plasma nanocoating properties are addressed. Surface characterization was undertaken utilizing surface contact angle, XPS and FTIR. The results from these studies provide information on the chemical composition and functional groups on the surface that may promote enhancement to host response. Mechanical stability of plasma nanocoatings was evaluated on coupons by tape test and stents after dilation by SEM imaging. Chemical stability of plasma nanocoatings was studied by

contact angle, FTIR and XPS spectra up to 2 years following coating deposition. Results from this chapter confirm the excellent adhesion of the coatings and good chemical stability.

In Chapter 4, biological responses of plasma nanocoatings are discussed. Cell-relation experiments such as single cell culture, co-culture, cell migration was performed with porcine artery coronary endothelial and smooth muscle cells. Blood compatibility of plasma nanocoating were assessed by platelet and fibrin adhesion test and protein adsorption test with ELISA assay. Results from this chapter strengthen the possibility of plasma nanocoatings in reducing in-stent restenosis and thrombosis.

Chapter 5 focuses on corrosion-related experiments. Immersion test (ASTM-G31-72), ion releasing test, cyclic polarization test, and cytotoxicity will be discussed to determine effects of plasma nanocoatings to corrosion potentials, corrosion rates, material weight loss, the plasma nanocoating surfaces after testing within simulated body fluid, the possible toxicity of plasma nanocoatings to cell growth. These enhancements may minimize the host inflammatory response on implantation due to reduced metal ion leakage.

Chapter 6 concludes this work and suggest some future work to further prove plasma coatings as a good choice for surface modification of cobalt chromium coronary stents.

Chapter 2

LITERATURE REVIEW:

CARDIOVASCULAR CORONARY STENTS

& PLASMA NANOCOATINGS

2.1. The development of vascular stents

Heart diseases:

Heart disease is the leading cause of death globally, representing 31% of all global deaths (approximately 17 million people die each year) [1,2]. Each year, nearly 1.4 million stents are implanted worldwide [3].

Cardiovascular stents:

In 1977, coronary balloon angioplasty was introduced. During angioplasty, a balloon-tipped catheter is inserted into the blocked or narrowed artery area and inflated to flatten plaque by briefly expanding the balloon, increasing the luminal artery diameter and restoring blood flow [4,5]. However, balloon angioplasty turned out to be a temporary solution because of the very high rate of restenosis [6]. About 30%-40% of patients undergoing balloon angioplasty had arterial narrowing of 50% within 6 months post-procedure [7]. The re-narrowing phenomenon of the artery is known as restenosis. In the case of balloon angioplasty, re-narrowing was mainly due to the arterial elastic forces – recoil and negative re-modelling.

The era of coronary stenting began in 1987 by the implantation of bare metal stents (BMS) in patients. A stent is a metallic mesh tube, acting as a scaffold to open the artery and restore blood flow. Stenting prevents vascular recoil and negative artery re-modelling; thus, the rate of restenosis reduces to 20%-30% after implantation [6,8,9]. However, this restenosis rate is not clinically negligible.

In-stent Restenosis:

Inflammatory responses and poor endothelialization in vessel walls due to artery damage during stent implantation encourage smooth muscle cell (SMC) proliferation and migration, leading to high in-stent restenosis rates in bare metal stents (BMSs) [1]. When a stent was inserted and inflated in lesion artery area, it not only flattens the plaque and restore blood flow, it also injures the endothelium layers – the topmost layer of luminal artery, and exposes the smooth muscle cell layer. The underlying mechanism of restenosis is neo-intimal accumulation which is caused primarily by the excessive smooth muscle cell (SMC) proliferation and migration [9,11]. The vessel wall injury at stent implantation is followed by leukocyte accumulation, inflammation, SMC migration, vessel wall remodeling, and ultimately restenosis [12]. Therefore, restenosis remains a major concern with BMSs.

First generation of Drug eluting stents:

Drug eluting stents (DES) were developed to reduce restenosis rates by carrying drugs (i.e., paclitaxel and sirolimus) that suppress SMC proliferation, but late thrombosis events remained a problem with first generation DES. The drugs contributed to poor endothelialization for first-generation DES, and the durable polymer coatings containing drugs further enhanced thrombosis risks. The in-stent restenosis rate in the first generation DES decreases to less than 13% [6] by releasing anti-proliferative drugs that

inhibit neointimal hyperplasia. Though DES reduce the incidence of restenosis, they come with the increased risk of late stent thrombosis due to inflammation and delayed re-endothelialization [9,13,14]. DES are susceptible to thrombotic events (early, late and very late stent thromboses). Late stent thrombosis is the formation of a blood clot inside the vessel wall at the stented site [15]. Late stent thrombosis may occur months or years after implantation and has become a complex problem. Clinical evidence revealed an increased risk of late-thrombosis (>1 year after stents were implanted) in 0.5-1% of patients undergoing DES implantation [7]. Stent thrombosis remains a catastrophic complication, being consistently associated with mortality rates of 25% [16]. DES are able to suppress excessive amount of SMC proliferation; however, at the same time the drug releasing from DES can inhibit endothelialization and therefore delay repairing of lesion vessels [14,17]. DES thrombosis rates in patients examined by clinical trials were remarkably higher than that observed in patients with BMS devices [15]. Additionally, polymer coatings containing anti-proliferation agents need to withstand the process of crimping and high-pressure expansion during stent implantation, causing cracking or peeling the polymer [17].

Second generation of Drug eluting stents:

The second-generation DES consisted of newer drugs (i.e., zotarolimus and everolimus) as well as more biocompatible coatings compared to first generation DES. Unfortunately, very late stent thrombosis can occur up to five years following implantation of second-generation DES. Patients have to take long-term duet anti-platelet therapy (DAPT) which is known for increasing chances of bleeding in certain high-risk patients, such as patients who have diabetes or scheduled for major surgery within weeks or months after stent implantation [18,19]. Biodegradable stents (BDS) are conceived to support the vessel wall temporarily followed by slow degradation; however, further improvement and validation are still required for current BDS [20,21]. Therefore, BMS has

still gained interest in spite of the growth of drug-eluting stents (DES) and bio-degradable stents (BDS).

Thus, developing novel stents that can effectively diminish restenosis and thrombosis without other serious clinical side effects will be meaningful for patients who cannot tolerate long term DAPT. Aside from developing DES, BMS surface modification is an effective approach to regulate bio-properties and improve cell response behavior, potentially reducing thrombosis and restenosis rates [22,23].

2.2. Stent materials

Another approach to prevent thrombosis and restenosis in BMS stent application is stent flexibility. It relates to the ease with which a stent could be tracked through the guide catheter, then crossed through lesions. Improved flexibility may be achieved by reducing stent strut thickness, resulting in smaller contact area of the stents with SMCs and consequently less inflammation and restenosis than thick strut designs [24,25]. The advantage of thinner stent struts links to both improved procedural and clinical outcomes. Thinner struts, however, cause even less X-ray attenuation, further lessening device visibility during deployment. Thus, a material that has high mechanical strength, good X-ray visibility, MRI compatibility, and good biocompatibility is promising for stent applications.

The most frequently implantable material for BMS is the 316L stainless steel because of its low cost, easy accessibility, excellent manufacturing properties, and acceptable compatibility. 316L stainless steel, however, cannot maintain strength with thin flexible struts due to its moderate compressive strength. In addition, thin-walled 316L devices would also have undesirably low radiopacity. L605 cobalt chromium (CoCr) alloys have higher mechanical strength and improved X-ray attenuation compared to 316L. L605

CoCr stent can have strut thicknesses in the region of 80–90 μm, compared to strut thicknesses of 130–140 μm for earlier 316L devices [26]. Although L605 CoCr alloys are known for high mechanical strength, good X-ray visibility, MRI compatibility, outstanding corrosion resistance and good biocompatibility, in-stent restenosis, thrombosis formation and endothelium damage still occur due to the invasive procedures of stent deployment [27]. Thus, surface modifications were performed to enhance biocompatibility, reducing restenosis and thrombosis.

Cobalt chromium (CoCr) L605 stents have been widely used because of their excellent mechanical and radiopaque properties and good biocompatibility [28,29]. Thin-strut stent design was claimed to reduce restenosis and thrombosis events in stenting implantation [21]. Despite containing thinner struts compared to stainless steel stents, CoCr L605 stents have minimal elastic recoil and also enhance X-ray visibility for implanting procedures [28]. Therefore, surface modification for cobalt chromium L605 stents can combine benefits of thin-struts design and modified stent surfaces to enhance stent performance.

2.3. Surface modification

2.3.1. Coating modification

So far, many techniques have been used to modify metallic stent surface for improving biocompatibility: non-coating and coating modification. For non-coating modification, Schieber [30] created linear patterning onto CoCr surfaces by direct laser interference patterning. The changes in surface topography, chemistry and wettability were beneficial for endothelialization without enhancement of platelet adhesion. Many studies focused on the surface modification of stainless steel 316L and cobalt chromium L605. Wawrzynska [31] used a carbon-based coating (graphene) onto stainless steel

316L- a common material for cardiovascular stents. The coating helped to enhance endothelial cell growth and decrease blood platelets. Maguire [32] investigated diamond-like carbon (DLC) coatings onto stainless steel with respect to bio-responses, mechanical stability, corrosion resistance. Doping with Si and the use of an a-Si:H interlayer made the film less hard and reduced the risk of film cracking due to superior mechanical tensile and compressive strength of DLC. Si doping was observed to be beneficial to bio-responses by enhancing human endothelial cells while minimizing platelet attachment. The coatings showed less inflammatory activity than the uncoated material. Braz [33] evaluated effect of surface modification of 316L stainless steel by low temperature plasma nitriding. Endothelial cell viability and corrosion resistance were improved on the material modified by plasma nitriding. Huang [34] reported the work of surface coating of Ti-O/Ti-N films onto stainless steel 316L coronary stents by plasma immersion ion implantation/deposition process. Mechanical characterization showed that the film was strongly adhesive to the substrate. The films enhanced biocompatibility of 316L stents by indicating no thrombus formation on coated stents during in vivo experiments. Rodriguez [35] reported surface modification for L605 CoCr alloys by direct plasma amination without any polymeric coating to assure coating stability and corrosion resistance. Different treatments including electropolishing, thermal treatments, and plasma immersion ion implantation were deployed to create surface chemical compositions favorable to cell viability and hemocompatibility. Liu [12] studied an ultra-thin Ti-O film deposited on L605 CoCr alloy coronary stents by metal vacuum arc source deposition. Results showed that Ti-O film modified stent was less susceptible to corrosion than bare material. Andrade [36] applied an electro-polishing pretreatment and oxygen plasma immersion ion implantation process on L605 CoCr stents to improve corrosion properties and cell proliferation. Higher cell viability was observed on the modified surface compared to untreated one. Podial [37] studied graphene coatings on Cu or Nitinol substrates for enhanced hemo-compatibility.

The study reported the lack of charge transfer between graphene and fibrinogen resulted in inhibiting platelet adhesion. No intro significant in vitro toxicity was exhibited for SMCs and ECs, confirming biocompatibility of graphene coatings.

2.3.2. Nitric oxide (NO)-containing coating

Nitric oxide (NO) is a molecule generated in healthy blood vessels. The release of NO by endothelial cells plays a critical role in maintaining patency and homeostasis of blood vessels [38]. NO-releasing stent coatings are very promising to meet biocompatibility and hemo-compatibility of biomaterials. ECs are primary source of NO in the vascular system and the continuous release of NO is fundamental to maintain healthy vasculature. NO is known to play a crucial role preventing thrombosis [39]. NO suppresses platelet aggregation, SMC migration and proliferation. It also promotes the endothelialization of foreign surfaces. Therefore, NO-releasing stent coating for bio-mimicking the functions of native endothelium appears to be a powerful strategy to address restenosis and thrombosis [12]. Gallino [40] used a low-pressure reactor to deposit an ultra-thin, stable, cohesive and adhesive plasma polymerized allylamine ($CH_2=CH—CH_2—NH_2$) coating with high selectivity towards primary amine groups onto stainless steel 316L. The coating was proven to be stable and adhesive to substrates, but biological responses of the coating were not mentioned in the study. Yang [41] fabricated a plasma polymerized allylamine thin film using an inductively coupled plasma at a 13.56 MHz pulsed radio frequency (RF). As a result, modified surface indicated inhibition in adhesion and activation of platelets and fibrinogen. The author found that the coating significantly enhanced endothelial cell proliferation, adhesion, and migration with the release of NO. Elnaggar [38] investigated a layer-by-layer coating with a NO donor-containing liposomes to control the release rate of NO from CoCr substrates. In vitro cell study indicated that NO release significantly promoted endothelial cell proliferation and

markedly prevented smooth muscle cell proliferation. In vivo study, the coating enhances results in luminal healing and inflammation. Qiu [42] applied heparin and nitric oxide (NO) on an amine-bearing film by plasma polymerized allylamine to develop an endothelium-mimetic coating. Heparin provides anti-coagulation and NO provides anti-platelet activity for the treated surface. In vivo study, the treatment improves the anti-thrombogenicity, re-endothelialization, and anti-restenosis.

2.4. Plasma nanocoatings

2.4.1. Plasma fundamentals

Plasma deposition has become a viable method for depositing biocompatible coatings. Plasma process relies on a precursor monomer gas, typically a carbon and silicon-rich species. Gas phase environment of glow discharges consists of electrons, various types of ions, excited-state species, and free radicals from direct current (DC) or radio frequency (RF) power sources. The monomer gas pressure necessary for non-equilibrium conditions is supplied below atmospheric pressure. Under non-equilibrium conditions, electron-gas molecule collisions are so infrequent that thermal equilibrium cannot be reached. Processing pressures are typically between 10 mTorr and 10 Torr [43].

Glow discharges are types of plasma formed by passing a current through a gas. Glow discharge owes its name to the fact that the plasma is luminous. There are some collision processes involving electrons that commonly happen in glow discharges, such as ionization, excitation, relaxation, and recombination. The most important of these collisions is ionization which plays key role in sustaining glow discharge. In ionization, a primary electron removes an electron from an atom, producing a positive ion and two electrons. For example, an argon atom is ionized by: $e + Ar = Ar^+ + 2e$. The two electrons

produced by ionization collision can be accelerated by electric field until they can ionize other atoms. By this multiplication process, the glow discharge is maintained.

The simplest type of glow discharge is direct-current (DC) glow discharge as depicted in **Figure 2.1**. A DC glow discharge can be generated by applying a potential between two electrodes in a gas at low pressure (0.01-10 Torr). A space between the two electrodes is filled by a bright glow known as the negative glow, the results of excitation and subsequent recombination processes. A sheath formed in front of the cathode is a dark region known as the dark space. There is a similar sheath in front of the anode known as the anode glow, but it is too thin to see clearly. Most of space between the two electrodes is filled with the positive column, but this region shrinks when the two electrodes are brought closer together.

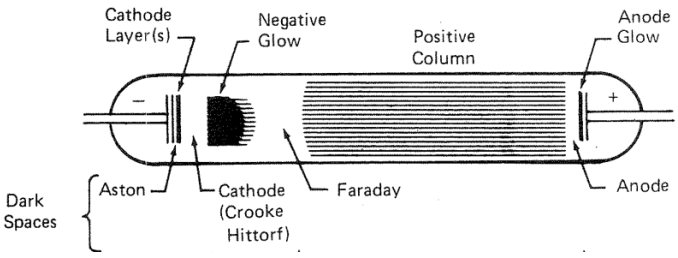

Figure 2.1: A normal DC glow discharge [43]

Initially, a small population of gas atoms is ionized through collisions between atoms. The ions which are positively charged are driven toward the cathode by electric potential, and the electrons are driven toward the anode. Those ions and electrons collide with other atoms and ionize them. As long as pressure is kept low enough, electrons can gain sufficient energy to ionize the gas molecules, resulting in ion bombardment of the cathode and sustainment of the discharges.

2.4.2. Plasma deposition

In plasma deposition (or plasma polymerization) process, plasma sources provide energy to activate gas monomers in vacuum to initiate the polymerization. The polymer generated by plasma polymerization process is known as favorably cross-linked, thoroughly branched, and extremely adhesive to substrates. The process is usually used to deposit a nano-scale thin film on various materials such as metals and polymers. The chemical composition and thin-film structure can be varied by selecting plasma conditions: power, pressure, precursor flow rate, and processing time.

Trimethylsilane (TMS) is one plasma precursor known for good reactivity in plasma, ability to form a thin film on substrate with stable performance [22,44,45] and relatively low health hazard [46–49]. In a DC glow discharge, the cathode is typically the substrate for plasma coating deposition. In order to facilitate plasma polymerization of TMS, DC power needs to be lower than that of normal glow discharge in which ionization glow (negative glow region) occurs. In TMS plasma deposition process, dissociation glow (cathode glow) take place because low-energy electrons cannot ionize TMS molecules to form ionization glow. Low-energy electrons break organic molecular bonds of TMS and make excited species. In other words, the formation of chemically reactive species (free radicals) is not from ionization, but from dissociation reactions.

If a carbon and silicon-containing gas, such as TMS [$(CH_3)_3SiH$] is used as the source, TMS can be presented by ABH in which A, B, and H stand for Si, C, and H, respectively. The dissociation reaction can be presented by: $ABH + e \rightarrow A^* + B^* + H + e$, where A^* and B^* are Si-based photon emitting species and C-based photon emitting species, respectively. The free radicals can be created by following reactions: $A^* \rightarrow A\bullet + h\nu_A$ and $B^* \rightarrow B\bullet + h\nu_B$, where A• and B• are chemically reactive species (free radicals),

$h\nu_A$ and $h\nu_B$ are represented photon energy in which h is Planck constant, ν_A and ν_B are Si and C frequencies of photon emission.

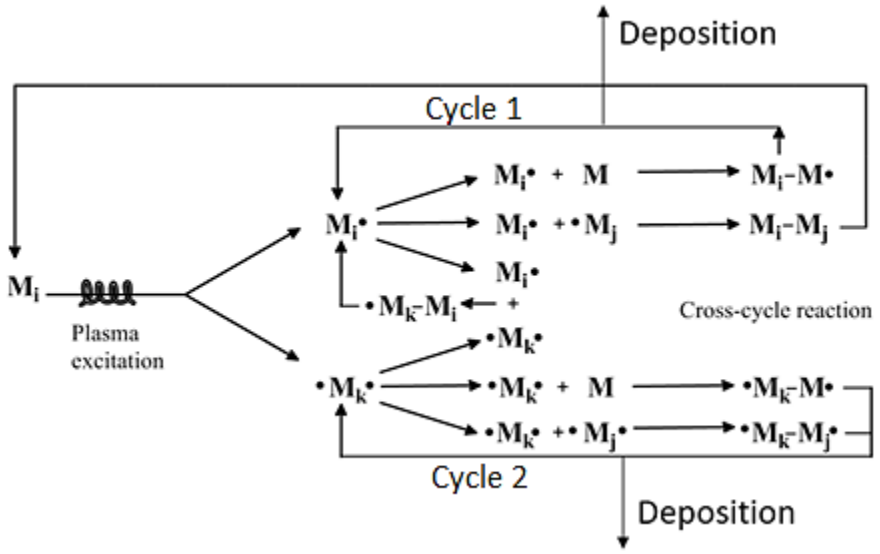

Figure 2.2: Diagram of plasma deposition's growth mechanism [50]

In **Figure 2.2**, $M_i\bullet$, $\bullet M_j$, $\bullet M_k\bullet$, $\bullet M_j\bullet$, etc, are reactive species (free radicals). In order to simplify the overall picture of gas phase reaction in glow discharge, substrates are not shown in **Figure 2.2**. In plasma glow discharge, positive or negative charged ions can participate in the polymer growth mechanism; however, the roles of ions in plasma polymerization can be neglected due to the ratio of neutral species over ions I roughly $10^6/1$. Reactions in cycle 1 and cycle 2 are the addition of reactive species to the monomer (M) or the combination of two reactive species. If the result products are new radicals (for example, M_i-M• in cycle 1 or $\bullet M_k$-M• and $\bullet M_k$-$M_j\bullet$ in cycle 2), cycles 1 and 2 will be either repeated or deposited on substrates through colliding as frequently as the kinetic theory of gases predicts. If the result product is a monomer (such as M_i-M_j in cycle 1), it will be activated/excited again by plasma environment.

Though H is not contributed in polymerization growth, it is attributed to negative glow in plasma polymerization. High-energy electron is shown by e^* in ionization reactions:

$$H + e^* \rightarrow H^+ + 2e$$

$$H + e^* \rightarrow H^* + e$$

$$H^* \rightarrow H\bullet + h\nu_H$$

where H^* and H• are excited molecule and free radical of H, respectively. The resulting plasma coating from TMS precursor is typically a hydrophobic, pinhole free film due the growth of mostly Si-based and C-based moieties in plasma polymerization.

2.4.3. Plasma modification

The purpose of plasma surface modification process is to change surface chemistry by incorporating desired functional groups. Similar to plasma deposition process, plasma surface modification deploys low plasma power to make dissociation reactions happened rather than ionization reactions. The difference of plasma surface modification and plasma deposition is the precursor. In plasma modification, precursors can be oxygen (O), nitrogen (N), or hydrogen (H), etc. as long as they are reactive in plasma glow discharge and tend to generate desire functional groups on substrate surfaces. Oxygen can be used to change the hydrophobic to hydrophilic surface [49,51]. Oxygen as well as nitrogen containing plasma has been shown to add N and O containing functional groups on substrate surfaces [52]. In plasma modification, free radical generation and radical incorporation to substrate surface are similar to plasma deposition process

2.4.4. Plasma applications

The application of non-equilibrium plasma method to deposit plasma nanocoatings and modify surface chemistry has been explored for years. This technique could benefit cardiovascular coronary stents. By managing plasma conditions, plasma surface chemistry can be controlled by adding inorganic oxide, carbide, or nitride, and so on.

Surface chemistry's adjustment can provide a various and expected surface properties, namely wettability, blood-compatibility, and biocompatibility.

There are some advantages of plasma deposition and modification techniques. First, plasma methods are well known as rapid, reliable, duplicatable, relatively inexpensive processes. Second, the plasma treated surface is clean, sterile, dry, and desired chemical, physical, and biological. Third, plasma treatment results in nano-scale coatings suitable to complex sample geometries like stents. The nanocoating is typically conformal and highly adhesive to substrates, void-free, chemically inert, and insulative.

In stent applications, it is expected that stent surfaces are clean, dry, reproductive, and reliable. Additionally, plasma nanocoatings require excellent adhesive and thoroughly coating conformal to avoid coating failures during crimping and expansion stent processes. More importantly, stent surfaces are expected to obtain unique surface characteristics relating to surface chemistry and biology which benefit stents to reduce in-stent restenosis and thrombosis.

2.5. References

[1] Y. Yang, P.K. Qi, Z.L. Yang, N. Huang, Nitric oxide-based strategies for applications of biomedical devices, Biosurface and Biotribology. 1 (2015) 177–201. https://doi.org/10.1016/j.bsbt.2015.08.003.

[2] T. Hu, C. Yang, S. Lin, Q. Yu, G. Wang, Biodegradable stents for coronary artery disease treatment: Recent advances and future perspectives, Materials Science and Engineering C. 91 (2018) 163–178. https://doi.org/10.1016/j.msec.2018.04.100.

[3] T. Simard, B. Hibbert, F.D. Ramirez, M. Froeschl, Y.X. Chen, E.R. O'Brien, The Evolution of Coronary Stents: A Brief Review, Canadian Journal of Cardiology. 30 (2014) 35–45. https://doi.org/10.1016/j.cjca.2013.09.012.

[4] Z. Yang, Y. Yang, K. Xiong, X. Li, P. Qi, Q. Tu, F. Jing, Y. Weng, J. Wang, N. Huang, Nitric oxide producing coating mimicking endothelium function for multifunctional vascular stents, Biomaterials. 63 (2015) 80–92. https://doi.org/10.1016/j.biomaterials.2015.06.016.

[5] J.E. Jones, Q. Yu, M. Chen, A chemical stability study of trimethylsilane plasma nanocoatings for coronary stents, Journal of Biomaterials Science, Polymer Edition. 28 (2017) 15–32. https://doi.org/10.1080/09205063.2016.1239947.

[6] K.S. Bohl, J.L. West, Nitric oxide-generating polymers reduce platelet adhesion and smooth muscle cell proliferation, (n.d.).

[7] G.M.D.M. Christopher Kaufmann, Long-term stability of self-assembled monolayers on electropolished L605 cobalt chromium alloy for stent applications, Journal of Biomedical Materials Research Part B: Applied Biomaterials. 98B (2011) 280–289.

[8] Z. Yang, Y. Yang, K. Xiong, X. Li, P. Qi, Q. Tu, F. Jing, Y. Weng, J. Wang, N. Huang, Nitric oxide producing coating mimicking endothelium function for multifunctional vascular stents, Biomaterials. 63 (2015) 80–92. https://doi.org/10.1016/j.biomaterials.2015.06.016.

[9] Y. Zhang, X. Wang, Z. Ma, B. Bai, J. Liu, L. Yang, G. Qin, E. Zhang, A potential strategy for in-stent restenosis: Inhibition of migration and proliferation of vascular smooth muscle cells by Cu ion, Materials Science and Engineering C. 115 (2020). https://doi.org/10.1016/j.msec.2020.111090.

[10] F. Lewis, P. Horny, P. Hale, S. Turgeon, M. Tatoulian, D. Mantovani, Study of the adhesion of thin plasma fluorocarbon coatings resisting plastic deformation for stent applications, Journal of Physics D: Applied Physics. 41 (2008). https://doi.org/10.1088/0022-3727/41/4/045310.

[11] Y. Xu, J.E. Jones, H. Yu, Q. Yu, G.D. Christensen, M. Chen, H. Sun, Nanoscale plasma coating inhibits formation of Staphylococcus aureus biofilm, Antimicrobial Agents and Chemotherapy. 59 (2015) 7308–7315. https://doi.org/10.1128/AAC.01944-15.

[12] H. Qiu, P. Qi, J. Liu, Y. Yang, X. Tan, Y. Xiao, M.F. Maitz, N. Huang, Z. Yang, Biomimetic engineering endothelium-like coating on cardiovascular stent through heparin and nitric oxide-generating compound synergistic modification strategy, Biomaterials. 207 (2019) 10–22. https://doi.org/10.1016/j.biomaterials.2019.03.033.

[13] C. Beythien, W. Terres, C.W. Hamm, In vitro model to test the thrombogenicity of coronary stents, Thrombosis Research, Volume 75, Issue 6, 15 September 1994, Pages 581-590.

[14] H. Liu, C. Pan, S. Zhou, J. Li, N. Huang, L. Dong, Improving hemocompatibility and accelerating endothelialization of vascular stents by a copper-titanium film, Materials Science and Engineering C. 69 (2016) 1175–1182. https://doi.org/10.1016/j.msec.2016.08.028.

[15] M.C. Loya, K.S. Brammer, C. Choi, L.H. Chen, S. Jin, Plasma-induced nanopillars on bare metal coronary stent surface for enhanced endothelialization, Acta Biomaterialia. 6 (2010) 4589–4595. https://doi.org/10.1016/j.actbio.2010.07.007.

[16] C.P. Kealey, S.A. Whelan, Y.J. Chun, C.H. Soojung, A.W. Tulloch, K.P. Mohanchandra, D. di Carlo, D.S. Levi, G.P. Carman, D.A. Rigberg, In vitro

hemocompatibility of thin film nitinol in stenotic flow conditions, Biomaterials. 31 (2010) 8864–8871. https://doi.org/10.1016/j.biomaterials.2010.08.014.

[17] B. Sivaraman, R.A. Latour, The relationship between platelet adhesion on surfaces and the structure versus the amount of adsorbed fibrinogen, Biomaterials. 31 (2010) 832–839. https://doi.org/10.1016/j.biomaterials.2009.10.008.

[18] H. Jinnouchi, Y. Sato, Q. Cheng, C. Janifer, M. Kutyna, A. Cornelissen, R. Wijeratne, A. Sakamoto, L. Guo, F.D. Kolodgie, S. Tunev, R. Virmani, A. v. Finn, Thromboresistance and endothelial healing in polymer-coated versus polymer-free drug-eluting stents: Implications for short-term dual anti-platelet therapy, International Journal of Cardiology. 327 (2021) 52–57. https://doi.org/10.1016/j.ijcard.2020.11.030.

[19] A.C. Perez, P. Jhund, D. Preiss, J. Kjekshus, J.J.V. McMurray, Effect of rosuvastatin on fatigue in patients with heart failure, J Am Coll Cardiol. 61 (2013) 1121–1122. https://doi.org/10.1016/j.jacc.2012.12.004.

[20] D. Sun, Y. Zheng, T. Yin, C. Tang, Q. Yu, G. Wang, Coronary drug-eluting stents: From design optimization to newer strategies, Journal of Biomedical Materials Research - Part A. 102 (2014) 1625–1640. https://doi.org/10.1002/jbm.a.34806.

[21] T. Hu, C. Yang, S. Lin, Q. Yu, G. Wang, Biodegradable stents for coronary artery disease treatment: Recent advances and future perspectives, Materials Science and Engineering C. 91 (2018) 163–178. https://doi.org/10.1016/j.msec.2018.04.100.

[22] J.E. Jones, Q. Yu, M. Chen, A chemical stability study of trimethylsilane plasma nanocoatings for coronary stents, Journal of Biomaterials Science, Polymer Edition. 28 (2017) 15–32. https://doi.org/10.1080/09205063.2016.1239947.

[23] P.K. Chu, J.Y. Chen, L.P. Wang, N. Huang, Plasma-surface modification of biomaterials, n.d.

[24] N. Foin, R.D. Lee, R. Torii, J.L. Guitierrez-Chico, A. Mattesini, S. Nijjer, S. Sen, R. Petraco, J.E. Davies, C. di Mario, M. Joner, R. Virmani, P. Wong, Impact of stent

strut design in metallic stents and biodegradable scaffolds, International Journal of Cardiology. 177 (2014) 800–808. https://doi.org/10.1016/j.ijcard.2014.09.143.

[25] S.Z.H. Rittersma, R.J. de Winter, K.T. Koch, M. Bax, C.E. Schotborgh, K.J. Mulder, J.G.P. Tijssen, J.J. Piek, Impact of strut thickness on late luminal loss after coronary artery stent placement, American Journal of Cardiology. 93 (2004) 477–480. https://doi.org/10.1016/j.amjcard.2003.10.049.

[26] B. O'Brien, W. Carroll, The evolution of cardiovascular stent materials and surfaces in response to clinical drivers: A review, Acta Biomaterialia. 5 (2009) 945–958. https://doi.org/10.1016/j.actbio.2008.11.012.

[27] S. Diaz-Rodriguez, P. Chevallier, C. Paternoster, V. Montaño-Machado, C. Noël, L. Houssiau, D. Mantovani, Surface modification and direct plasma amination of L605 CoCr alloys: on the optimization of the oxide layer for application in cardiovascular implants, RSC Advances. 9 (2019) 2292–2301. https://doi.org/10.1039/C8RA08541B.

[28] R.I.M. Asri, W.S.W. Harun, M. Samykano, N.A.C. Lah, S.A.C. Ghani, F. Tarlochan, M.R. Raza, Corrosion and surface modification on biocompatible metals: A review, Materials Science and Engineering C. 77 (2017) 1261–1274. https://doi.org/10.1016/j.msec.2017.04.102.

[29] Y. Zhang, X. Wang, Z. Ma, B. Bai, J. Liu, L. Yang, G. Qin, E. Zhang, A potential strategy for in-stent restenosis: Inhibition of migration and proliferation of vascular smooth muscle cells by Cu ion, Materials Science and Engineering C. 115 (2020). https://doi.org/10.1016/j.msec.2020.111090.

[30] R. Schieber, F. Lasserre, M. Hans, M. Fernández-Yagüe, M. Díaz-Ricart, G. Escolar, M.P. Ginebra, F. Mücklich, M. Pegueroles, Direct Laser Interference Patterning of CoCr Alloy Surfaces to Control Endothelial Cell and Platelet Response for Cardiovascular Applications, Advanced Healthcare Materials. 6 (2017). https://doi.org/10.1002/adhm.201700327.

[31] M. Wawrzyńska, I. Bil-Lula, A. Krzywonos-Zawadzka, J. Arkowski, M. Łukaszewicz, D. Hreniak, W. Stręk, G. Sawicki, M. Woźniak, M. Drab, K.

Frączkowska, M. Duda, M. Kopaczyńska, H. Podbielska, D. Biały, Biocompatible Carbon-Based Coating as Potential Endovascular Material for Stent Surface, BioMed Research International. 2018 (2018). https://doi.org/10.1155/2018/2758347.

[32] P.D. Maguire, J.A. McLaughlin, T.I.T. Okpalugo, P. Lemoine, P. Papakonstantinou, E.T. McAdams, M. Needham, A.A. Ogwu, M. Ball, G.A. Abbas, Mechanical stability, corrosion performance and bioresponse of amorphous diamond-like carbon for medical stents and guidewires, in: Diamond and Related Materials, 2005: pp. 1277–1288. https://doi.org/10.1016/j.diamond.2004.12.023.

[33] J.K.F.S. Braz, G.M. Martins, V. Sabino, J.O. Vitoriano, C.A.G. Barboza, A.K.M.C. Soares, H.A.O. Rocha, M.F. Oliveira, C. Alves Júnior, C.E.B. Moura, Plasma nitriding under low temperature improves the endothelial cell biocompatibility of 316L stainless steel, Biotechnology Letters. 41 (2019) 503–510. https://doi.org/10.1007/s10529-019-02657-7.

[34] Y.X.L.P.Y. N. Huang, Surface modification of coronary artery stent by Ti–O/Ti–N complex film coating prepared with plasma immersion ion implantation and deposition, Nuclear Instruments and Methods in Physics Research B. 242 (2006) 18–21.

[35] B.J. Tefft, S. Uthamaraj, A. Harbuzariu, J.J. Harburn, T.A. Witt, B. Newman, P.J. Psaltis, O. Hlinomaz, D.R. Holmes, R. Gulati, R.D. Simari, D. Dragomir-Daescu, G.S. Sandhu, Nanoparticle-mediated cell capture enables rapid endothelialization of a novel bare metal stent, Tissue Engineering - Part A. 24 (2018) 1157–1166. https://doi.org/10.1089/ten.tea.2017.0404.

[36] L.M. de Andrade, C. Paternoster, V. Montaño-Machado, G. Barucca, M. Sikora-Jasinska, R. Tolouei, S. Turgeon, D. Mantovani, Surface modification of L605 by oxygen plasma immersion ion implantation for biomedical applications, MRS Communications. 8 (2018) 1404–1412. https://doi.org/10.1557/mrc.2018.202.

[37] R. Podila, T. Moore, F. Alexis, A.M. Rao, Graphene coatings for enhanced hemo-compatibility of nitinol stents, RSC Advances. 3 (2013) 1660–1665. https://doi.org/10.1039/c2ra23073a.

[38] M.A. Elnaggar, S.H. Seo, S. Gobaa, K.S. Lim, I.H. Bae, M.H. Jeong, D.K. Han, Y.K. Joung, Nitric Oxide Releasing Coronary Stent: A New Approach Using Layer-by-Layer Coating and Liposomal Encapsulation, Small. 12 (2016) 6012–6023. https://doi.org/10.1002/smll.201600337.

[39] , J. S. Stinson B. J. O'Brien, A platinum–chromium steel for cardiovascular stents, Biomaterials. 31 (2010) 3755–3761.

[40] E. Gallino, S. Massey, M. Tatoulian, D. Mantovani, Plasma polymerized allylamine films deposited on 316L stainless steel for cardiovascular stent coatings, Surface and Coatings Technology. 205 (2010) 2461–2468. https://doi.org/10.1016/j.surfcoat.2010.09.047.

[41] Z. Yang, Q. Tu, M.F. Maitz, S. Zhou, J. Wang, N. Huang, Direct thrombin inhibitor-bivalirudin functionalized plasma polymerized allylamine coating for improved biocompatibility of vascular devices, Biomaterials. 33 (2012) 7959–7971. https://doi.org/10.1016/j.biomaterials.2012.07.050.

[42] H. Qiu, P. Qi, J. Liu, Y. Yang, X. Tan, Y. Xiao, M.F. Maitz, N. Huang, Z. Yang, Biomimetic engineering endothelium-like coating on cardiovascular stent through heparin and nitric oxide-generating compound synergistic modification strategy, Biomaterials. 207 (2019) 10–22. https://doi.org/10.1016/j.biomaterials.2019.03.033.

[43] B. Chapman, Glow discharge processes: Sputtering and plasma etching, John Wiley & Sons, NewYork, 1980.

[44] D.J. Marchand, Z.R. Dilworth, R.J. Stauffer, E. Hsiao, J.H. Kim, J.G. Kang, S.H. Kim, Atmospheric rf plasma deposition of superhydrophobic coatings using tetramethylsilane precursor, Surface and Coatings Technology. 234 (2013) 14–20. https://doi.org/10.1016/j.surfcoat.2013.03.029.

[45] Y. Ma, M. Chen, J.E. Jones, A.C. Ritts, Q. Yu, H. Sun, Inhibition of Staphylococcus epidermidis biofilm by trimethylsilane plasma coating, Antimicrobial Agents and Chemotherapy. 56 (2012) 5923–5937. https://doi.org/10.1128/AAC.01739-12.

[46] D.J. Marchand, Z.R. Dilworth, R.J. Stauffer, E. Hsiao, J.H. Kim, J.G. Kang, S.H. Kim, Atmospheric rf plasma deposition of superhydrophobic coatings using tetramethylsilane precursor, Surface and Coatings Technology. 234 (2013) 14–20. https://doi.org/10.1016/j.surfcoat.2013.03.029.

[47] R. di Mundo, F. Palumbo, F. Fracassi, R. D'Agostino, Thin film deposition in capacitively coupled plasmas fed with bis(dimethylamino)-dimethylsilane and oxygen: An FTIR study, Plasma Processes and Polymers. 6 (2009) 506–511. https://doi.org/10.1002/ppap.200800206.

[48] H.K. Yasuda, Q.S. Yu, Deposition of trimethylsilane in glow discharges, Journal of Vacuum Science & Technology A: Vacuum, Surfaces, and Films. 19 (2001) 773–781. https://doi.org/10.1116/1.1365137.

[49] J.E. Jones, M. Chen, Q. Yu, Corrosion resistance improvement for 316L stainless steel coronary artery stents by trimethylsilane plasma nanocoatings, Journal of Biomedical Materials Research - Part B Applied Biomaterials. 102 (2014) 1363–1374. https://doi.org/10.1002/jbm.b.33115.

[50] Hirotsugu Yasuda, Luminous Chemical Vapor Deposition and Interface Engineering, Surfactant Science Series, Marcel Dekker - New York (2005).

[51] M. Morra, E. Occhiello, R. Marola, F. Garbassi, P. Humphrey, A.D. Johnsont, On the Aging of Oxygen Plasma-Treated Polydimethylsiloxane Surfaces, 1990.

[52] A. Vesel, I. Junkar, U. Cvelbar, J. Kovac, M. Mozetic, Surface modification of polyester by oxygen- And nitrogen-plasma treatment, Surface and Interface Analysis. 40 (2008) 1444–1453. https://doi.org/10.1002/sia.2923.

Chapter 3

SURFACE PROPERTY EVALUATION

OF PLASMA NANOCOATINGS

3.1. Abstract

TMS plasma nanocoatings (20 ~ 30 nm thick) were deposited onto L605 cobalt chromium (CoCr) coupons and stents to improve biocompatibility for stenting application. Direct current (DC) glow discharges were utilized for Trimethysilane (TMS) plasma coatings to enhance coating stability and adhesion. The TMS plasma nanocoated surfaces were then treated with NH_3/O_2 plasma modification to tailor their surface chemistry and properties.

Coating thickness was determined by spectroscopic reflectometry. Surface wettability was analyzed by contact angle measurement. X-ray photoelectron spectroscopy (XPS) and Fourier transform infrared spectroscopy (FTIR) were used to characterize the coating surface chemistry. Scanning electron microscope (SEM) was used to evaluate morphology of plasma nanocoating on stents and coupons. Coating adhesion was examined by tape test for plasma nanocoated coupons and stent dilation process to check stent coating cracks or delamination.

Results show that TMS plasma coatings possessed Si– and C–rich composition, while NH_3/O_2 post-treated TMS plasma nanocoatings mostly contain O (39.39 at.%), Si (31.92 at.%), C (24.12 at.%) and N (2.77 at.%). The NH_3/O_2 post-treated TMS plasma nanocoatings were hydrophilic with water contact angle of 48.5° and stable at 48-50° over two years, though the contact angle increased a little due to hydrophobicity recovery with

storage time. Surface elemental compositions were found mostly unchanged after two-year aging in dry condition. TMS plasma nanocoatings showed excellent adhesion to the L605 coupon surfaces and no crack or peeling off in SEM images taken on stent surfaces in dilation test. These results suggest that the ultra-thin, mildly hydrophilic, strong adhesion, N and O containing plasma nanocoatings is promising to stent applications.

3.2. Introduction

3.2.1. Plasma nanocoatings

Plasma coating is a potential approach for stents to be more biocompatible and blood-compatible. As stated in Chapter 2, nitric oxide (NO) incorporated into plasma coating can reduce in-stent restenosis and thrombosis events. In order to improve stability, corrosion resistance, and ion-releasing resistance, plasma coating deposition can be applied to stent surfaces prior to plasma modification which creates NO in this plasma coating. In order to enhance plasma coating adhesion to stent surfaces, a plasma cleaning process needs to be included and considered as plasma pre-treatment.

Which gases should be used in plasma processes: plasma cleaning pre-treatment, plasma deposition, and plasma modification? Typically, argon (Ar) or oxygen (O) can be utilized for this sputtering/etching process to remove surface contaminations or impurities prior to deposition [1]. Oxygen is the most common gas used in plasma cleaning process due to its low cost and wide availability. Oxygen plasmas are considered higher sputtering level than the process with Ar, leading to more effective cleaning. By using oxygen, in plasma discharge it combines with hydrogen (H) and carbon (C) – main elements in organic contaminations – to become H_2O and CO_2 which are pumped out of plasma chamber.

In plasma deposition process, Si-containing coatings are commonly employed to reduce surface wear and corrosion, acting as insulating barrier layers to protect bare material [2-4]. Amorphous silicon carbide (a-SiC:H) coatings have been investigated for improving stent biocompatibility. It was found that such silicon carbide coatings could block electron transfer reactions between the blood protein fibrinogen and the underlying metallic stent and thus halt thrombus formation. Pre-clinical studies have shown that surface passivation of stents by a-SiC:H coating could reduce thrombogenecity and possibly improve the biocompatibility of stent surfaces. Clinical trials have generally shown low rates of stent thrombosis in patients with stenotic lesions [5]. Diamond-like carbon (DLC) coatings have been investigated with respect to biocompatibility, mechanical stability, and corrosion resistance. Results showed that these coatings stimulate less inflammatory activity than uncoated materials and produce comparable responses to already existing polyurethane coatings [6].

TMS was chosen as a precursor molecule for many plasma deposition studies because it has good reactivity in plasma and has a relatively low health hazard. TMS was more mechanically stable an could resist to various environment factors [7]. TMS plasma techniques produce hydrophobic coatings [2–4,7]. Nitrogen and oxygen modification can change the surface wettability of silicon and silicon-based materials to be more hydrophilic. The presence of Si-N and Si-N-O improve the hydrophilicity of nitrogen-implanted silicon due to the more polar contribution of the bonding states [2].

In plasma modification process, gases containing nitrogen (N) and O can be introduced to plasma to integrate NO into plasma coatings. The signaling molecule NO is desired to incorporate into stent surface due to its potential to reduce in-stent restenosis and thrombosis. Compared to N_2 and other N-containing gases, NH_3 is more easily ionized, thus more reactive in glow discharge [2] Additionally, the treatment time for N_2

plasma modification could be longer than NH_3 due to the triple bond energy of N_2 being higher than N-H single bond in NH_3. Surface treated with O_2 plasma can introduce polar functional groups containing O, leading to the hydrophilic surface [8]. Hydrophilicity is one of key factors involved in the biocompatibility of stents. There has been research focusing on NH_3 and O_2 gas mixture for surface plasma treatment, such as modified stainless steel 316L stents with NH_3 and O_2 plasma gas mixture that achieved good results in reducing platelet and leukocyte adhesion. Additionally, no inflammation, hemolysis and thrombosis were found on 316L stainless steel treated with NH_3/O_2 [9]. The existence of NO groups promotes endothelialization while inhibiting smooth muscle cell (SMC) attachment and proliferation [10–12]. Stainless steel treated with NH_3/O_2 plasma had chemical and biological characteristics distinct from untreated stainless steel. Plasma-treated stainless steel became more hydrophilic. Surface resistance to platelet and leukocyte attachment was enhanced [13]. TMS plasma coatings deposited onto 316L stainless steel by DC and radiofrequency (RF) plasma deposition have potential application in preventing restenosis and platelet aggregation on cardiovascular stents. The modification with NH_3/O_2 change the wettability and surface chemistry to be beneficial for the biocompatibility of treated materials [9]. Ammonia, which contain hydrogen, is more easily ionized than nitrogen and the formation of hydrogen-containing nitrogen species are more chemically active [2].

3.2.2. Surface characterization

Surface characterization is necessary for plasma coatings because plasma deposition and modification produce different characteristics in comparison with conventional polymerization processes. In the plasma, many reactive species are created such as mainly free radicals, ions, excited molecules, photons and free energetic electrons. These species react in many ways, and their products range from low molecular weight species to highly branched and cross-linked polymers [7]. The high energy plasma

reaction is complex and less specific than typical polymerization polymer products. Surface characterization for plasma coatings gives a better understanding of coating thickness, surface wettability, surface chemistry and surface morphology.

Wettability is one of key factors involved in the biocompatibility of stents. The more hydrophobic the surface, the greater extent of protein adsorption [14]. Albumin has a higher affinity for hydrophilic surface, and in contrast, fibrinogen adsorption increases with increasing surface hydrophobicity [15]. DLC coatings with contact angle lower than 65° showed a significant enhancement in cell viability and albumin to fibrinogen ratio [16]. Hydrophilic coatings on nickel titanium inhibited the number of adhered platelets compared to uncoated surfaces [17]. A hydrophilic polydopamine coating on cobalt chromium stents showed a reduction in platelet activation and adhesion [18]. A hydrophilic copper-titanium film on 316L stainless steel exhibited a good hemocompatibility and biocompatibility in vitro [19]. Hydrophilic surface modification of CoCr L605 alloys using atmospheric pressure plasma jet improved the biocompatibility by accelerating endothelial cell migration and proliferation compared to untreated samples [20]. Therefore, the increased hydrophilicity of the surface is advantageous against thrombus formation.

A stent is a flexible metal coil or open-mesh tube that is crimped onto a balloon catheter and surgically inserted into a narrowed artery, then expanded and pressed into the vascular wall at up to 10-20 atm pressure, providing a scaffold to hold the artery open. As mentioned, metallic stent surfaces face to two main complications: in-stent restenosis and thrombosis. Coating surface treatment is one of the promising solutions for those complications. Stents may locally undergo large deformation due to tension, compression, rotation as the extension and extraction during clinical operation. The large deformation can cause failures in coating layer such as cracking and delamination which result in a severe problem in the life time of the coated stents. This is due to the mismatch in

mechanical properties between the metal and coatings and the poor adhesion between layers [21]. Coating failures on stent surfaces were addressed after undergoing dilation process and checked with SEM imaging [6,22–24]. Failure analysis on stent surfaces showed that DLC film was delaminated at almost all regions of stents without Si buffer, while film cracking and peeling were significantly suppressed on DLC coated stent with Si buffer deposited layers [6,24]. Practical deformation behavior of Ta coatings on stents were examined using SEM. It indicated severe crack formation, propagation and delamination, leading to fragmentation and detachment from the substrate, though Ta coatings show good results in radiopacity, ion-release suppression, and good cellular responses [23].

Surface coatings with hard and rigid bio-ceramics (TiN, TiCN, Al_2O_3, SiC, BN, and Si_3N_4) fail in stenting applications due to the cracking of these coatings because of the expansion during stent dilatation [25]. Coatings applied on stents should be smooth to reduce friction during insertion, bio-inert [6], highly conformal and pin-hole free, and have excellent adhesion to their substrates [9]. To improve coating adhesion, oxygen plasma pre-treatment can be carried out to clean and activate surfaces prior to plasma deposition. Si-containing films are rather brittle and usually possess compressive stresses [26]. Tape test is usually used for coating adhesion evaluation. The adhesion of atmospheric plasma coated onto aluminum alloy [27] and polycarbonate [28] were assessed by the coating came off due to tape test (ASTM D33590).

In this study, TMS plasma nanocoatings are deposited onto CoCr L605 substrates, followed by NH_3/O_2 plasma modification. Surface wettability was evaluated by contact angle measurement and surface morphology was studied by SEM. FTIR and XPS analysis were performed to identify surface chemistry of the plasma nanocoatings. Aging study was performed on plasma nanocoated coupons and assessed with contact angle

measurement and XPS to assure surface chemical stability. Tape test and stent dilation process were used to examine coating adhesion and failure behaviors.

3.3. Materials and methods

3.3.1. Materials and reagents

L605 CoCr sheets (AMS 5537) purchased from HighTemp Metals (Sylmar, CA, USA) were sectioned into circular coupons (diameter of 15 mm) and square coupons (10 mm × 10 mm). Coupons were cleaned with a Detergent 8 solution (Alconox, Inc., White Plains, NY, USA) for 3 h at room temperature in a tumbling jar; rinsed three times with deionized (DI) water by tumbling; rinsed three times with acetone, and dried at room temperature with a KimWipe.

L605 CoCr stents (diameter × length = 1.3 mm × 12 mm, Resonetics Israel Ltd., Or Akiva, Israel) required a cleaning process recommended by the stent manufacturer. Stents were held in a sample rack immersed in a beaker containing ethanol for 15 min. The beaker containing stents was then transferred to an ultrasonic bath held at 50°C. The stents were sonicated in ethanol for 30 min. Each stent was finally rinsed on the sample rack with fresh ethanol using a squeeze bottle for 3 seconds. Clean stents were dried in air for 15 min.

3.3.2. Plasma nanocoating by DC-based glow discharge

Anhydrous ammonia (purity > 99.99%) was purchased from Airgas (Holts Summit, MO, USA). Oxygen (purity > 99.6%) was purchased from Praxair (Columbia, MO, USA). TMS (purity > 97%) was purchased from Gelest, Inc. (Morrisville, PA, USA). An 80-L bell-jar reactor was used to generate DC glow discharges as shown in **Figure 3.1**. Samples were attached to a titanium holder positioned between two titanium electrodes in parallel.

The holder acted as the cathode whereas the two square titanium electrodes served as the electrically grounded anodes. The reactor was sealed and evacuated to a base pressure less than 1 mTorr using mechanical and booster pumps connected in series. Flow rates were controlled with MKS mass flow controllers (MKS Instruments, Andover, MA) and an MKS 247D readout. The pressure inside the plasma reactor was allowed to stabilize at 50 mTorr for all plasma processing steps using an MKS pressure controller. Pre-treatment with oxygen plasma is used to remove organic contaminants on samples surfaces. Oxygen plasma flow rate was set to 1 standard cubic centimeter per minute (sccm). At pressure stabilization, oxygen was excited with DC power supply at 20 W in order to form the plasma. Plasma pre-treatment was conducted for 2 min. Following plasma pre-treatment, the reactor was pumped to base pressure and TMS introduced to the reactor at a flow rate of 1 sccm. When TMS pressure stabilized at 50 mTorr, plasma was initiated at 5 W DC power for 20 seconds (coupon samples) and 10 seconds (stent samples). Plasma post-treatment of the TMS-based nanocoating was carried out with a mixture of NH_3/O_2. NH_3 and O_2 flow rates were 2 sccm and 1 sccm, respectively. At pressure stabilization (50 mTorr), plasma was initiated at 5 W DC power for 2 min. Details of main parameters used in the three processes are listed in **Table 3.1**.

Table 3.1: Plasma nanocoating parameters

Pre-treatment	Deposition	Post-treatment
Pressure P = 50 mTorr	Pressure P = 50 mTorr	Pressure P = 50 mTorr
Power W = 20 W	Power W = 5 W	Power W = 5 W
O_2 Flow rate = 1 sccm	TMS Flow rate = 1 sccm	NH_3/O_2 Flow rate ratio = 2:1 sccm
Time = 120 s	Time = 10 s ÷ 20 s	Time = 120 s

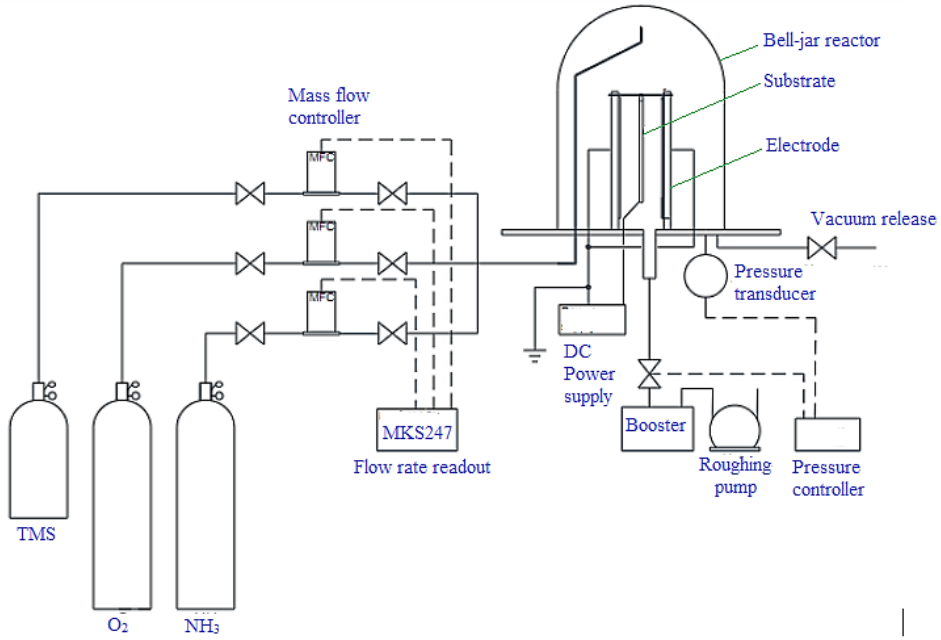

Figure 3.1: Schematic illustration of the plasma apparatus used in this study

3.3.3. Coating thickness

Plasma nanocoating thickness was determined by using a microscope-mounted thin-film measurement device (Filmetrics F40-UV, KLA Corporation, Milpitas, CA, USA). The thickness range of the device is 4 nm – 40 μm. A small sample area is non-destructively analyzed by reflecting light off the nanocoating. The reflectance spectrum is analyzed over a wavelength range (200-2000 nm). The Filmetrics software performs curve fitting of the reflectance spectrum to determine the nanocoating thickness. For coating analysis, the refractive index (n_i) is 1.65, as verified by previous researchers for TMS-based nanocoatings.

3.3.4. Contact angle

Surface contact angles for uncoated L605, TMS, and TMS+NH_3/O_2 plasma nanocoatings were measured using a 1.2 - 1.3 μL droplet of deionized water deposited onto square coupons and a contact angle meter/Goniometer - DMe 210 (Kyowa Interface

Science Co., Ltd., Eden Prairie, MN, USA) with FAMAS software. Nanocoating stability was assessed by storing the nanocoated coupons in Pyrex dishes at 25 °C for 96 weeks. At least six contact angle measurements were obtained per condition in order to get the mean contact angle and standard deviation.

3.3.5. FTIR spectroscopy

Fourier-transform infrared spectroscopy (FTIR) - a Agilent Cary 660 FTIR spectrometers (Agilent Technologies Inc., Santa Clara, CA, USA) - was conducted to determine bonding states within plasma nanocoating deposited onto silicon wafers. Silicon wafers were sectioned in 15mm x 15mm squares. FTIR scan was carried out from 400 to 3700 cm^{-1} with sample count of 32.

3.3.6. XPS measurements

Nanocoating surface chemistry on L605 square coupons was analyzed by XPS. A Kratos AXIS Ultra DLD X-ray Photoelectron Spectrometer (Kratos Analytical Inc., Chestnut Ridge, NY, USA) utilizing a monochromatic Al Kα X-ray (1486.6 eV) source operating at 150 W was utilized to characterize the coatings to a depth of about 10 nm. The X-ray source take-off angle was set at 90 degrees relative to the coupon surface, and the spot size was 200 μm x 200 μm. The survey was performed at 10 mA and 15 kV. Survey spectra were recorded in the binding energy scale from 1200 to -5 eV, and dwell time of 100 ms with two sweeps to resolve peaks. The sample was loaded into the load lock and pumped down to less than $5x10^{-7}$ torr and transferred into the sample analysis chamber. Data was collected at pressures approximately $5x10^{-9}$ torr. Binding energies in the survey and high-resolution spectra were calibrated with respect to C1s at 284.6 eV adventitious peak. The acquired data were analyzed by using the Casa XPS software package. Peak fitting was performed using Gaussian de-convolution function.

3.3.7. Adhesion test

Adhesion of plasma nanocoating was performed by following ASTM D3359. Although this is a rather qualitative test, interfaces failing in this test are considered to have poor adhesion. Uncoated L605 and plasma nanocoated coupons (4 cm $\times$ 3 cm) were used for this adhesion tape test. Clean and dry areas that are free of surface imperfections were selected. Grid area with six cuts in each direction were scraped onto plasma nanocoated surfaces, and pressure-sensitive tape was thoroughly adhered over the lattice patterns and then detached. Adhesion was assessed by optical imaging. The adhesion scale was rated from 0B to 5B as listed in ASTM D3359. Each test was repeated three times.

Adhesion of plasma nanocoating to stents was determined by crimping and expanding process that mimics stent dilation procedures. A stent was positioned on a balloon catheter and crimped by Model CX with J-Crimp Station (Blockwise Engineering LLC, Tempe, AZ, USA) to a final crimping diameter of 0.8 mm. The crimped stent was expanded at 12 atm to reach a diameter of 3.2 mm. Stents were examined under environmental SEM - Quanta 600 FEG equipped with a Schottky Field Emitter (FEI Company, Hillsboro, Oregon, USA) for coating failure investigation. An accelerating voltage of 10 kV with probe currents of 4.5 μA was used for all operations.

3.3.8. Statistics

Results were expressed as mean $\pm$ standard deviation (SD) of the mean for each treatment group. Each experiment was repeated for three times independently, if not indicated otherwise. Data were analyzed using one-way ANOVA followed by the Turkey's test. A *p*-value of 0.05 or less was considered significant.

3.4. Results and Discussion

3.4.1. Plasma coating thickness

The average of plasma nanocoating thickness determined onto 6 coupon samples was 23 ± 1.4 nm. The plasma nanocoating is thicker on coupons than that on stents under the same plasma coating parameters due to stent size is much smaller than coupons.

3.4.2. Surface wettability

Water contact angle measurements provided evidence of nanocoatings with different surface chemistries. Uncoated L605 contact angle was 74 ± 0.8° (**Figure 3.2**). Following deposition of the TMS nanocoating, the contact angle increased to 99 ± 1.2°, indicating hydrophobic surface. However, with TMS+NH_3/O_2 surface modification, the plasma nanocoating water contact angle dramatically decreased to 3 ± 0.4° and then gradually increased to 48.5 ± 0.9° after 96 weeks (2 years) storage in clean and dry conditions. Hydrophobic recovery occurs due to thermal motion and diffusion of polar groups attached to the nanocoatings. Groups or chain segments at the surface of the coating have greater freedom than those in the bulk and tend to be arranged to equilibrate with chemical environment. The rearrangement directly affects the durability of the hydrophilic surface and subsequent water contact angle stabilization over the aging period. Hydrophilic durability after one year can be explained by the formation of cross-linkage that suppresses the rearrangement of the polar group on hydrophilic surface [29–31]. All TMS+NH_3/O_2 plasma nanocoated samples utilized in this study have aged for three months prior to any surface characterization experiments and bio-related testing. **Figure 3.2** (b and c) also shows photography of spherical water droplets on coupon and stent surfaces. Water droplets spread out on modified TMS+NH_3/O_2 coupons and “absorbed” in

modified stent meshes, indicating that TMS+NH_3/O_2 substrates are more hydrophilic than uncoated L605 and TMS plasma nanocoated counterparts.

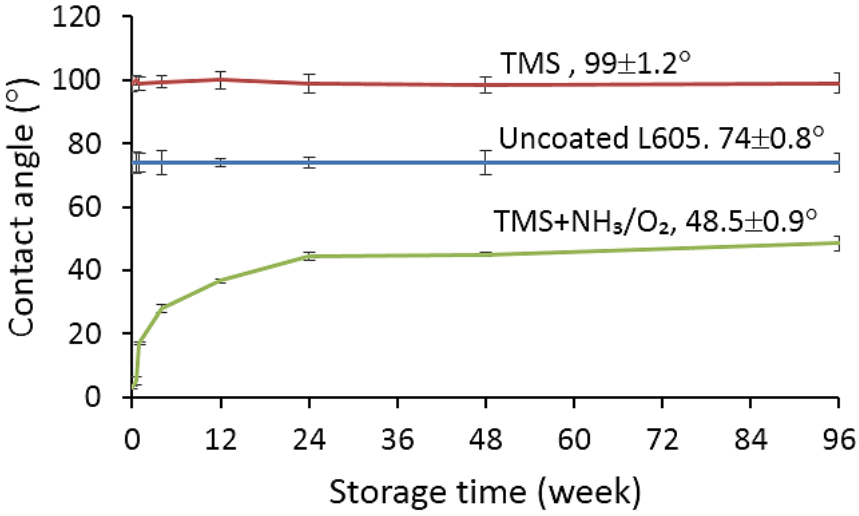

a)

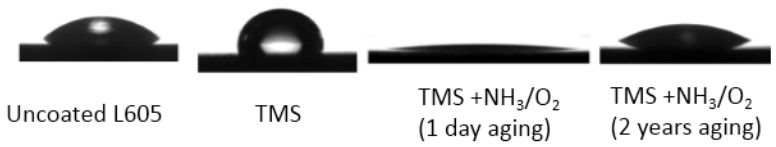

b)

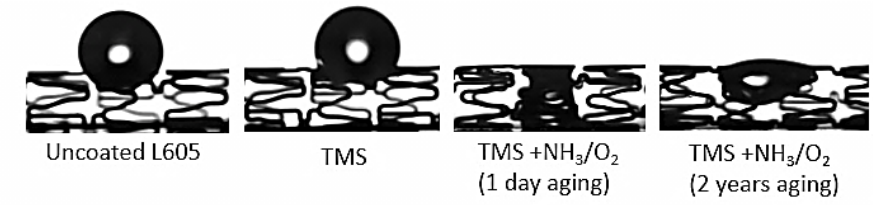

c)

Figure 3.2: a) Surface static contact angle for uncoated L605, TMS, and TMS+NH_3/O_2 plasma nanocoated coupons up to 96 weeks, b) Photography of spherical water droplets on uncoated L605 and plasma nanocoated coupons, c) Photography of spherical water droplets on uncoated and plasma nanocoated stents

3.4.3. Surface functional groups

FTIR absorbance spectra acquired from plasma nanocoating surfaces are shown in **Figure 3.3** and characteristic absorption bands are assigned in **Table 3.2**. Compare to original TMS monomer structure, the FTIR spectra of TMS plasma nanocoating features are similar, reflecting that it has not been excessively fragmented [31]. In the range of 400 to 3700 cm^{-1}, the broad band at 3320 cm^{-1} observed on both plasma nanocoating spectra can be attributed to OH stretching - one of the most hydrophilic groups. For TMS spectrum, it may be explained by the presence of oxygen impurity in the reactor (residual O_2 or H_2O) or by its absorption after the plasma nanocoating exposure to the atmospheric air [32]. For TMS+NH_3/O_2 spectrum, the intensity of OH-related peak increased due to NH_3/O_2 plasma modification, indicating that oxygen radicals during NH_3/O_2 plasma diffused into inner structures of the coating to form Si-OH [33]. Polar functionalities Si-OH are associated with improved wettability, which can be explained by the hydrophilicity of NH_3/O_2 treated plasma nanocoating. The presence of organic C-H stretching peaks at 2865 cm^{-1} (symmetric stretching in CH_2), 2931 cm^{-1} (asymmetric stretching in CH_2) and 2962 cm^{-1} (asymmetric stretching in CH_3) [34–37] are expected, suggesting the existence of plasma nanocoating. Other C-H stretching peaks at 1587 cm^{-1} (asymmetric deformation in CH_3), 1479 cm^{-1} (asymmetric bending in CH_3), and 1365 cm^{-1} (symmetric bending in CH_3) [33–36] are observed, suggesting radicals existed in plasma modification process. Si-H peaks are present in plasma nanocoating spectra by signals at 2109 cm^{-1} and 1845 cm^{-1} (stretching) [6,32,34,37], indicating that TMS yields radicals SiH-$(CH_3)_2$ which are then incorporated in the surface layer to give free Si-H [38]. Organosilicon Si-CH_3 groups are revealed in TMS spectrum by a small band at 1250 cm^{-1} (symmetric bending) and a strong band at 798 and 825 cm^{-1} (CH_3 rocking in Si-$(CH_3)_3$ units) [33,34]. CH_3 functional group and Si-based structure generated more hydrophobic character for TMS plasma

nanocoating [39]. In TMS+NH_3/O_2 plasma nanocoating spectrum, Si-CH_3 groups are shown at 796 cm^{-1} (CH_3 rocking in Si-$(CH_3)_3$ units), but no signal bands around 1250 cm^{-1}, implying that some Si-CH_3 groups were dissociated in NH_3/O_2 plasma. Peaks in the region of 979 cm^{-1} to 1234 cm^{-1} correspond to Si-O-Si or Si-O-C. The Si-O-Si/C and Si-H peaks indicate that some of the Si-CH_3 bonds composed of the TMS molecules were dissociated in the plasma, and their fragments reacted with each other or with dissociated oxygen from air or from NH_3/O_2 plasma to form new bonds [6]. Si-C groups are also observed with bands appearing at 711 and 732 cm^{-1} in plasma nanocoating spectra. A very small but important peak appeared at 808 cm^{-1} can be attributed to the existence of Si-N group [3] in TMS+NH_3/O_2 plasma nanocoating due to the post-treatment with NH_3/O_2. Peaks in the region 2300 - 2400 cm^{-1} can be attributed to CO_2 molecule coming from ambient air or residues formed during oxidation of organics [4,33].

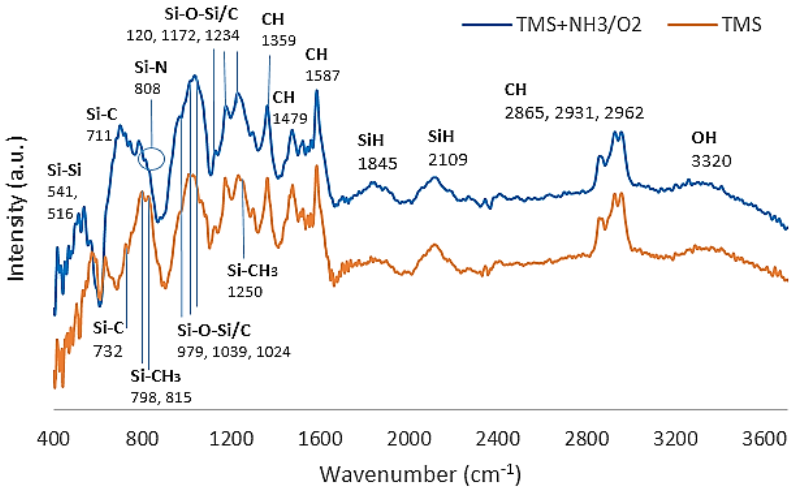

a)

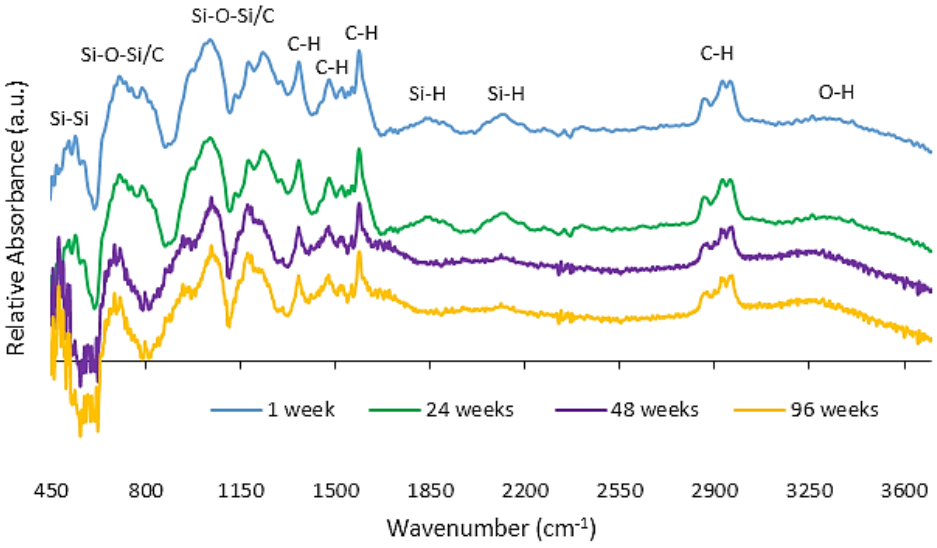

b)

Figure 3.3: a) FTIR spectra for uncoated L605, TMS, and TMS+NH_3/O_2 plasma nanocoated samples; b) FTIR spectra for TMS+NH_3/O_2 plasma nanocoating after 1 week, 24 weeks, 48 weeks, and 96 weeks.

The FTIR spectra for TMS+NH_3/O_2 plasma nanocoating up to 96-week aging are shown in **Figure 3.3 b**. Spectra detected at 48 and 96 weeks displayed a slightly change in absorbance intensity compared to spectra for 1 week and 24 weeks. Peaks for Si-O-Si/C are present at nearly consistent levels, but the peak at 1234 cm^{-1} assigned for Si-O-Si/C declines significantly in intensity at 48 weeks and 96 weeks. Si-H groups at 1845 and 2109 cm^{-1} almost disappear after 48 weeks of aging.

Table 3.2: FTIR peak assignments for plasma nanocoatings

Assignments	Wavenumber (cm^{-1})	Type	References
O-H	3320	Stretching	[32,34]
C-H	2962 2931 2865	Asymmetric stretching in CH_3 Asymmetric stretching in CH_2 Symmetric stretching in CH_2	[34,40]
	1587	Asymmetric deformation in CH_3	[36]
	1479	Asymmetric bending in CH_2	[36,41]
	1365	Symmetric deformation CH_3	[36]
Si-H	2109, 1845 965	Stretching Deformation	[32,37,40]
Si-CH_3	1250	Symmetric bending	[37]
	798, 825	CH_3 rocking in Si-$(CH_3)_3$	[32,34,36,42]
Si-O-Si Si-O-C	1234, 1172, 1120 1039, 1024, 979 792, 757, 732, 711	Asymmetric stretching	[37,41,42]
Si-N	819	Asymmetric stretching	[43]
Si-Si	516, 541	Stretching	[34,36]

3.4.4. Surface compositions

XPS survey spectra for uncoated L605 and plasma nanocoated samples are shown in **Figure 3.4**. The elemental chemical compositions (at.%) within surfaces are provided in **Table 3.3 and 3.4**. In **Figure 3.4** a, XPS survey spectrum for uncoated L605 prior to oxygen plasma treatment shows the presence of N 1s peak; whereas, N 1s peak disappears in XPS spectrum of samples treated with oxygen plasma. In **Table 3.3**, surface atomic concentrations for uncoated L605 before and after oxygen plasma indicate that N 1s percentage reduced from 0.81 at.% to 0 and C 1s declined from 34.98 at.% to 25.15 at.% as uncoated L605 samples were treated with oxygen plasma, implying the clean uncoated L605 prior to plasma nanocoating process. The contamination removal is considered beneficial to the adhesion of plasma nanocoatings to the L605 substrates. The increase of O 1s percentage from 44.7 at.% to 61.4 at.% confirms that the uncoated L605 surface not only contains O inherently in its oxide layer, but also O incorporated by oxygen plasma treatment.

In **Figure 3.4 b** and **Table 3.4**, a small amount of carbon (23.33 $\pm$ 0.88 at.%) observed on the surface of uncoated L605 sample was characteristic of a low contamination with just adventitious carbon. The presence of Si 2p (36.28 $\pm$ 1.32 at.%), Si 2s and the increase of C 1s (from 23.33 $\pm$ 0.88 at.% to 47.42 $\pm$ 1.6 at.%) indicate that TMS plasma nanocoatings was deposited onto uncoated L605 surfaces.

The O 1s percentage (16.31 $\pm$ 0.28 at.%) detected from TMS plasma nanocoating surface decreased compared to the O 1s amount (50.03 $\pm$ 2.02 at.%) on uncoated L605 surface, implying that oxide layer on the top surfaces of uncoated L605 was mostly replaced by TMS plasma nanocoatings. O 1s contents in TMS plasma nanocoating spectra can be attributed to oxygen in Si-O-Si/C or contamination from ambient air. In

TMS+ NH_3/O_2 spectrum, the O 1s amount increases to 39.39 ± 1.06 at.% due to oxygen in NH_3/O_2 post-treatment. Conversely, C 1s reduces to 24.12 ± 1.7 at.% due to the etching effect or the plasma modification of NH_3/O_2, in which N, O, and H radicals can react or combine to the plasma nanocoated surfaces. The N 1s concentration is 2.77 ± 0.19 at.%, while no trace of N 1s was observed on the surface of uncoated L605 and TMS plasma nanocoating coupons. N was incorporated into TMS plasma nanocoatings by NH_3/O_2 plasma post-treatment. The increase of oxygen and nitrogen concentration was attributed to reactions of free radicals created by plasma treatment with mixture of NH_3 and O_2. The ratio of O/Si increases almost three times in TMS+NH_3/O_2 compared to that for TMS, while the ratio of C/Si decreases by half. It can be explained that compared to TMS plasma nanocoatings, post-treated surfaces are dominant with O, resulting more hydrophilic surface properties. Conversely, TMS plasma nanocoatings contains more C, leading to surface hydrophobicity.

The XPS core level spectra using the Gaussian distribution of C 1s, O 1s and Si 2p in plasma nanocoated samples are depicted in **Figure 3.4 c**. The C 1s in TMS plasma nanocoating showed peaks at 284.4 eV and 285.1 eV corresponding to C-C and C-H [44]. Similarly, in TMS+NH_3/O_2 plasma nanocoating, the binding energy of 285.3 eV was assigned to C-H. Other peaks at 287.5 eV and 289.3 eV can be assigned as C=O and O=C-O functional groups [45,46]. In TMS+NH_3/O_2 plasma nanocoating, area percentage of C-C or C-H groups increased to 85%, whereas C=O and O=C-O groups accounted for 6% and 9%, respectively. Though the amounts of polar groups C=O and O=C-O were small, they played important roles in hydrophilicity of TMS+NH_3/O_2 plasma nanocoating. XPS core level O 1s spectrum for TMS plasma nanocoating showed two Si-O peaks, the first one represented Si-O in SiO_2 at binding energy 532.7 eV and the second bigger peak at 533.3 eV corresponding to Si-O-Si. The O 1s peak in TMS+NH_3/O_2 plasma nanocoating

is symmetrical and contains no discernable asymmetry or structure. It can be assigned to C-O in Si-O-C [44,47–49] or O=C-O [50]. The Si peaks at 101.2 eV and 102.4 eV in TMS plasma nanocoating are attributed to the presence of O-Si-C and O-Si-O, respectively [51,52]. High resolution Si 2p spectrum for TMS+NH_3/O_2 plasma nanocoating presents Si-N at 101.8 eV and O-Si-OH at 104.2 eV [52]. The peak position shift to 104.2 eV can be attributed to the siloxane unit with a hydroxyl group substituted for a methyl group. XPS high resolution spectra confirmed the existence of C-O, C=O and O-H polar groups in TMS+NH_3/O_2 plasma nanocoating, whereas C-H, C-C, Si-O-Si, O-Si-O were detected in TMS plasma nanocoating. This result determines the existence of N and O containing functionality groups in TMS+NH_3/O_2 plasma nanocoating. XPS N 1s core spectra (**Figure 3.4 c**) revealed the existence of characteristic peak of N-Si at 395.65 eV and N-C at 397.43 eV [53,54] due to the larger electronegativity of C than Si. The direct N to O bond has binding energy of 402 eV or higher [54]. The peak is not present, and any N-O bonding may be present below the XPS threshold of detection. This result determines the existence of N and O containing functionality groups in TMS+NH_3/O_2 plasma nanocoating.

XPS survey spectra in **Table 3.4** and **Figure 3.4** was performed to study the changes of chemical structure and composition of TMS+NH_3/O_2 plasma coatings. In **Figure 3.4** d, all spectra show similar peaks of O 1s (529 eV), N 1s (400 eV), C 1s (285 eV), and Si 2p (101 eV). After 2-year surface aging, ratios of O 1s, N 1s and C 1s to Si 2p were almost the same as shown in **Table 3.4**, serving as strong evidence of the chemical stability of plasma nanocoating with NH_3/O_2 plasma post-treatment.

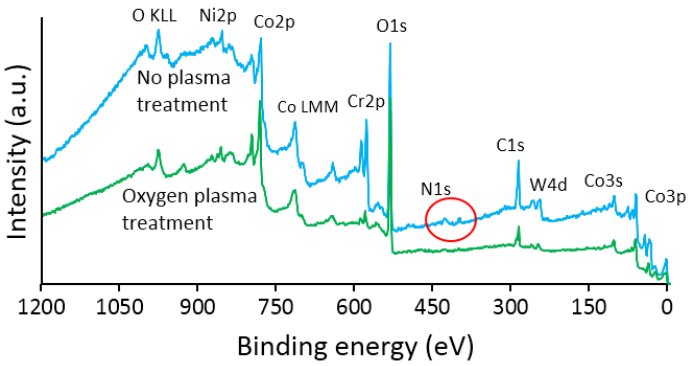
O KLL
Ni2p
Co2p
O1s
No plasma treatment
Co LMM
Cr2p
C1s
N1s
W4d
Co3s
Co3p
Oxygen plasma treatment
Intensity (a.u.)
1200
1050
900
750
600
450
300
150
0
Binding energy (eV)

a)

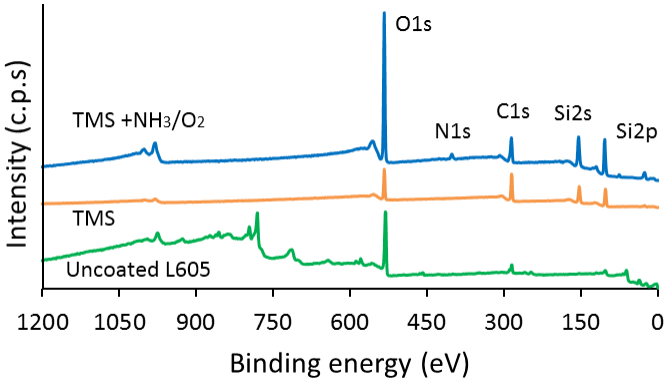
O1s
TMS +NH3/O2
N1s
C1s
Si2s
Si2p
TMS
Uncoated L605
Intensity (c.p.s)
1200
1050
900
750
600
450
300
150
0
Binding energy (eV)

b)

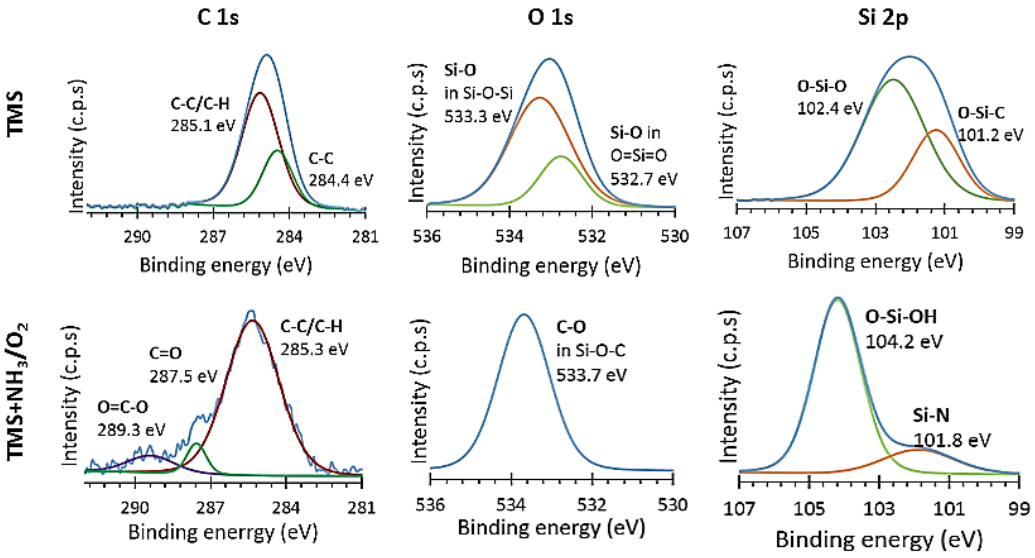
C 1s
O 1s
Si 2p
TMS
TMS+NH3/O2
Intensity (c.p.s)
C-C/C-H
285.1 eV
C-C
284.4 eV
Si-O
in Si-O-Si
533.3 eV
Si-O in
O=Si=O
532.7 eV
O-Si-O
102.4 eV
O-Si-C
101.2 eV
C=O
287.5 eV
C-C/C-H
285.3 eV
O=C-O
289.3 eV
C-O
in Si-O-C
533.7 eV
O-Si-OH
104.2 eV
Si-N
101.8 eV
290
287
284
281
536
534
532
530
107
105
103
101
99
Binding energy (eV)
Binding enerrgy (eV)

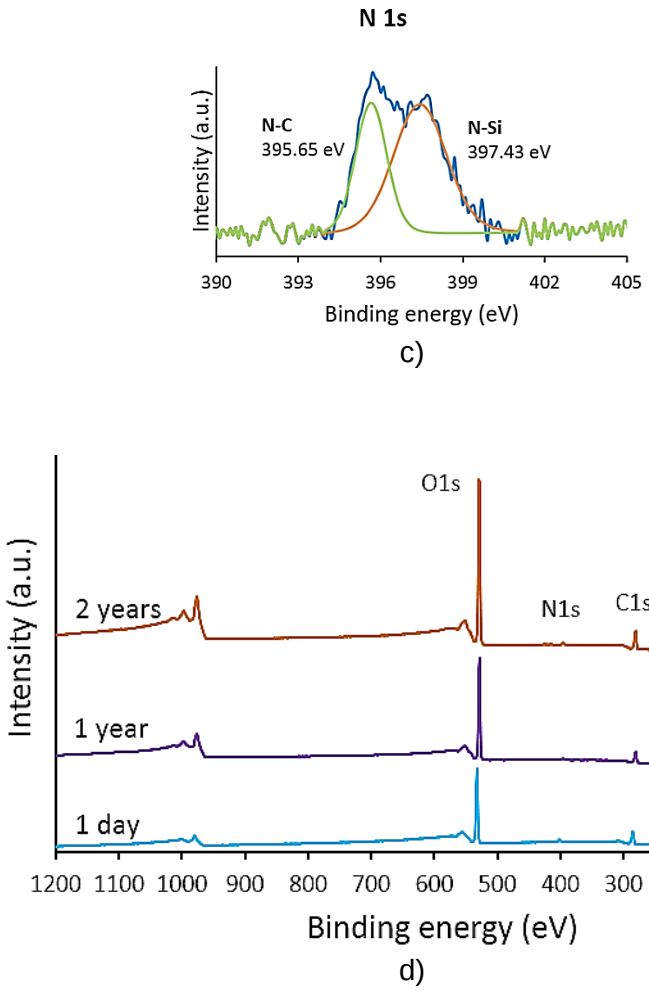

Figure 3.4: a) XPS survey spectra for uncoated L605 before and after oxygen plasma treatment; b) XPS survey spectra for uncoated L605, TMS, and TMS+NH_3/O_2 plasma nanocoatings; c) XPS core level spectra; d) XPS survey spectra for TMS+NH_3/O_2 plasma nanocoatings after 1 day, 1 year and 2 years following plasma treatment.

Table 3.3: Atomic concentrations for uncoated L605 with and without oxygen plasma

	O 1s (at.%)	C 1s (at.%)	N 1s (at.%)	Co 2p (at.%)	Cr 2p (at.%)	Ni 2p (at.%)	W 4d (at.%)
No Plasma	44.70	34.98	0.81	7.1	10.01	0.74	1.21
O_2 plasma	61.40	25.15	0	9.91	1.58	1.48	0.48

Table 3.4: Surface composition of plasma nanocoated samples

	O 1s (at.%)	N 1s (at.%)	C 1s (at.%)	Si 2p (at.%)	O/Si	N/Si	C/Si
Uncoated L605	50.03 ±2.02	0	23.33 ±0.88	0	N/A	N/A	N/A
TMS	16.31 ±0.28	0	47.42 ±1.60	36.28 ±1.32	0.45	0	1.31
TMS+NH_3 /O_2	39.39 ±1.06	2.77 ±0.19	24.12 ±1.70	31.92 ±1.08	1.23	0.086	0.76

3.4.5. Surface morphology

The surface morphology and crystallographic texture in micro scale of uncoated L605 and plasma nanocoated coupons are shown by SEM backscatter images in **Figure 3.5 a**. The uncoated L605 surface is mainly composed of equiaxed grains with random crystallographic orientation. The average grain size is about 50 μm. At the same magnification, grain boundaries in plasma nanocoated coupons were not clearly seen because of the plasma coating.

Mechanical stability test is to evaluate any coating defects such as cracking or peeling off because stents are subjected to large strains during crimping and expansion in implantation procedure [55]. These defects may result in inflammation and un-favored biological responses. In order to insert stents into cardiovascular arteries, a stent is

crimped onto a balloon catheter. Along with a guide catheter and a guide wire, the stent mounted on the balloon catheter is tracked to the lesion area and expanded to open artery and restore blood flow. The evaluation of the plasma nanocoating on stent surface after the stents undergo plastic compression and expansion is necessary. SEM images at high magnification provide evidence of any possible failures on stent surfaces such as cracking and coating detachment. **Figure 3.5 b** shows the images obtained using SEM of uncoated L605 and plasma nanocoated stents. These images were acquired following stent crimping and expansion processes. At low magnification, plasma nanocoated stent surfaces look smoother and more conformal without any defects compared to uncoated L605 stents, but at higher magnification many folding lines were found vertically and horizontally on both stent surfaces due to crimping and expanding processes. Neither cracking nor delamination were observed at this magnification.

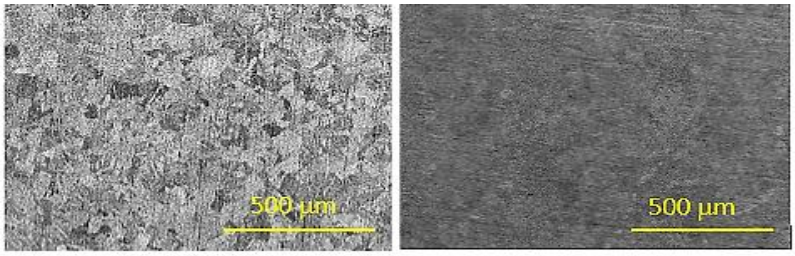

a)

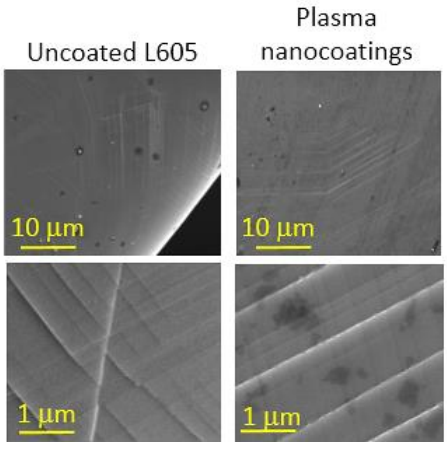

b)

Figure 3.5: SEM images: a) Uncoated L605 vs. plasma nanocoated coupon surfaces; b) Uncoated L605 vs. plasma nanocoated stent surfaces

3.4.6. Plasma nanocoating adhesion

Adhesion is highly important for the practical application of coatings. The resistance and the film removal degree were observed by SEM imaging when the tape was removed. Adhesion was rated by comparing film pulled-off against an established standard (ASTM 3359). **Figure 3.6 a** shows SEM images of plasma treated samples after tape test. Edges of lattice patterns are completely smooth with no detached layer near the cuts. Residual materials from plasma nanocoating piled up on both sides of grooves are chips produced by plastic material deformation. The adhesion of plasma nanocoating to its substrate was classified as 5B – the highest rating scale for adhesion evaluation – in which film removal was approximately 0%. The test was repeated in two other locations in the same sample, and test results of 5B classification were verified.

Mechanical stability testing evaluates coating defects such as cracking or peeling off. Stent coatings are susceptible to cracking and delamination because they are subjected to large strains during crimping and expansion during implantation procedure [7]. These defects may result in inflammation and unfavorable biological responses. In order to insert stents into coronary arteries, a stent is crimped onto a balloon catheter. Along with a guide catheter and a guide wire, the stent mounted on the balloon catheter is tracked to the lesion area and expanded to open the artery and restore blood flow. The evaluation of the plasma nanocoating on stents following plastic compression and expansion is necessary. SEM images at high magnification provide evidence of any possible failures on stent surfaces such as cracking and coating detachment. **Figure 3.6 b** shows the images obtained using SEM of uncoated L605 and plasma nanocoated stents. These images were acquired following stent crimping and expansion processes.

At low magnification, plasma nanocoated stent surfaces appeared smoother and more conformal without any defects compared to uncoated L605 stents, but at higher magnification many folding lines were found vertically and horizontally on both stent surfaces due to crimping and expanding processes. Neither cracking nor delamination were observed at this magnification. At very high magnification, post-dilated surface texture of uncoated L605 and plasma nanocoated stents contains multiple shallow and shaft pits and ridges due to dilation processes. No sign of micro-cracking and delamination were observed for plasma nanocoated stents with coating thickness about 20-25 nm.

The adhesion of plasma nanocoatings may be improved by surface contamination removal during oxygen plasma pre-treatment. As shown in **Figure 3.4 a** and **Table 3.3**, in XPS spectrum for uncoated L605 after oxygen plasma treatment, N 1s percentage became zero and the C 1s percentage reduced, implying less contamination on uncoated L605 surfaces prior to plasma deposition process. In plasma deposition, adhesion of plasma nanocoatings to substrates is attributed to Si-O bonds of the oxide layer on the top surface of uncoated L605 and Si-containing radicals generated by TMS. A very thin coating layer (20-30 nm) which minimizes internal stresses occurring in plasma nanocoatings is another reason plasma nanocoated stents did not undergo cracking and delamination during dilation process.

At very high magnification, post-dilated surface texture of uncoated L605 and plasma nanocoated stents contains multiple shallow and shaft pits and ridges due to dilation processes. No sign of micro-cracking and delamination were observed for plasma nanocoated stents with coating thickness about 20-25 nm, but micro-cracks were found at coating thickness of 40-45 nm, and micro-delamination were detected clearly at thick plasma nanocoating as 60-65 nm (**Figure 3.6 b**). The thicker the coating, the more severe cracking and delamination were observed. Crack length and delamination size were about

1 μm, so tiny compared to stent strut thickness of 80 μm [56]; however, the impact of those tiny failures can be addressed in biological assessments.

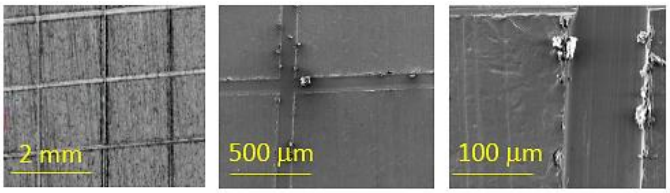

a)

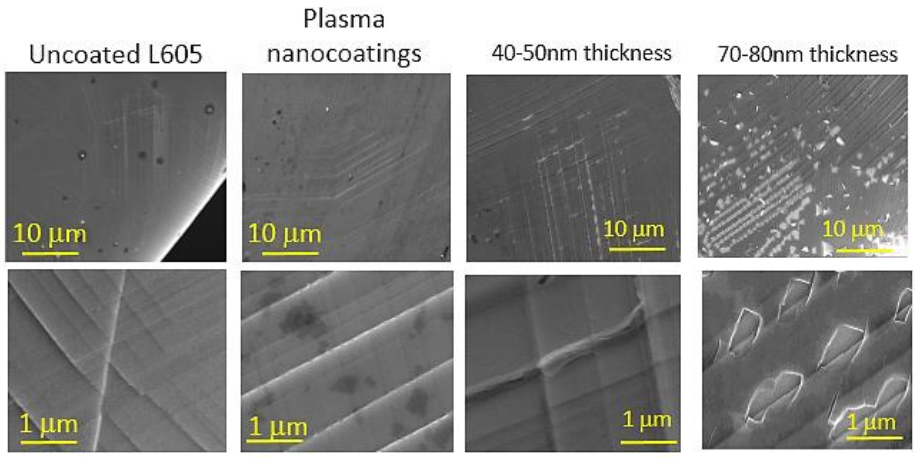

b)

Figure 3.6: SEM images: a) plasma nanocoated samples in tape test; b) plasma nanocoating failures at different coating thickness.

3.5. Conclusions

NH_3/O_2 modified TMS plasma nanocoatings of 20-30 nm thickness were deposited onto CoCr L605 coupons and coronary artery stents, using glow discharges sustained with a DC power supply. The smooth, conformal, moderately hydrophilic plasma nanocoatings containing N and O functional groups are desirable for stent surfaces. Long-term usage of the plasma nanocoatings was confirmed by chemical stability assessment. The plasma nanocoatings were not prone to stress cracking upon dilatation catheter

expansion, thereby preventing exposure of the bare metal substrate, leading to better biocompatibility.

3.6. References

[1] D.F. O'Kane, K.L. Mittal, Plasma cleaning of metal surfaces, J Vac Sci Technol. 11 (1974) 567–569. https://doi.org/10.1116/1.1318069.

[2] G.J. Wan, P. Yang, R.K.Y. Fu, Zh.Q. Yao, N. Huang, P.K. Chu, Improvement of nitrogen retained dose using ammonia as a precursor in nitrogen plasma immersion ion implantation of silicon, Journal of Vacuum Science & Technology A: Vacuum, Surfaces, and Films. 23 (2005) 1346–1349. https://doi.org/10.1116/1.1991870.

[3] A.M. Wr, H. Szymanowski, J. Kowalski, Plasma Polymerization of Carbosilanes: Tetramethylsilane as a Model Monomer for Reactivity Study of Silylmethyl Groups, Plasma Chemistry and Plasma Processing volume 10, pages277–289, 1990.

[4] J.L.C. Fonseca, S. Tasker, D.C. Apperley, J.P.S. Badyal, Plasma-Enhanced Chemical Vapor Deposition of Organosilicon Materials: A Comparison of Hexamethyldisilane and Tetramethylsilane Precursors, 1996.

[5] M. Unverdorben, B. Sippel, R. Degenhardt, K. Sattler, R. Fries, B. Abt, E. Wagner, H. Koehler, G. Daemgen, M. Scholz, H. Ibrahim, K.H. Tews, B. Hennen, H.K. Berthold, C. Vallbracht, Comparison of a silicon carbide-coated stent versus a noncoated stent in human beings: the Tenax versus Nir Stent Study's long-term outcome., American Heart Journal. 145 (2003). https://doi.org/10.1067/mhj.2003.90.

[6] P.D. Maguire, J.A. McLaughlin, T.I.T. Okpalugo, P. Lemoine, P. Papakonstantinou, E.T. McAdams, M. Needham, A.A. Ogwu, M. Ball, G.A. Abbas, Mechanical stability, corrosion performance and bioresponse of amorphous diamond-like carbon for medical stents and guidewires, in: Diamond and Related Materials, 2005: pp. 1277–1288. https://doi.org/10.1016/j.diamond.2004.12.023.

[7] D.J. Marchand, Z.R. Dilworth, R.J. Stauffer, E. Hsiao, J.H. Kim, J.G. Kang, S.H. Kim, Atmospheric rf plasma deposition of superhydrophobic coatings using tetramethylsilane precursor, Surface and Coatings Technology. 234 (2013) 14–20. https://doi.org/10.1016/j.surfcoat.2013.03.029.

[8] T. Murakami, S.-I. Kuroda, Z. Osawa, Dynamics of Polymeric Solid Surfaces Treated with Oxygen Plasma: Effect of Aging Media after Plasma Treatment, 1998.

[9] J.E. Jones, Q. Yu, M. Chen, A chemical stability study of trimethylsilane plasma nanocoatings for coronary stents, Journal of Biomaterials Science, Polymer Edition. 28 (2017) 15–32. https://doi.org/10.1080/09205063.2016.1239947.

[10] B.J. O'Brien, J.S. Stinson, S.R. Larsen, M.J. Eppihimer, W.M. Carroll, A platinum-chromium steel for cardiovascular stents, Biomaterials. 31 (2010) 3755–3761. https://doi.org/10.1016/j.biomaterials.2010.01.146.

[11] H. Qiu, P. Qi, J. Liu, Y. Yang, X. Tan, Y. Xiao, M.F. Maitz, N. Huang, Z. Yang, Biomimetic engineering endothelium-like coating on cardiovascular stent through heparin and nitric oxide-generating compound synergistic modification strategy, Biomaterials. 207 (2019) 10–22. https://doi.org/10.1016/j.biomaterials.2019.03.033.

[12] M.A. Elnaggar, S.H. Seo, S. Gobaa, K.S. Lim, I.H. Bae, M.H. Jeong, D.K. Han, Y.K. Joung, Nitric Oxide Releasing Coronary Stent: A New Approach Using Layer-by-Layer Coating and Liposomal Encapsulation, Small. 12 (2016) 6012–6023. https://doi.org/10.1002/smll.201600337.

[13] M. Chen, P.O. Zamora, L. Peñ, P. Som, S. Osaki, NH_3/O_2 mixed gas plasmas alter the interaction of blood components with stainless steel, Journal of Biomedical Materials Research, Volume 67A, Issue 3, 1 December 2003, 994-1000 2003.

[14] Lyuba I. Mikhalovska, Matteo Santin, Stephen P. Denyer, Fibrinogen adsorption and platelet adhesion to metal and carbon coatings, Thromb Haemost 2004; 92(05): 1032-1039 2004.

[15] B. Clarke, P. Kingshott, X. Hou, Y. Rochev, A. Gorelov, W. Carroll, Effect of nitinol wire surface properties on albumin adsorption, Acta Biomaterialia. 3 (2007) 103–111. https://doi.org/10.1016/j.actbio.2006.07.006.

[16] W.J. Ma, A.J. Ruys, R.S. Mason, P.J. Martin, A. Bendavid, Z. Liu, M. Ionescu, H. Zreiqat, DLC coatings: Effects of physical and chemical properties on biological

response, Biomaterials. 28 (2007) 1620–1628. https://doi.org/10.1016/j.biomaterials.2006.12.010.

[17] V. Milleret, S. Buzzi, P. Gehrig, A. Ziogas, J. Grossmann, K. Schilcher, A.S. Zinkernagel, A. Zucker, M. Ehrbar, Protein adsorption steers blood contact activation on engineered cobalt chromium alloy oxide layers, Acta Biomaterialia. 24 (2015) 343–351. https://doi.org/10.1016/j.actbio.2015.06.020.

[18] N. Bricout, F. Chai, J. Sobocinski, A. Hertault, W. Laure, A. Ung, P. Woisel, J. Lyskawa, N. Blanchemain, Immobilisation of an anti-platelet adhesion and anti-thrombotic drug (EP224283) on polydopamine coated vascular stent promoting anti-thrombogenic properties, Materials Science and Engineering C. 113 (2020). https://doi.org/10.1016/j.msec.2020.110967.

[19] H. Liu, C. Pan, S. Zhou, J. Li, N. Huang, L. Dong, Improving hemocompatibility and accelerating endothelialization of vascular stents by a copper-titanium film, Materials Science and Engineering C. 69 (2016) 1175–1182. https://doi.org/10.1016/j.msec.2016.08.028.

[20] Z. Yang, Q. Tu, J. Wang, X. Lei, T. He, H. Sun, N. Huang, Bioactive Plasma-Polymerized Bipolar Films for Enhanced Endothelial Cell Mobility, Macromolecular Bioscience. 11 (2011) 797–805. https://doi.org/10.1002/mabi.201000474.

[21] B. Sivaraman, R.A. Latour, The relationship between platelet adhesion on surfaces and the structure versus the amount of adsorbed fibrinogen, Biomaterials. 31 (2010) 832–839. https://doi.org/10.1016/j.biomaterials.2009.10.008.

[22] F. Lewis, P. Horny, P. Hale, S. Turgeon, M. Tatoulian, D. Mantovani, Study of the adhesion of thin plasma fluorocarbon coatings resisting plastic deformation for stent applications, Journal of Physics D: Applied Physics. 41 (2008). https://doi.org/10.1088/0022-3727/41/4/045310.

[23] C. Park, S. Kim, H.E. Kim, T.S. Jang, Mechanically stable tantalum coating on a nano-roughened NiTi stent for enhanced radiopacity and biocompatibility, Surface and Coatings Technology. 305 (2016) 139–145. https://doi.org/10.1016/j.surfcoat.2016.08.014.

[24] H.J. Kim, M.W. Moon, K.R. Lee, H.K. Seok, S.H. Han, J.W. Ryu, K.M. Shin, K.H. Oh, Mechanical stability of the diamond-like carbon film on nitinol vascular stents under cyclic loading, Thin Solid Films. 517 (2008) 1146–1150. https://doi.org/10.1016/j.tsf.2008.08.175.

[25] C. Sella, J.C. Martin, J. Lecoeur, A. le Chanu, M.F. Harmand, A. Naji, J.P. Davidas, Biocompatibility and corrosion resistance in biological media of hard ceramic coatings sputter deposited on metal implants, 1991.

[26] D. Hegemann, H. Brunner, C. Oehr, Plasma treatment of polymers for surface and adhesion improvement, in: Nuclear Instruments and Methods in Physics Research, Section B: Beam Interactions with Materials and Atoms, 2003: pp. 281–286. https://doi.org/10.1016/S0168-583X(03)00644-X.

[27] T.S.M. Mui, L.L.G. Silva, V. Prysiazhnyi, K.G. Kostov, Surface modification of aluminium alloys by atmospheric pressure plasma treatments for enhancement of their adhesion properties, Surface and Coatings Technology. 312 (2017) 32–36. https://doi.org/10.1016/j.surfcoat.2016.08.024.

[28] T. Gururaj, R. Subasri, K.R.C.S. Raju, G. Padmanabham, Effect of plasma pretreatment on adhesion and mechanical properties of UV-curable coatings on plastics, Applied Surface Science. 257 (2011) 4360–4364. https://doi.org/10.1016/j.apsusc.2010.12.060.

[29] H.J. Griesser, D. Youxian, A.E. Hughes, T.R. Gengenbach, A.W.H. Mau, Shallow Reorientation in the Surface Dynamics of Plasma-Treated Fluorinated Ethylene Propylene Polymer, 1991. https://pubs.acs.org/sharingguidelines.

[30] K. Tsougeni, N. Vourdas, A. Tserepi, E. Gogolides, C. Cardinaud, Mechanisms of oxygen plasma nanotexturing of organic polymer surfaces: From stable super hydrophilic to super hydrophobic surfaces, Langmuir. 25 (2009) 11748–11759. https://doi.org/10.1021/la901072z.

[31] M. Morra, E. Occhiello, R. Marola, F. Garbassi, P. Humphrey, A.D. Johnsont, On the Aging of Oxygen Plasma-Treated Polydimethylsiloxane Surfaces, 1990.

[32] M. Kihel, S. Sahli, A. Zenasni, P. Raynaud, Y. Segui, Dielectric properties of SiOx like films deposited from TMS/O2 mixture in low pressure microwave plasma, Vacuum. 107 (2014) 264–268. https://doi.org/10.1016/j.vacuum.2014.02.022.

[33] C.S. Yang, Y.H. Yu, H.J. Lee, K.M. Lee, C.K. Choi, The effect of the CH4 plasma treatment on deposited SiOC(-H) films with low dielectric constant prepared by using TMS/O2 PECVD, in: Thin Solid Films, 2005: pp. 150–154. https://doi.org/10.1016/j.tsf.2004.07.019.

[34] J.L.C. Fonseca, D.C. Apperley, J.P.S. Badyal, Plasma Polymerization of Tetramethylsilane, 1993. https://pubs.acs.org/sharingguidelines.

[35] M. Chen, S. Osaki, P.O. Zamora, M. Potekhin, Effect of Nitrogen and Oxygen Incorporated into TMSAA Plasma Coating on Surface-Bound Heparin Activity, (2003).

[36] C.W. Kan, C.H. Kwong, S.P. Ng, Surface modification of polyester synthetic leather with tetramethylsilane by atmospheric pressure plasma, Applied Surface Science. 346 (2015) 270–277. https://doi.org/10.1016/j.apsusc.2015.03.111.

[37] C.M. Weikart, Y. Matsuzawa, L. Winterton, H.K. Yasuda, Evaluation of plasma polymer-coated contact lenses by electrochemical impedance spectroscopy, 2000.

[38] B. O'Brien, W. Carroll, The evolution of cardiovascular stent materials and surfaces in response to clinical drivers: A review, Acta Biomaterialia. 5 (2009) 945–958. https://doi.org/10.1016/j.actbio.2008.11.012.

[39] C. Bayram, A.K. Mizrak, S. Aktürk, H. Kurşaklioğlu, A. Iyisoy, A. Ifran, E.B. Denkbaş, In vitro biocompatibility of plasma-aided surface-modified 316L stainless steel for intracoronary stents, Biomedical Materials. 5 (2010). https://doi.org/10.1088/1748-6041/5/5/055007.

[40] R. di Mundo, F. Palumbo, F. Fracassi, R. D'Agostino, Thin film deposition in capacitively coupled plasmas fed with bis(dimethylamino)-dimethylsilane and oxygen: An FTIR study, Plasma Processes and Polymers. 6 (2009) 506–511. https://doi.org/10.1002/ppap.200800206.

[41] C.S. Yang, Y.H. Yu, H.J. Lee, K.M. Lee, C.K. Choi, The effect of the CH4 plasma treatment on deposited SiOC(-H) films with low dielectric constant prepared by using TMS/O2 PECVD, in: Thin Solid Films, 2005: pp. 150–154. https://doi.org/10.1016/j.tsf.2004.07.019.

[42] M. Chen, S. Osaki, P.O. Zamora, M. Potekhin, Effect of Nitrogen and Oxygen Incorporated into TMSAA Plasma Coating on Surface-Bound Heparin Activity, (2003).

[43] G. Lucovsky, ' J Yang, S.S. Chao, J.E. Tyler, W. Czubatyj, Nitrogen-bonding environments in glow-discharge-deposited a-Si:H films, 1983.

[44] M. Lehocký, H. Drnovská, B. Lapčíková, A.M. Barros-Timmons, T. Trindade, M. Zembala, L. Lapčík, Plasma surface modification of polyethylene, in: Colloids and Surfaces A: Physicochemical and Engineering Aspects, Elsevier, 2003: pp. 125–131. https://doi.org/10.1016/S0927-7757(03)00242-5.

[45] L.M. de Andrade, C. Paternoster, V. Montaño-Machado, G. Barucca, M. Sikora-Jasinska, R. Tolouei, S. Turgeon, D. Mantovani, Surface modification of L605 by oxygen plasma immersion ion implantation for biomedical applications, MRS Communications. 8 (2018) 1404–1412. https://doi.org/10.1557/mrc.2018.202.

[46] Z. Zheng, L. Ren, W. Feng, Z. Zhai, Y. Wang, Surface characterization of polyethylene terephthalate films treated by ammonia low-temperature plasma, Applied Surface Science. 258 (2012) 7207–7212. https://doi.org/10.1016/j.apsusc.2012.04.038.

[47] Y. Chen, Q. Gao, H. Wan, J. Yi, Y. Wei, P. Liu, Surface modification and biocompatible improvement of polystyrene film by Ar, O 2 and Ar + O 2 plasma, Applied Surface Science. 265 (2013) 452–457. https://doi.org/10.1016/j.apsusc.2012.11.027.

[48] A. Kaynak, T. Mehmood, X.J. Dai, K. Magniez, A. Kouzani, Study of radio frequency plasma treatment of PVDF film using Ar, O2 and (Ar + O2) gases for improved polypyrrole adhesion, Materials. 6 (2013) 3482–3493. https://doi.org/10.3390/ma6083482.

[49] S.M. Pawde, K. Deshmukh, Surface characterization of air plasma traeted poly vinylidene fluoride and poly methyl methacrylate films, Polymer Engineering and Science. 49 (2009) 808–818. https://doi.org/10.1002/pen.21319.

[50] G.P. Lopez, D.G. Castner, B.D. Ratner, XPS 0 1s Binding Energies for Polymers Containing Hydroxyl, Ether, Ketone and Ester Groups, 1991.

[51] G.G. Lara, G.F. Andrade, M.F. Cipreste, W.M. da Silva, P.L. Gastelois, D.A. Gomes, M.C. de Miranda, W.A. de Almeida Macedo, M.J. Neves, E.M.B. de Sousa, Protection of normal cells from irradiation bystander effects by silica-flufenamic acid nanoparticles, Journal of Materials Science: Materials in Medicine. 29 (2018). https://doi.org/10.1007/s10856-018-6134-5.

[52] S.R. Darmakkolla, H. Tran, A. Gupta, S.B. Rananavare, A method to derivatize surface silanol groups to Si-alkyl groups in carbon-doped silicon oxides, RSC Advances. 6 (2016) 93219–93230. https://doi.org/10.1039/c6ra20355h.

[53] D.Q. Yang, E. Sacher, A spectroscopic study of CNx formation by the keV N2+ irradiation of highly oriented pyrolytic graphite surfaces, Surface Science. 531 (2003) 185–198. https://doi.org/10.1016/S0039-6028(03)00492-8.

[54] L. Rosenberger, R. Baird, E. McCullen, G. Auner, G. Shreve, XPS analysis of aluminum nitride films deposited by plasma source molecular beam epitaxy, Surface and Interface Analysis. 40 (2008) 1254–1261. https://doi.org/10.1002/sia.2874.

[55] V. Milleret, A. Ziogas, S. Buzzi, R. Heuberger, A. Zucker, M. Ehrbar, Effect of oxide layer modification of CoCr stent alloys on blood activation and endothelial behavior, Journal of Biomedical Materials Research - Part B Applied Biomaterials. 103 (2015) 629–640. https://doi.org/10.1002/jbm.b.33232.

[56] I.B.A. Menown, R. Noad, E.J. Garcia, I. Meredith, The platinum chromium element stent platform: From alloy, to design, to clinical practice, Advances in Therapy. 27 (2010) 129–141. https://doi.org/10.1007/s12325-010-0022-9.

Chapter 4

BIOLOGICAL RESPONSES OF PLASMA NANOCOATINGS

4.1. Abstract

In-stent restenosis and stent thrombosis remain challenges in cardiovascular stent technology. Surface modification is considered an effective method to adjust bio-related responses such as cell proliferation and blood compatibility without changing biomaterial bulk properties. In this study, NH_3/O_2 plasma modified TMS plasma nanocoatings (20-30 nm) were deposited onto L605 cobalt chromium substrates using a low pressure, non-equilibrium plasma glow discharge to selectively improve cell proliferation of endothelial cells (ECs), while inhibiting adhesion and activation of smooth muscle cells (SMCs) and platelets.

Nitric oxide (NO)-like functionality was indirectly detected in ODQ experiments. Bio-related behavior of the plasma nanocoatings was evaluated by MTT assay, cell counting, SEM imaging, protein tests, platelet adhesion tests, and clotting formation tests for porcine coronary artery endothelial cell (PCAEC) and smooth muscle cell (PCASMC) growth. Results revealed that TMS plasma nanocoatings with NH_3/O_2 plasma modification maintained similar level of PCAEC proliferation while PCASMC viability decreased by 73% after 7-day incubation comparing to cells on uncoated L605 surfaces. PCAEC and PCASMC cell co-culture and migration studies were also conducted. In cell co-culture, the cell ratio of PCAEC/PCASMC on NH_3/O_2 plasma modified TMS plasma nanocoatings was 1.5-fold higher than that of uncoated L605. Migration test showed comparable PCAEC

migration distance for uncoated L605 and NH_3/O_2 plasma modified TMS plasma nanocoatings; however, PCASMC migration distance reduced 6-fold on TMS plasma nanocoatings without NH_3/O_2 plasma modification. Lower adhered platelets distribution (70% decrease) and less platelet activation were found on the NH_3/O_2 plasma modified TMS plasma nanocoating surfaces comparing to uncoated L605. Thus, these in vitro test results indicate that both restenosis and thrombosis might be prevented strongly by TMS plasma nanocoatings with NH_3/O_2 modification.

4.2. Introduction

In-stent restenosis is one of the most common problems resulting in stent failure [1]. Typically, stent implantation causes endothelial damage, leading to SMC proliferation [2]. The lack of endothelium and inflammatory responses in vessel walls are thought to encourage SMC proliferation and migration, resulting in high restenosis rates of 30-50% [3–5]. Thrombosis – another crucial stent complication because of the associated incidences of deaths (~20% - 40%) [6,7]- involves a series of biochemical process like platelet distribution, aggregation, and coagulation [2,8]. Endothelium is the natural barrier to prevent thrombosis and the interaction of cells with biomaterials is an important key for successful long-term implantation of medical devices [9]. Thus, complete and rapid reendothelialization on vessel wall surface presents the most advantageous way to prevent in-stent restenosis and thrombosis. In addition to functional surfaces promoting EC while inhibiting SMC, the anti-platelet and anti-thrombogenic ability is also important because platelet attachment and activation are primary indicators of lack of hemo-compatibility to assess blood-containing biomaterials.

Protein adsorption is one of the fundamental aspects of hemo-compatibility. In fact, protein adsorption is the first event happened when blood contacts to biomaterials [10,11].

Platelets consume and block blood flow, leading to stent failure and other complications in patients [12]. Cells and other components in the blood diffuse much more slowly than proteins and so arrive on a surface already partly or fully coated with adsorbed proteins. Typically, two types of protein - albumin and fibrinogen - are usually taken into consideration. Albumin is regarded as the most abundant protein in human blood plasma and one of the first proteins to adsorb to the biomaterial surfaces [13–15]. Albumin is considered as “non-adhesive” to platelets due to the absence of binding sites for platelet receptors [16], resulting in greatly reduced coagulation and thrombosis. Fibrinogen – a common blood protein - is thought to be a biochemical marker in platelet adhesion, aggregation process, and thrombosis because of its binding to platelets [10,17–19]. Fibrinogen plays a role as a molecular bridge for the aggregation of platelets [20] or serves as a mediator layer between surfaces and platelets [16].

Protein adsorption can be affected by surface roughness, surface chemistry and molecular structure (surface charge, surface energy, surface contact angle) [12,13]. Effect of surface wettability to protein adsorption was reported in many studies. The more hydrophobic the surface, the greater the adsorption of protein [12,16]. Proteins tends to adsorb more strongly to non-polar groups, and charged surfaces [21]. Additionally, fibrinogen affinity is higher with increasing hydrophobicity [23]. Surface chemistry such as the presence of CH_3 and OH monolayers can promote the fibrinogen attachment [12]. Albumin molecules adsorb to hydrophilic surfaces through hydrogen bonding and interact more strongly than that on hydrophobic surfaces [22]. Protein concentration is another factor affecting protein adsorption.

Effects of fibrinogen conformation to platelet adhesion is controversial and inconsistent. It remains controversial whether platelet adhesion is in response to the adsorbed amount or the adsorbed conformation of fibrinogen [23]. Studies have provided

definitive proof that the conformation of adsorbed fibrinogen is critical determinant of platelet adhesion and activation because conformation determines that whether the platelet binding sides will be exposed or not [14,19]. It is reported that platelets do not adhere to native fibrinogen in blood stream, they interact with absorbed fibrinogen whose conformation changes at biomaterial surfaces. There are two steps to protein adsorption: First, protein molecules adhere to the surface; then they rearrange on that surface [16]. Unfolding fibrinogen can attach to a biomaterial surface by side-on binding, leading to fewer fibrinogen molecules covering the surface. Folded fibrinogen adheres to the surface by end-on binding, leading to a larger amount of fibrinogen molecules adhering to the surface and higher surface coverage. However, the unfolded protein conformation was proven to adhere more platelets than folded state [16]. Fibrinogen underwent a greater degree of unfolding with increasing surface hydrophobicity [12,24]. This implies that the folded conformation of adsorbed fibrinogen on hydrophilic surface with minimal conformation changes has no affinity to attach and activate platelets.

It is well established in literature review that NO-releasing materials are anti-thrombotic [25]. NO may change fibrinogen structure and conformation. The existence of NO can increase the amount of adsorbed fibrinogen, but decrease the adhered platelets on biomaterials [12]. The increase of fibrinogen was not enough to interfere with the anti-platelet effects of NO [25]. Bioactive coatings containing nitrogen (N) and oxygen (O) functional groups can be a promising solution to surface modification [26,27]. NO is a gaseous signaling molecule produced in vascular endothelial layers. It is evident in acceleration of reendothelialization, prevention of thrombosis, inhibition of SMCs proliferation and attachment, and minimization of leukocyte activation [2,28,29]**.** It should be emphasized that platelet attachment is a normal response to vascular trauma and a fundamental step in halting blood loss. Furthermore, circulating leukocytes adhere to the

vasculature in order to promote tissue repair. Unfortunately, platelet/leukocyte interactions become more debilitating in the presence of vascular implants. Extensive platelet and leukocyte aggregates form in response to the vascular irritation caused by stents. The platelet/leukocyte complexes result in thrombosis potentially resulting in embolization and myocardial infarction. Prevent platelet adhesion and activation by modifying surface chemistry and properties [12].

EC adherence to the SMC layer is critical in the formation of a proper intimal layer. ECs comprise the normal luminal lining of the blood vessel and block the formation of blood clots on the arterial surface. A disruption to the endothelial lining could lead to vasoconstriction and potential tissue death. Acceleration of covering the stent surface by ECs can reduce the risk of thrombosis. Moreover, ECs have the ability to regulate platelet aggregation and SMC proliferation. SMCs are well established for the cause of restenosis by hyperplasia, resulting in implantation failure. Endothelialization represents the most effective way to inhibit stenting complications [24].

Hydrophilicity is one of key factors involved in the biocompatibility of stents. The adsorption of proteins onto biomaterials plays an important role because within a second of implantation, protein adsorption onto the implanted materials will occur [12]. The more hydrophobic the surface, the greater extent of protein adsorption [10]. Albumin is generally believed to greatly reduce the acute inflammatory response and minimize adhesion and aggregation of platelets, thus reducing the possibility of thrombus formation [12]. Albumin has a higher affinity for hydrophilic surface, and in contrast, fibrinogen adsorption increases with increasing surface hydrophobicity. Diamond-like carbon (DLC) coatings with contact angle lower than 65° showed a significant enhancement in cell viability and albumin to fibrinogen ratio [11]. Hydrophilic coatings on nickel titanium inhibited a significant decrease in the number of adhered platelets compared to uncoated surfaces

[13]. A polydopamine coatings on cobalt chromium stents were hydrophilic surfaces and showed a reduction in platelet activation and adhesion [14]. A hydrophilic copper-titanium film on 316L stainless steel exhibited a good hemocompatibility and biocompatibility in vitro [15]. Hydrophilic surface modification of CoCr L605 alloys using atmospheric pressure plasma jet improved the biocompatibility by accelerating endothelial cell migration and proliferation compared to untreated samples [16]. Therefore, the increased hydrophilicity of the surface is advantageous against thrombus formation.

The aim of this study is to evaluate blood and bio compatibility of plasma nanocoatings. Cell culture, cell migration, protein adsorption, platelet adhesion and activation were evaluated.

4.3. Materials and Methods

4.3.1. Sample preparation

See Chapter 3 – section 3.3.1 in page 30.

4.3.2. Plasma nanocoating preparation

See Chapter 3 – section 3.3.2 in page 30.

4.3.3. Porcine coronary artery smooth muscle and endothelial cell cultures

Porcine coronary artery endothelial cells (PCAECs) and porcine coronary artery smooth muscle cells (PCASMCs) were provided as gifts from Biomedical Sciences Dept., University of Missouri, Columbia, MO. The PCAECs and PCASMCs were re-suspended and cultured in DMEM (1X) and DMEM/F12 growth media, respectively. PCAECs and PCASMCs were grown in T-75 flasks in 15 mL respective growth media. Cells were grown in a humidified atmosphere with 5% CO_2 at 37°C. Culture media were replaced every 2

days for both PCASMCs and PCAECs until the cells reached a confluence of 70%. Cells were detached from the culture flasks with 0.25 wt.% trypsin/EDTA (Sigma-Aldrich, St. Louis, MO, USA) and counted with a hemo-cytometer. PCAEC and PCASMC concentrations were adjusted to 10,000 cells/mL. Either PCAEC or PCASMC were seeded onto individual 15-mm-diameter coupons of uncoated L605, TMS, and TMS+NH_3/O_2 plasma nanocoatings at passages 7 or 8. The coupons were UV-sterilized for 15 min per side prior to cell culture. Each cell line was cultured with coupons in 24-well cell-culture plates up to 7 days. Cell proliferation was evaluated by microscopic observation and quantitatively in two methods: measuring the metabolic activity of the cells by MTT assay and cell counting with an automated cell counter.

4.3.4. Cell viability

Relative viable cell densities were obtained through MTT assay. Following time points of 1-, 3-, 7-day cell culture, the seeded coupons were incubated in 3-(4, 5-dimethylthiazol-2-yl)-2, 5-diphenyltetrazolium (MTT) solution (0.5 mg/mL, 37°C, 5% CO_2) for 4h. Following incubation, the top liquid medium was removed, leaving the purple formazan crystal undisturbed. The formazan crystals were dissolved in DMSO, and the optical absorbance at the wavelength of 570 nm was measured using a micro plate reader. Data are from triplicate samples for both PCAEC and PCASMC-seeded coupons.

For cell counting method, after 1-day, 3-day, and 7-day culture, cells were rinsed 2 times with DPBS, then immersed for 10 min in incubator at 37°C in 0.25 wt.% Trypsin-EDTA solution (Sigma-Aldrich, St. Louis, MO, USA) diluted with DPBS. Trypsin was neutralized by mixing with media containing FBS and cells were stained by Trypan blue (Sigma-Aldrich, St. Louis, MO, USA) to discriminate viable and non-viable cells. Cell

proliferation was determined by a Countess automated cell counter (SPW Industrial, Laguna Hills, CA, USA) at different time points.

4.3.5. Cell morphologies

PCASMCs or PCAECs were seeded on uncoated L605 and plasma nanocoated samples. Each cell type was grown for 1 day, 3 days, and 7 days. At respective sampling day, cells were rinsed one time with DPBS and fixed by sodium cacodylate (2% glutaraldehyde and 2% paraformaldehyde) for 30 min in room temperature. Then the cells were dehydrated in a graded series of ethanol (50%, 60%, 70%, 80%, 90% and 100%) for 10 min each and dried at room temperature in ambient air. The cell attachment and morphology were examined by an FEI Quanta 600 FEG Environmental SEM (FEI Company, Hillsboro, Oregon, USA).

4.3.6. NO-releasing detection by ODQ solution

TMS+NH_3/O_2 plasma nanocoated circular coupons (diameter = 15 mm) were UV-sterilized for 15 min per side in 24-well plates prior to the test. PCASMCs were suspended and cultured in 1H- [1,2,4] oxadiazolo[4,3-a] quinoxalin-1-one (ODQ) treated and non-treated SMC culture medium. ODQ irreversibly binds guanylate cyclase within smooth muscle cells. ODQ binding occurs at a heme group that binds NO. When NO binds, cGMP is produced and smooth muscle cells adopt a contractile phenotype and no longer proliferate. ODQ binding reduces cGMP production, causing the smooth muscle cells to proliferate. ODQ was mixed with DMSO to a final ODQ concentration of 20mM. Stock ODQ is diluted 1/1000 in complete smooth muscle cell culture medium (ODQ solution/culture medium). The same volume of DMSO was added to DMEM/F12 culture medium as non-treated ODQ culture medium. The 24-well plates were put inside an

incubator containing humidified atmosphere with 5% CO2 at 37°C. PCASMC proliferation was determined quantitatively by MTT assay after 1- and 3-day incubation.

4.3.7. Cell co-culture

The co-culture of PCASMCs and PCAECs was conducted according to the protocol described by Qiu et al. [30]. The PCASMCs and PCAECs were separately grown to 70-80% confluence and isolated by 0.25% trypsin-EDTA solution. When cells were completely detached, cell suspensions were centrifuged for 5 min at 1000 rpm, then re-suspended in 1 mL of fresh culture medium without fetal bovine serum (FBS). In order to discriminate PCASMCs and PCAECs on co-culture samples clearly, two different colors (orange and green) were utilized for cell trackers in co-culture experiments. The orange tracker (CMTMR) and green tracker (CMFDA) (Invitrogen, Waltham, MA, USA) were used for PCASMCs and PCAECs, respectively. Cell trackers CMTMR or CMFDA were added to 1 mL PCASMCs and 1 mL PCAECs respectively, with ratio 1:1000, and incubated for 1h at 37°C and 5% CO_2 humidified. After incubation, cells were centrifuged and re-suspended in PBS twice. After the last centrifugation, cells were re-suspended in DMEM culture medium (Gibco, USA) containing 4.5 g/L glucose, 4.5 g/L L-glutamine, 10% FBS, 100 U/mL penicillin, and 100 μg/mL streptomycin. Cells were counted by using a hemacytometer. Cells were seeded onto coupons placed inside 24-well plates at concentrations of 25,000 cells/mL for both PCAECs and PCASMCs. Culture media volume inside wells was 1 mL. The competitive cell proliferation and adhesion was examined by using the Zeiss Axiovert 200M inverted fluorescence microscope after 1 day and 3 days. Cell numbers were determined by ImageJ software. At least 5 images with 10X magnification were taken on each sample and results were averaged.

4.3.8. Cell migration

Cell migration tests utilized L-shaped L605 coupons as substrates (**Figure 4.1**). Horizontal and vertical parts of the L-shaped samples have the same dimensions (10 mm x 10 mm x 0.4 mm). The horizontal parts of all samples were uncoated L605 materials. During coating process, horizontal parts were covered by other uncoated L605 wafers in order to block surface modification. The vertical parts coated with TMS, TMS+NH_3/O_2 plasma nanocoatings correspond to TMS and TMS+NH_3/O_2 plasma nanocoated L-shaped samples, respectively. Uncoated L605 L-shaped sample served as the control. All samples were placed in 24-well cell culture plates with uncoated L605 sides attaching to the bottom of the plate wells. Cells were seeded at densities of 50,000 cells/mL and cultured for 24 h to ensure the formation of a confluent cell layer. After 24 h, culture media was replaced with fresh media. After 7 days, samples were washed with PBS and fixed with sodium cacodylate (2% glutaraldehyde and 2% paraformaldehyde) for 30 min at room temperature. Cell migration over the treated vertical portion was inspected by an FEI Quanta 600 FEG Environmental SEM (FEI Company, Hillsboro, Oregon, USA).

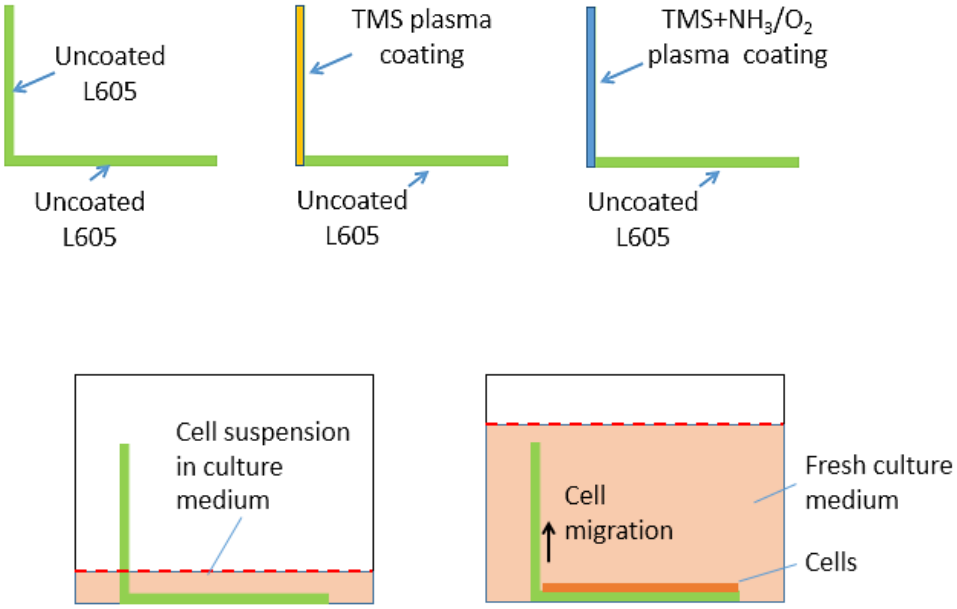

Figure 4.1: Schematic diagram for cell migration test.

4.3.9. Protein test

Protein adsorption on uncoated L605 and plasma nanocoated coupons was determined by an enzyme-linked immunosorbent assay (ELISA) approach. A test group are metal coupons (10 mm x 10 mm) of three conditions: uncoated L605, TMS plasma nanocoatings with and without NH_3/O_2 post-treatment, covered by 20% (vol/vol) human plasma in PBS at 37°C for one night. To evaluate fibrinogen adsorption, a blank is another group of coupons with those three nanocoating conditions, overlaid with 1% bovine serum albumin (BSA). To determine albumin adsorption, another blank group of coupons with those three nanocoating conditions was coated with 5% low-fat milk.

All coupons in the test group were washed 3 times with PBS. Then, the solution (the primary antibody) of PBS including a 1:1500 goat anti-human fibrinogen dilution (Sigma-Aldrich, St. Louis, MO, USA) and 1% BSA was used to incubate the all coupons of the test group. The test group's coupons were immersed into solution of low-fat milk (5%) and anti-human albumin of rabbit (the primary antibody) (Cell Sig-naling Technology, Danvers, MA, USA) for albumin adsorption measurement. Coupons in the blank group were submerged in triplicate in the corresponding antibody. After incubated in test group and blank groups (1% BSA group and 5% low-fat milk group) at 37°C for 1 h, all coupons was cleaned with PBS. Those coupons were incubated for 1h in a fresh 24-well plate containing PBS-BSA or PBS-milk (consisting of 1:250 dilutions of the respective horseradish peroxidase (HRP)-conjugated polyclonal IgG), then washed gently with PBS.

At room temperature, the chromogenic substrate 2, 2=-azinobis(3-ethylbenzo-thiazoline-6-sulfinic acid) (ABTS; Thermo Fisher Scientific Inc., Rockford, IL, USA) incubates coupons for 10 min. A micro-reader was used to measure absorbance

(wavelength of 410 nm). To calibrate, subtract the average absorbance of respective 1% BSA blank group from the final absorbance of either fibrinogen. Similarly, subtract the average absorbance of the low-fat milk (5%) of blank group from the final albumin absorbance.

4.3.10. Platelet adhesion- Static condition

An *in vitro* model to test the platelet adhesion onto uncoated L605, TMS, and TMS+NH_3/O_2 samples was performed. Platelet attachment on coupon surfaces was observed by SEM. All steps were performed under sterile conditions. Porcine whole blood containing sodium (Na) heparin from Innovative Research (Novi, MI, USA) was centrifuged (200 g, 15 min, 25°C) to get platelet rich plasma (PRP). Samples were then incubated in 24-well plates in 1 mL blood for 2 h at 37°C. After incubation, samples were rinsed in PBS to get rid of non-adherent cells. For SEM analyses, specimens were fixed with sodium cacodylate (2% glutaraldehyde and 2% paraformaldehyde) for 30 min at room temperature and dried in an ethanol gradient, starting from 50% ethanol to 100%. Samples were kept in each ethanol dilution for 10 min followed by drying at room temperature.

4.3.11. Clotting assay

Porcine whole blood from Innovative Research (Novi, MI, USA) contained Na heparin to slow but not stop clotting. All steps were performed under sterile conditions. The blood (3 mL) and DMEM/F12 (12 mL) were warmed up separately to 37°C, then add the DMEM/F12 medium amount to the blood to get blood dilution of 1:4 ratio. Samples (3 uncoated L605 coupons, 3 TMS plasma nanocoated coupons, and 3 TMS+NH_3/O_2 plasma nanocoated coupons) were placed in a 24-well plate and sterilized under UV for 15 min each side. 1 mL of the blood and DMEM/F12 mixture was added into each well containing

coupon sample. The 24-well plate was placed on a platform shaker (120 cycles/min) inside a 37°C incubator for 1 h. After incubation, samples were rinsed well with PBS twice, and transferred to a new 24-well plate. Samples were fixed with buffer formalin at room temperature for 30 min and stained with crystal violet (CV) at room temperature for 10 min. The CV solution was made of 0.05 g CV powder, 2 mL ethanol, and DI water to get final solution of 50 mL total. The CV can detect all clotted material including fibrin and platelets. The stained specimens were rinsed thoroughly in water and PBS. Aliquot 1 mL glacial acid mixture (acid and DI water with 1:10 ratio) to each well containing samples and put the plate onto the shaker for 10 min. The absorbance was monitored at 595 nm.

4.3.12. Statistical analysis

Results were all expressed as mean ± standard deviation (SD) of the mean for each treatment group. Each experiment was repeated independently three times, if not indicated otherwise. Data were analyzed using one-way ANOVA. A *p*-value of 0.05 or less was considered significant.

4.4. Results and Discussion

4.4.1. Nitric oxide (NO) releasing

Direct NO release from the nanocoating is difficult to ascertain. NO is likely present at nano-molar concentrations, making it difficult to measure NO with commercially available Griess kits. We sought to test the potential effects of NO by blocking its cell signaling pathway in vitro. The NO impact to cardiovascular system is mainly related to the activation of soluble guanylate cyclase (sGC) by NO [29]. As NO binds and activates sGC, cGMP is synthesized from GTP, which leads to relaxation processes including prevention of platelet adhesion and activation and reduced SMC proliferation. ODQ - a

NO-sensitive guanylyl cyclase inhibitor – has high affinity to sGC which is the only known receptor for NO. When ODQ was added to culture media, ODQ binds to sGC, reducing sGC receptors available for NO binding. The activation of sGC by NO is minimized, decreasing NO-cGMP signaling resulting in smooth muscle cell proliferation. As shown in **Figure 4.2 a**, at day 1 the effect of ODQ was not pronounced, leading to similar MTT absorbance for samples immersed in treated and non-treated culture medium. At day 3, the viability level of PCASMCs on TMS+NH_3/O_2 plasma nanocoatings incubated in culture medium with ODQ solution was 95% higher ($p < 0.05$) compared to non-ODQ sample, indicating the effect of ODQ solution on modified plasma nanocoatings. It can be explained that ODQ solution bound to sGC and hindered NO-cGMP signaling, causing more PCASMC proliferation. Conversely, for the sample incubated in non-treated ODQ culture medium, NO activated sGC and supported NO-cGMP, preventing PCASMC growth. Uncoated L605 samples with and without ODQ treatment showed indistinguishable level of SMC viability, indicating the absence of interaction between NO and sGC. In **Figure 4.2 a**, SEM images of SMC attachment on uncoated L605 and plasma nanocoated samples under different ODQ treatment were shown. In agreement with MTT absorbance graph, SMC imaging reveals almost identical proliferation for uncoated L605 with and without ODQ treatment, whereas ODQ non-treated TMS+NH_3/O_2 plasma nanocoated samples show fewer cells than ODQ-treated nanocoated samples.

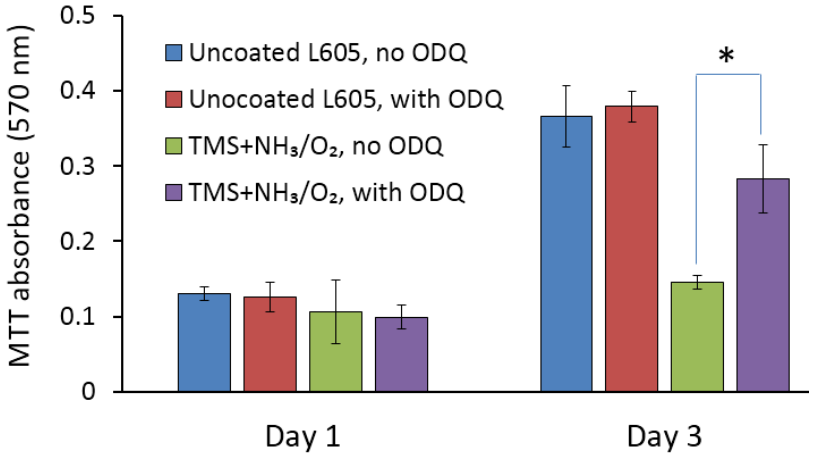

a)

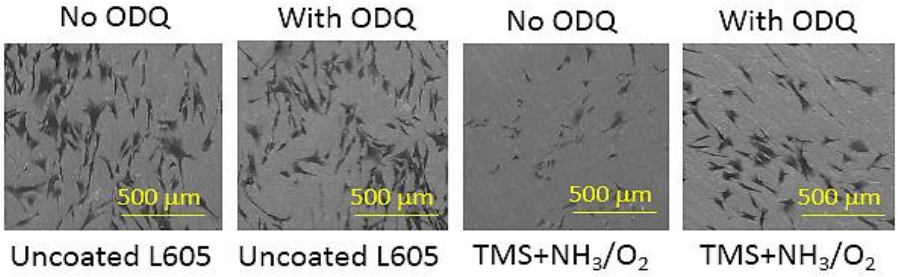

b)

Figure 4.2: a) SMC proliferation by MTT assay at day 1 and day 3 incubation on uncoated L605 and TMS+NH_3/O_2 plasma nanocoated coupons with and without ODQ treatment. Plotted values are means ±SD (n=3), *p < 0. 05; b) Imaging of SMC proliferation.

4.4.2. PCAEC and PCASMC adhesion and proliferation

ECs and SMCs, two main cell types in coronary vasculature, play important roles in restenosis. The proliferation and migration of SMCs promote restenosis, but endothelial coverage is essential to inhibit restenosis. Two methods of cell proliferation evaluation performed in this research (MTT assay and cell counting) convey equivalent results of cell behavior on uncoated L605 and plasma nanocoated surfaces.

Figure 4.3 shows the proliferation of PCAECs and PCASMCs cultured for 1 day, 3 days and 7 days. In **Figure 4.3 a**, MTT absorbance for PCAECs on uncoated L605 surface was significantly higher than that of plasma nanocoated ones ($p < 0.005$) at day 1 and day 3. However, after 7-day incubation, PCAEC viability levels on uncoated L605 and TMS+NH_3/O_2 plasma coated surfaces were comparable. TMS plasma nanocoating without NH_3/O_2 plasma modification was not favorable for PCAEC proliferation due to obviously low MTT absorbance ($p < 0.005$), especially at day 7 of cell culture. In **Figure 4.3 b**, PCASMCs on uncoated L605 samples were roughly doubled after 7-day incubation, while they were not supported by plasma nanocoated surfaces. PCASMCs dominated on uncoated L605 at all time-points ($p < 0.005$). At day 1, the difference in PCASMC viability level on uncoated L605 and plasma nanocoating surfaces was approximately 55% ($p < 0.005$). At day 7, PCASMCs viability difference was 73% ($p < 0.005$) on TMS+NH_3/O_2 plasma nanocoating surfaces compared to uncoated L605. These results suggested that TMS+NH_3/O_2 plasma nanocoating was the best choice in enhancing PCAECs and inhibiting PCASMCs, potentially minimizing in-stent restenosis.

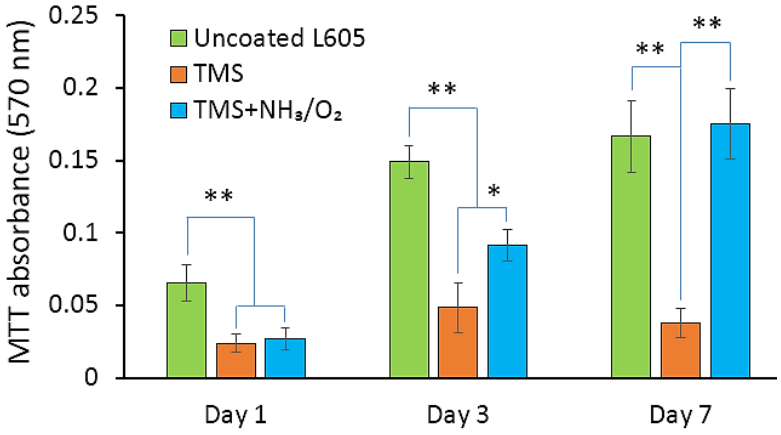

a)

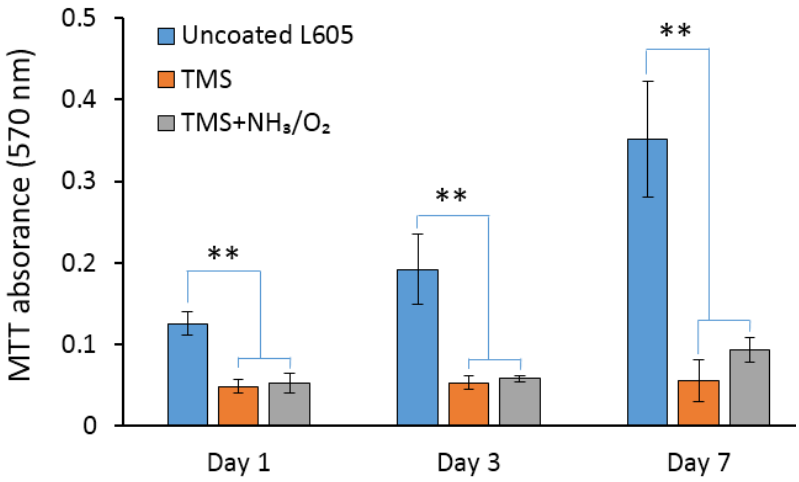

b)

Figure 4.3: Cell proliferation by MTT assay for a) ECs and b) SMCs after 1-, 3-, 7-day incubation on uncoated L605, TMS, and TMS+ NH_3/O_2 plasma nanocoated coupons. Plotted values are means ±SD (n=3), *p < 0. 05 and **p < 0.005.

Figure 4.4 show absolute cell counts for PCAECs and PCASMCs after 3-, 5-, 7-day incubation. At all three time points, PCAECs counted on uncoated L605 surfaces and TMS+NH_3/O_2 plasma nanocoatings were comparable (p > 0.05). The PCAEC amount found on TMS plasma nanocoatings was significantly lower than that for uncoated L605 and TMS+NH_3/O_2 surfaces (p < 0.005), indicating that TMS is not suitable for PCAEC proliferation. PCASMC cell counts detected on uncoated L605 surfaces increase rapidly after each time point compared to those on plasma nanocoatings (p < 0.005). After day 7, PCASMCs identified on TMS+NH_3/O_2 plasma nanocoated surfaces were reduced about 62% compared to uncoated L605 samples. Similarly, to PCAECs, PCASMC proliferation on surfaces of TMS plasma nanocoatings without modification indicated low growth level. Therefore, TMS+NH_3/O_2 plasma nanocoatings may be suitable candidate materials for preventing restenosis due to PCASMC inhibition, but poor endothelialization is a big problem for TMS plasma nanocoatings.

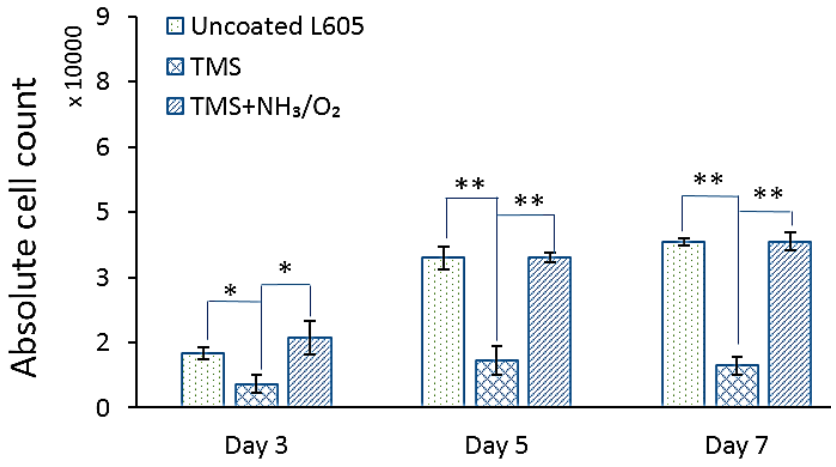

a)

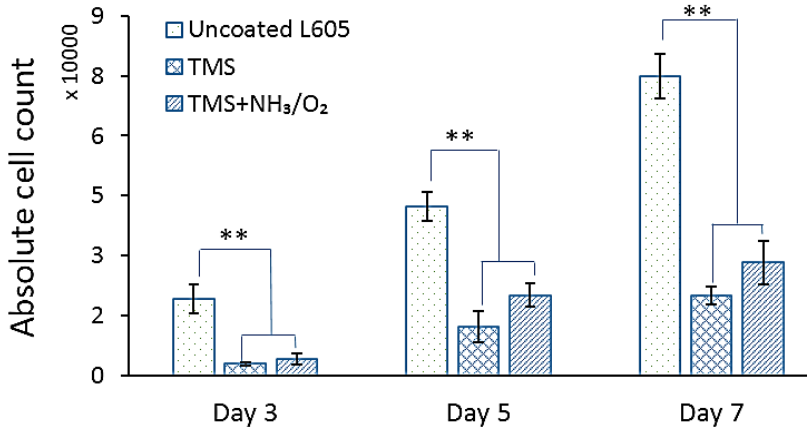

b)

Figure 4.4: Absolute cell counts after 1, 3, 7 days on uncoated L605, TMS, and TMS+ NH_3/O_2 plasma nanocoated coupons, performed with automated cell counting: a) PCAECs, b) PCASMCs. Plotted values are means ±SD (n=3), *p < 0. 05, **p < 0.005.

The growth of PACECs and PACSMCs were observed by SEM images as shown in **Figure 4.5**. In agreement with results indicated in **Figure 4.4** and **4.3**, uncoated L605 surfaces were favorable for both PCAECs and PCASMCs, while TMS+NH_3/O_2 plasma nanocoatings supported PCAECs and prevented PCASMC proliferation. SEM images show that cells spread and grow robustly on uncoated L605 surface. Compared to PCAEC proliferation on uncoated L605 surfaces, TMS+NH_3/O_2 plasma nanocoating showed less

density at day 1, but became more uniform at day 3 and very dense at day 7. PCAEC cell morphology indicated that after 1 and 3 days, PCAEC were spindle-like and spread but not very flat on TMS+NH_3/O_2 plasma nanocoating, but after 7 days they became more confluent, elongated and interacted with each other, suggesting TMS+NH_3/O_2 substrate is favorable for the attachment and growth of PCAECs. From day 1 to day 7 of cell culture, very few PCASMC cells were observed on TMS+NH_3/O_2 plasma nanocoating, exhibiting a remarkable inhibitory effect on SMCs adhesion compared to that of uncoated L605. TMS plasma nanocoating without modification shows lowest PCASMC amount, but it is not beneficial for stent application due to the very low PCAEC growth. These results reinforce the MTT assay that TMS+NH_3/O_2 plasma nanocoating promotes PCAEC growth while preventing PCASMC attachment and proliferation.

In **Figure 4.5 c**, cell morphologies were investigated with SEM images at high magnification. PCAECs look healthy on both uncoated L605 and TMS+NH_3/O_2 plasma nanocoating – cells spread and flatten in multi-angular shapes with visible filopodia to form bridges among cells. PCASMCs on uncoated L605 show robust state with spreading and directional cells, implying the PCASMC are migrating along the bare metal. In contrast, a few PCASMCs were found on TMS+NH_3/O_2 plasma nanocoating, yet they were mostly rounded and showed poor migration. PCAECs and PCASMCs detected on TMS plasma nanocoating without plasma post-treatment showed smaller and round shape, indicating TMS plasma nanocoatings are not favorable surfaces for cells.

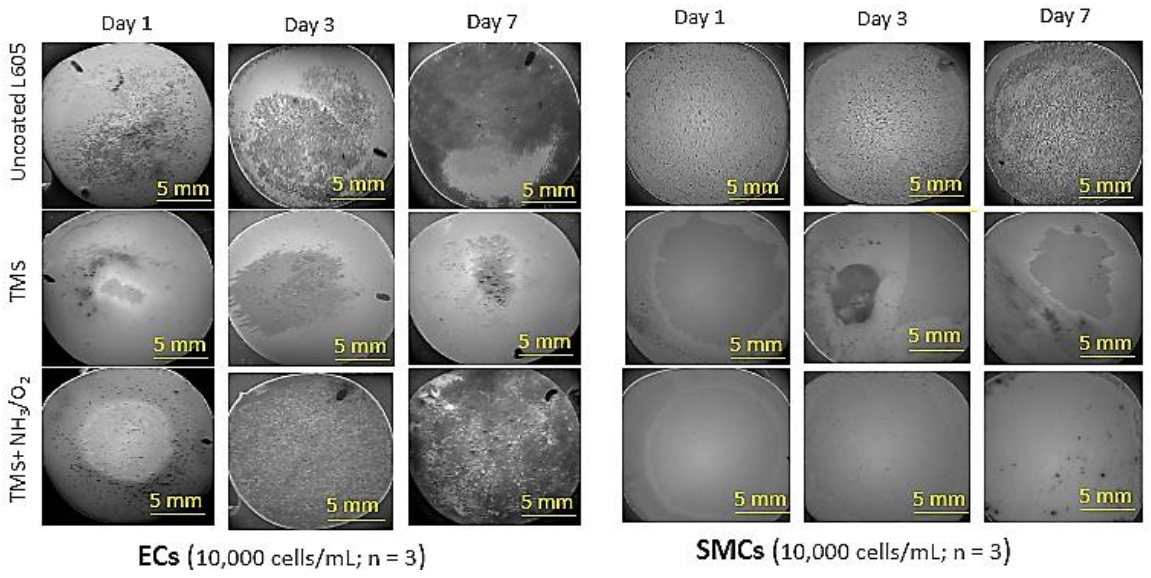
Day 1
Day 3
Day 7
Day 1
Day 3
Day 7
Uncoated L605
TMS
TMS+ NH3/O2
5 mm
ECs (10,000 cells/mL; n = 3)
SMCs (10,000 cells/mL; n = 3)

a)

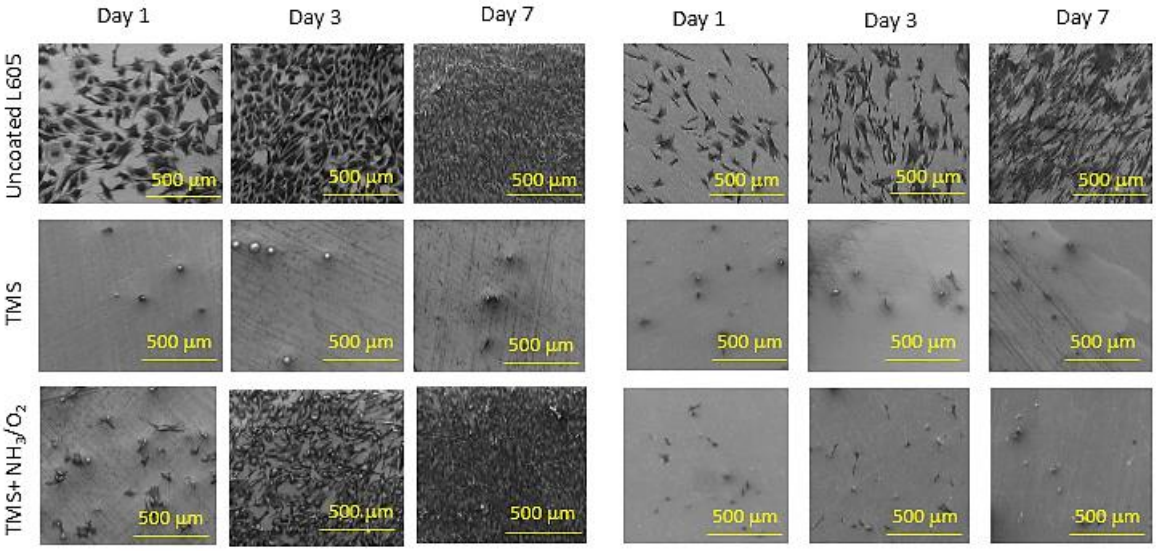
Day 1
Day 3
Day 7
Day 1
Day 3
Day 7
Uncoated L605
TMS
TMS+ NH3/O2
500 µm

b)

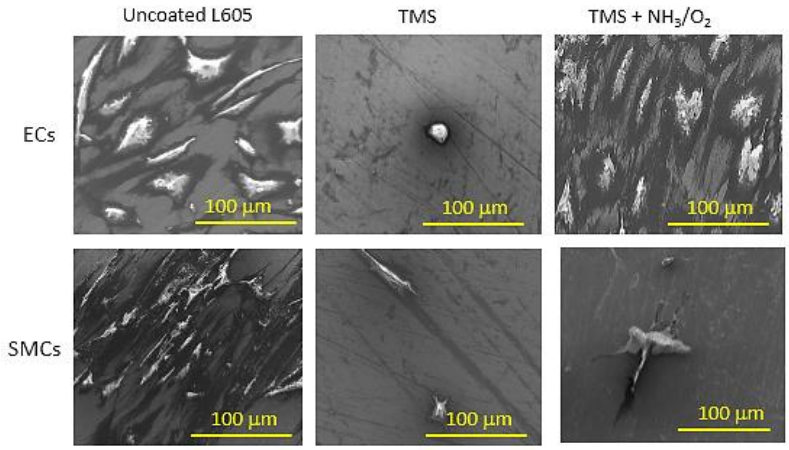

c)

Figure 4.5: EC and SMC attachment and proliferation onto uncoated L605, TMS, TMS+NH_3/O_2 plasma nanocoatings after 1-, 3-, 7-day incubation: a) At low magnification (scale bar = 5 mm), b) at higher magnification (scale bar = 500 μm), c) Cell morphology (scale bar = 100 μm).

After stenting implantation, SMCs and ECs compete directly on stent surfaces. The interaction between PCAECs and PCASMCs in the coronary arteries plays a significant role in vascular wall remodeling and then in-stent restenosis. **Figure 4.6** displays fluorescent images and the quantification levels of adhered PCAECs and PCASMCs in cell co-culture after 1 day and 3 days on uncoated L605 and plasma nanocoated coupons. Over time, PCAEC proliferation and attachment were enhanced compared to PCASMC. Particularly, the cell ratio of PCAECs over PCASMCs on TMS+NH_3/O_2 plasma nanocoatings was the highest with nearly 55% increase at day 1 ($p < 0.005$) and day 3 ($p < 0.05$) than those of uncoated L605 surfaces. This ratio enhancement demonstrates the outstanding selectivity of TMS+NH_3/O_2 for PCAEC growth. In accordance with the MTT results and SEM images for PCAECs and PCASMCs, TMS alone did not support attachment of PCASMCs and PCAECs.

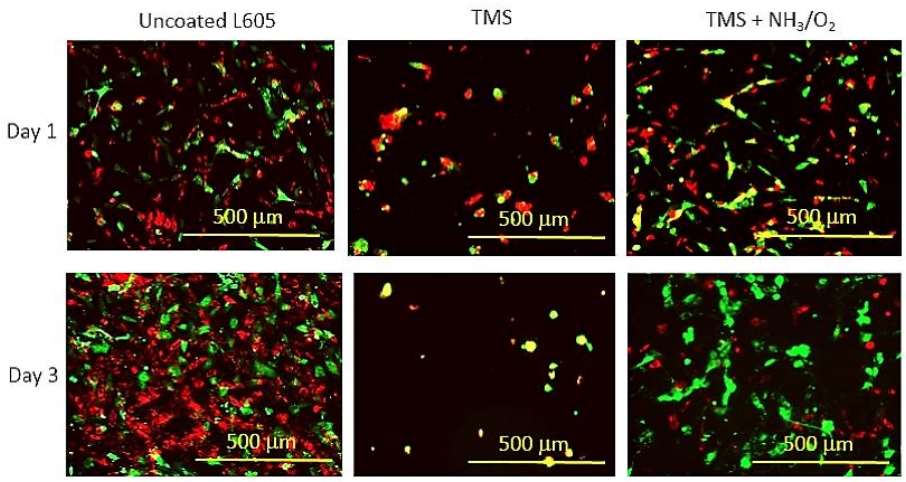

a)

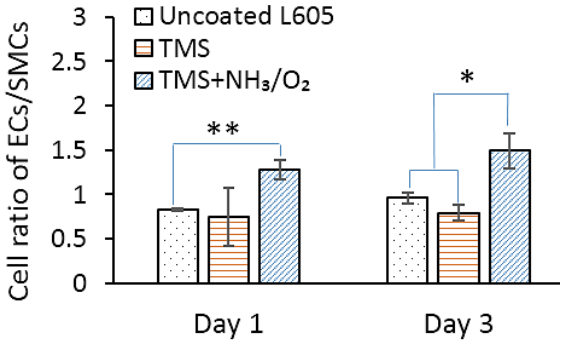

b)

Figure 4.6: a) Fluorescent micrographs showing ECs and SMCs proliferation and adhesion onto uncoated L605, TMS, TMS+NH_3/O_2 plasma nanocoatings after 1 and 3 days. b) EC/SMC cell ratio graph determined from the fluorescent micrographs by ImageJ. Indicating values are mean ± SD (n = 3), *$p < 0.05$, **$p < 0.005$.

Upon adhesion to a surface, it is important for PCAECs to be able to migrate and proliferate because this is necessary for the formation of healthy endothelium. However, the migration of PCASMCs to a stent may cause in-stent restenosis event; thus, different concerns were raised for the migration behaviors of PCAECs and PCASMCs. The migration of PCASMCs and PCAECs are shown in **Figure 4.7**. Migration distances of

PCAECs on uncoated L605 and TMS + NH_3/O_2 plasma nanocoated coupons were almost the same at 1.35 mm after 7 days. However, significant difference in migration distances of PCASMCs were observed on TMS + NH_3/O_2 plasma nanocoated and uncoated L605 samples. In particular, migration distance of SMCs on TMS+NH_3/O_2 plasma nanocoatings decreased nearly 8.5-fold than that on uncoated L605 surface ($p < 0.005$). PCASMC and PCAEC migration distance on TMS plasma nanocoating was much shorter than those on uncoated L605 and TMS+NH_3/O_2 ($p < 0.005$), confirming that TMS plasma coating is a non-favorable cell supporting surface as indicated in aforementioned MTT assay and SEM images.

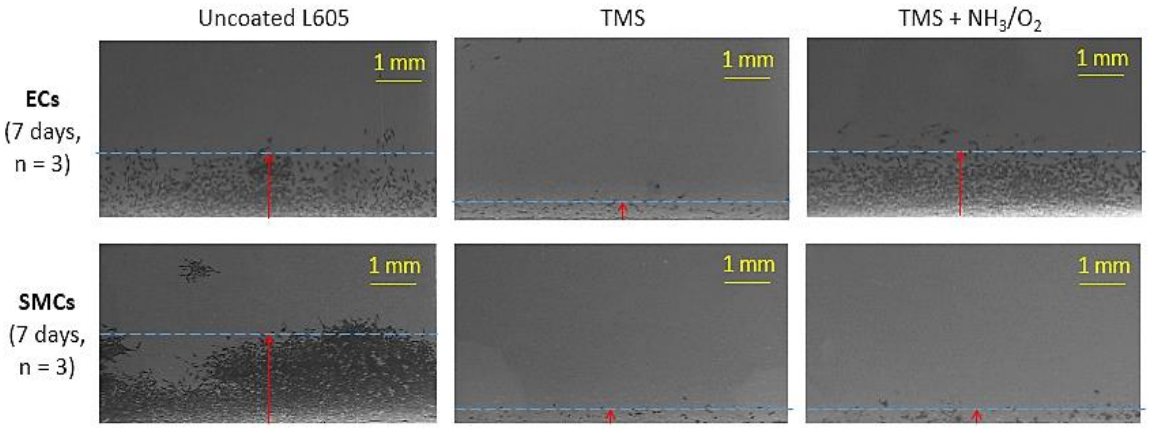

a)

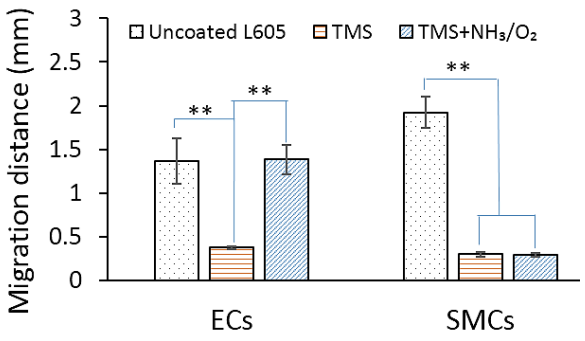

b)

Figure 4.7: a) Migration of ECs and SMCs onto uncoated L605, TMS, TMS+ NH_3/O_2 plasma nanocoatings after 7 days. b) Migration distance graph determined by ImageJ. Indicating values are mean ±SD (n = 3), $^{**}p < 0.005$.

4.4.3. Protein adsorption

Figure 4.8 plots albumin and fibrinogen (Fg) adsorption for uncoated L605 and plasma nanocoated coupons, determined by ELISA assay. **Figure 4.8 a** show that albumin adsorption is more favorable on uncoated L605 and TMS plasma nanocoated surfaces than TMS+NH_3/O_2 plasma nanocoatings ($p < 0.005$). The reason for this probably derives from the relation between surface wettability and protein attachment. The more hydrophobic the surface, the greater the adsorption of protein [12,16]. Data of contact angle listed in **Figure 3.2** indicates that TMS+NH_3/O_2 plasma nanocoating is much more hydrophilic (48.5°) than the uncoated L605 sample (74°) and TMS plasma nanocoating without modification (99°), which correlates well with the data of albumin adsorption. The relation of albumin and polar component on surfaces are reported [31], in which the more polar groups incorporated, the less albumin attaches to surfaces. TMS+NH_3/O_2 plasma nanocoating surfaces containing –OH, C-O, C=O polar groups as characterized by FTIR and XPS (in Chapter 3) is less albumin adhesive compared to non-polar TMS plasma nanocoating and uncoated L605 surfaces.

In **Figure 4.8 b**, plasma nanocoatings exhibit higher Fg adsorption compared to uncoated L605 ($p < 0.05$). Fg affinity is known for increasing with hydrophobicity [12,16] however comparable Fg adsorbed levels on TMS plasma nanocoatings treated with and without NH_3/O_2 reveal that there should be other factors that could explain for Fg adsorption. Conformation of Fg could be a potential reason [14,19,23,31]. Unfolding Fg can attach to a biomaterial surface in by side-on binding, leading to smaller amounts of Fg covering the surface. Folded Fg adheres to the surface by end-on binding and larger

amounts of Fg adheres to the surface, leading to higher surface coverage [24]. Unfolded state of protein was proven to adhere more platelets than folded state [16]. Though adsorbed Fg amount on TMS+NH_3/O_2 plasma nanocoating is higher than that determined on uncoated L605, those adsorbed Fg molecules could be in folded native state, hiding their binding sites to platelets. Fg underwent a greater degree of unfolding with increasing surface hydrophobicity [12,32]. This implies that the folding conformation of adsorbed Fg on hydrophilic surface with minimal conformation changes has no affinity to attach and activate platelets.

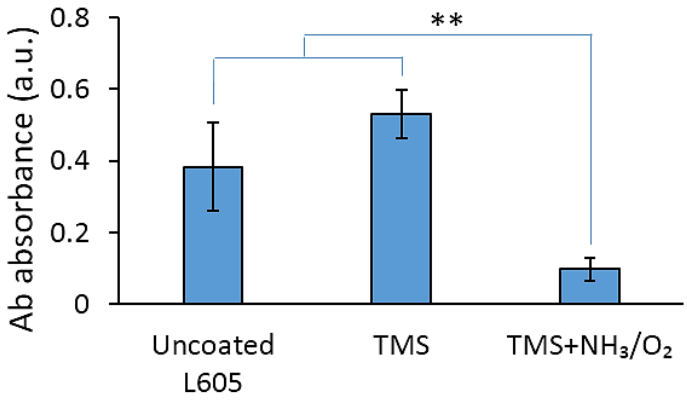

a)

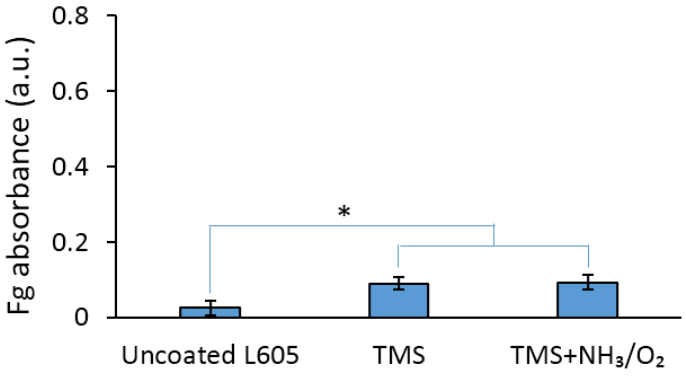

b)

Figure 4.8: (a) Albumin and (b) fibrinogen adsorption on uncoated L605 and plasma nanocoated samples determined by ELISA. Indicating values are mean ± SD (n = 3), *p < 0.05, **p < 0.005.

4.4.4. Platelet, fibrin and clotting adhesion

Platelet adhesion test was performed for uncoated L605 and plasma nanocoated samples, then evaluated by SEM images. Platelet adhesion result is shown in **Figure 4.9**. Adhered platelet density on plasma nanocoated coupon samples (about 150 platelets/mm^2) were much lower ($p < 0.005$) than that on uncoated L605 surfaces (about 600 platelets/mm^2). The adhered platelets on the uncoated L605 samples display spherical structures of about 4-μm size and marked with long pseudopodia. The size and shape of adhered platelets are similar as reported in literature in which platelets attached to cobalt chromium alloy are approximately 4-5 μm hedgehog-like structures [32].

Though similar platelet density on plasma nanocoated surfaces, platelets on TMS+NH_3/O_2 plasma nanocoatings were observed with more circular shape and less pseudopodia. Based on the activation state and structure, levels of activation can be divided in four states: 1) inactivated state when platelets are typical discoid and round shape, 2) beginning state (or dendritic state), 3) partly spread, and 4) fully spread [33,34]. Platelets on the TMS+NH_3/O_2 plasma nanocoatings appear to be in inactivated form, whereas adhered platelets on TMS plasma nanocoating and uncoated L605 are in beginning or partly spread states. Large number of adhered platelets and the high degree of platelet activation can trigger thrombosis events on cobalt chromium alloy [35,36]. In **Figure 4.9 c**, platelet adhesion on uncoated L605 stent surfaces is mostly in dendritic state – the beginning state of platelet activation; whereas, almost no adhered platelets were detected on TMS+NH_3/O_2 plasma nanocoated stent surfaces.

Numerous groups reported the essential effect of fibrinogen on platelet attachment. Some groups believed that adsorbed fibrinogen amount critically promotes platelet adhesion and activation [15,37], whereas other groups determine platelet binding

is more influenced by adsorbed fibrinogen conformation [19,33]. Platelet adhesion is strongly correlated with the degree of adsorption-induced unfolding of fibrinogen and with essentially no correlation with adsorbed fibrinogen amount [37]. Fibrinogen shows more affinity (**Figure 4.8**) for plasma nanocoating, but fewer adhered platelets and smaller degree of platelet activation were found on NH_3+O_2 plasma nanocoatings. Thus, it is reasonable that adsorbed fibrinogen on plasma nanocoating surface retains its native conformation that inhibits platelet binding and activation. It is in accordance to studies [13,37] that proteins adsorbing to hydrophilic surfaces keep a close-to-native conformational state, leading to reduced platelet adhesion.

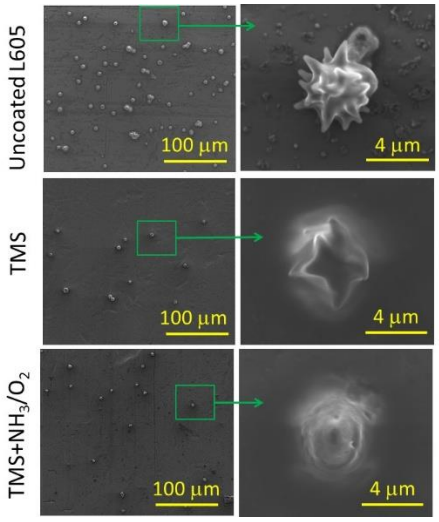

a)

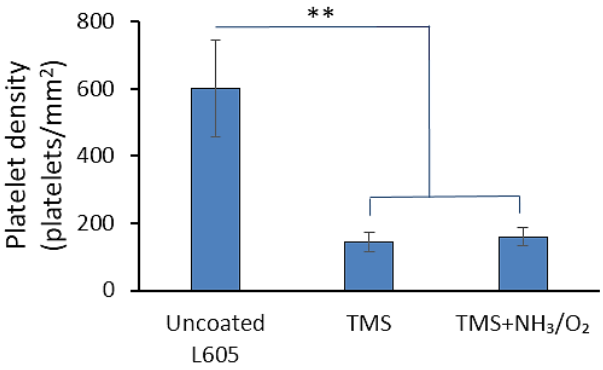

b)

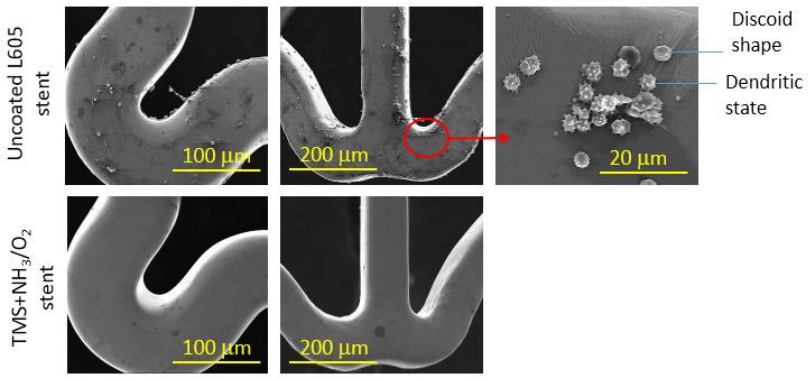

c)

Figure 4.9: Platelet adhesion on uncoated L605 and plasma nanocoated surfaces under static condition. a) SEM images of platelets on coupons; b) Platelet density (Indicating values are mean ± SD (n = 3), $^{**}p < 0.005$); c) SEM images of platelets on stents.

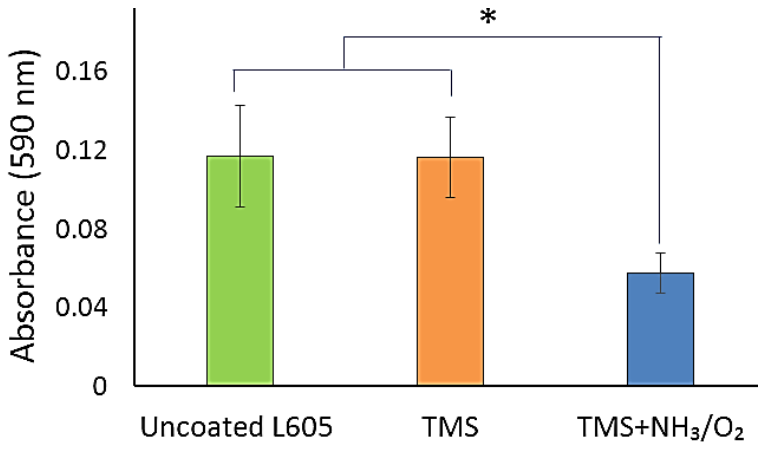

Figure 4.10: Clotting levels determined on uncoated L605, TMS, and TMS+NH_3/O_2 plasma nanocoatings. Indicating values are mean ± SD (n = 3), $^{*}p < 0.05$.

The reduced level of clotting attachment to TMS+NH_3/O_2 plasma nanocoatings ($p < 0.05$) in **Figure 4.10** suggest that modified plasma coatings can resist the formation of thrombosis events by clotting reduction. An in vitro circulation model using whole blood to stimulate the in vivo thrombosis responses to uncoated L605 and plasma nanocoating.

4.4.5. Effect of surface wettability to biological responses

CoCr L605 is known as a good biocompatible material which promotes cell growth on its surfaces [39]. The cell attachment is attributed to L605 mild hydrophilicity (contact angle of 74°). Additionally, the top-most layer of CoCr L605 is composed mainly of cobalt oxides and chromium oxides that promote cell viability [40]. Contact angle can be considered a key determinant of cell attachment. Highly hydrophilic (0 - 20°) surfaces may result in poor endothelial cell attachment which could limit stent surface endothelialization, which will ultimately limit long-term stent functions [7]. Low surface energy and high

contact angle prevent cell adhesion and spreading to a greater extent than materials that have lower contact angle [41]. Moderately wettable surfaces (contact angle between 20 - 40°) provide the best cell adhesion for the biomaterials [42,43]. Thus, hydrophobic TMS plasma nanocoatings (contact angle of 99°) inhibit SMC and EC growth, but mildly hydrophilic TMS+NH_3/O_2 plasma nanocoating (contact angle of 48.5°) exhibited comparable EC spreading and adhesion to uncoated L605, leading to healthy endothelium. The TMS + NH_3/O_2 plasma nanocoatings were aged from approximately 3° after treatment to 48.5° after 2 years as shown in **Figure 3.2**, assisting cell attachment and proliferation. Without aging, modified plasma surfaces are not favorable to cell adhesion, resulting in in-biocompatible surfaces. Cell proliferation and attachment were influenced by surface wettability change. On TMS plasma nanocoating surfaces, PCAEC and PCASMC attachment was prevented due to the hydrophobic surfaces. The reason can be the protein interface between cells and substrates. If the surface is hydrophobic, adsorbed proteins will denature.[30,44]. In **Figure 4.3-4.7,** PCAECs and PCASMCs fail to spread on TMS plasma nanocoating surfaces which are hydrophobic with contact angle of 99°. However, if the surface is too hydrophilic, proteins fail to attach, resulting in poor cell adhesion. Protein attachment is ideal on moderately hydrophilic surfaces, leading to cell spreading and binding on the substrates [44]. Contact angles of 74° and 48.5° for uncoated L605 and TMS+NH_3/O_2 plasma nanocoated surfaces, respectively, are considered favorable for cell growth. In **Figure 4.5**, cells look robust and spreading on uncoated L605 and TMS+NH_3/O_2 plasma nanocoating. Compared to spreading cells, elongated cells are considered more proliferative and prone to migration [30]. PCAEC morphology on TMS+NH_3/O_2 looks more elongated and directional compared to PCAECs detected on uncoated L605, potentially resulting in higher PCAEC proliferation and migration on TMS+NH_3/O_2 plasma nanocoatings. Highly hydrophilic surface reduced

platelet adhesion when compared to mildly hydrophilic or hydrophobic surfaces [39,45]. It was found that albumin – a common blood protein which prevents platelet deposition – tends to be absorbed by hydrophilic surfaces [7]. In addition, fibrinogen – another key blood protein that promotes platelet attachment- is accumulated by hydrophilic surfaces but keeps fibrinogen in a close-to-native conformational state minimizing platelet accumulation [39].

Surface wettability is not only the essential factor influencing cell growth. Unlike the similarity of PCAEC proliferation on uncoated L605 and TMS+NH_3/O_2 plasma nanocoatings, PCASMCs were inhibited by TMS+NH_3/O_2 plasma nanocoatings but supported by uncoated L605 as shown in **Figure 4.3-4.7**. NO can be contributed to that phenomenon because NO plays a crucial role in inhibition of SMC proliferation and adhesion.

4.4.6. Effect of NO-generating coatings to biological responses

In **Figure 3.4** and **Table 3.4**, N and O incorporation into plasma nanocoatings and they can be present in the form of numerous chemical groups, such as NO. There are some mechanisms for NO inhibitory effect on SMCs, one of them is to stop collagen production and DNA synthesis in SMCs [46].

NO has been known as an ideal candidate for surface modification to enhance biocompatibility because NO can prevent thrombosis formation, SMC proliferation and migration, platelet and leukocyte adhesion and activation, and simulate endothelialization [2,28]. Though NO releasing rates in healthy vasculature is low ($0.5\text{-}4 \times 10^{-10}$ mol $\times$ $cm^{-2} \times$ min^{-1}), it plays crucial roles in vasculature [29]. N and O containing plasma nanocoatings were evident in XPS spectra with the high surface concentration of O (~ 39.39 at. %) and very tiny concentration of N (2.6 at. %). Concentration of N1s incorporated into coatings

by plasma techniques for surface modification need such small amount starting at 1.23 at. % [47]. The NO-releasing plasma coating was proven by ODQ experiments in which PCASMCs were influenced by ODQ treatment. ODQ has high affinity for sGC - the only-known receptors of NO [28,29].

Though the TMS+NH_3/O_2 plasma nanocoating supports PCAEC cell attachment and growth, it strongly restricted the proliferation of PCASMC. Thus, aside from wettability effect, there must be other factors affecting cell proliferation and binding. The obvious decrease of PCASMC proliferation and migration on TMS + NH_3/O_2 plasma nanocoating can be attributed by the existence of N and O tailored in the coating. NO may also cause the reduced platelet adhesion and the less platelet activation shown on TMS+NH_3/O_2 plasma nanocoated surfaces. NO inhibits SMCs, platelet adhesion and platelet activation in the similar mechanism. NO-mediated inhibition of platelet function and SMC proliferation occurs primarily through elevations in cGMP [48]. The increase of cGMP in platelets and SMCs was due to activation of sGC by NO [29,49].

PCAEC and PCASMC migration and proliferation on TMS plasma nanocoated samples without NH_3/O_2 plasma surface modification were very limited due to the hydrophobicity that is not favorable for cell growth. The selectivity to enhance PCAEC migration while inhibiting PCASMC migration is the key factor of cardiovascular stents for accomplishing the regeneration of a healthy endothelium. NO-releasing stent surface may be an effective way to supply NO and maintain physiological processes in vascular system. ODQ test was used to confirm the NO presence by its effect on SMC growth.

4.5. Conclusions

In vitro biological tests were performed on uncoated L605 and NH_3/O_2 plasma modified TMS plasma nanocoatings deposited on cobalt chromium L605 surfaces. The *in*

vitro test results revealed that the hydrophilic surfaces containing N element exhibit good biocompatibility and hemocompatibility.

Protein test results showed that fibrinogen adsorption was higher on NH_3/O_2 plasma modified TMS plasma nanocoating surfaces and albumin adsorption was highest on uncoated L605 surfaces. However, platelet adhesion and activation test conducted on L605 stents and coupons showed a remarkable reduction of platelet adhesion and activation on NH_3/O_2 plasma modified TMS plasma nanocoating surfaces compared to uncoated L605. Similarly, fibrin deposition test in circulation model indicated that more fibrin was detected on uncoated L605 than the NH_3/O_2 plasma modified TMS plasma nanocoatings. Such behavior suggests that thrombus formation may be minimized on the stent surface.

Cell culture results show that on uncoated L605 surfaces, both PCAECs and PCASMCs proliferated. In contrast, TMS plasma nanocoatings inhibited PCAECs and PCASMCs proliferation and adhesion with very few cells on their surfaces. NH_3/O_2 plasma modified TMS plasma nanocoatings were more favorable to PCAECs by displaying PCAECs comparable to that on uncoated L605 surfaces; and at the same time prevented the proliferation and attachment of PCASMCs. The competition of PCAECs and PCASMCs in cell co-culture reveals that NH_3/O_2 plasma modified TMS plasma nanocoatings exhibited adhesion and proliferation selectively toward PCAECs. The cell migration test indicates that NH_3/O_2 plasma modified TMS plasma nanocoatings werefavorable for PCAEC migration, but prevented the migration of PCASMCs.

In summary, NH_3/O_2 plasma modified TMS plasma nanocoatings shoed the capability of inhibiting the survivability of PCASMCs, reducing the number of adhered platelets, minimizing platelet activation, and accelerating the proliferation of PCAECs.

Therefore, NH_3/O_2 plasma modified TMS plasma nanocoatings are good candidate materials for preventing restenosis and thrombosis in stent applications.

4.6. References

[1] Y. Zhang, X. Wang, Z. Ma, B. Bai, J. Liu, L. Yang, G. Qin, E. Zhang, A potential strategy for in-stent restenosis: Inhibition of migration and proliferation of vascular smooth muscle cells by Cu ion, Materials Science and Engineering C. 115 (2020). https://doi.org/10.1016/j.msec.2020.111090.

[2] N. Lyu, Z. Du, H. Qiu, P. Gao, Q. Yao, K. Xiong, Q. Tu, X. Li, B. Chen, M. Wang, G. Pan, N. Huang, Z. Yang, Mimicking the Nitric Oxide-Releasing and Glycocalyx Functions of Endothelium on Vascular Stent Surfaces, Advanced Science. 7 (2020). https://doi.org/10.1002/advs.202002330.

[3] A. Curcio, D. Torella, C. Indolfi, Mechanisms of smooth muscle cell proliferation and endothelial regeneration after vascular injury and stenting, Circulation Journal. 75 (2011) 1287–1296. https://doi.org/10.1253/circj.CJ-11-0366.

[4] D. Sun, Y. Zheng, T. Yin, C. Tang, Q. Yu, G. Wang, Coronary drug-eluting stents: From design optimization to newer strategies, Journal of Biomedical Materials Research - Part A. 102 (2014) 1625–1640. https://doi.org/10.1002/jbm.a.34806.

[5] M.N. Babapulle, M.J. Eisenberg, Coated stents for the prevention of restenosis: Part I, Circulation. 106 (2002) 2734–2740. https://doi.org/10.1161/01.CIR.0000038982.49640.70.

[6] D.R. Holmes, D.J. Kereiakes, S. Garg, P.W. Serruys, G.J. Dehmer, S.G. Ellis, D.O. Williams, T. Kimura, D.J. Moliterno, Stent Thrombosis, J Am Coll Cardiol. 56 (2010) 1357–1365. https://doi.org/10.1016/j.jacc.2010.07.016.

[7] J.M. Seeger, M.D. I, E. Bigatan, N. Klingman, D. Amery, C. Widenhouse, E.P. Goldberg, Hydrophilic surface modification of metallic endoluminal stents, Journal of Vascular Surgery, Volume 22, Issue 3, September 1995, Pages 327-336.

[8] T. Simard, B. Hibbert, F.D. Ramirez, M. Froeschl, Y.X. Chen, E.R. O'Brien, The Evolution of Coronary Stents: A Brief Review, Canadian Journal of Cardiology. 30 (2014) 35–45. https://doi.org/10.1016/j.cjca.2013.09.012.

[9] J.W. Shim, I.H. Bae, D.S. Park, K.S. Lim, S.Y. Lee, E.J. Jang, J.K. Park, J.H. Kim, M.H. Jeong, Evaluation of ion implantation for anti-thrombogenic coronary stent in vitro and in vivo, Journal of Industrial and Engineering Chemistry. 54 (2017) 290–297. https://doi.org/10.1016/j.jiec.2017.06.003.

[10] Y. Wu, F.I. Simonovsky, B.D. Ratner, T.A. Horbett, The role of adsorbed fibrinogen in platelet adhesion to polyurethane surfaces: A comparison of surface hydrophobicity, protein adsorption, monoclonal antibody binding, and platelet adhesion, Journal of Biomedical Materials Research - Part A. 74 (2005) 722–738. https://doi.org/10.1002/jbm.a.30381.

[11] B. Clarke, P. Kingshott, X. Hou, Y. Rochev, A. Gorelov, W. Carroll, Effect of nitinol wire surface properties on albumin adsorption, Acta Biomaterialia. 3 (2007) 103–111. https://doi.org/10.1016/j.actbio.2006.07.006.

[12] Y. Zang, K.C. Popat, M.M. Reynolds, Nitric oxide-mediated fibrinogen deposition prevents platelet adhesion and activation, Biointerphases. 13 (2018) 06E403. https://doi.org/10.1116/1.5042752.

[13] C.P. Kealey, S.A. Whelan, Y.J. Chun, C.H. Soojung, A.W. Tulloch, K.P. Mohanchandra, D. di Carlo, D.S. Levi, G.P. Carman, D.A. Rigberg, In vitro hemocompatibility of thin film nitinol in stenotic flow conditions, Biomaterials. 31 (2010) 8864–8871. https://doi.org/10.1016/j.biomaterials.2010.08.014.

[14] B. Sivaraman, R.A. Latour, The Adherence of platelets to adsorbed albumin by receptor-mediated recognition of binding sites exposed by adsorption-induced unfolding, Biomaterials. 31 (2010) 1036–1044. https://doi.org/10.1016/j.biomaterials.2009.10.017.

[15] Y. Tanaka, K. Kurashima, H. Saito, A. Nagai, Y. Tsutsumi, H. Doi, N. Nomura, T. Hanawa, In vitro short-term platelet adhesion on various metals, Journal of Artificial Organs. 12 (2009) 182–186. https://doi.org/10.1007/s10047-009-0468-1.

[16] E. Jia, X. Zhao, Y. Lin, Z. Su, Protein adsorption on titanium substrates and its effects on platelet adhesion, Applied Surface Science. 529 (2020). https://doi.org/10.1016/j.apsusc.2020.146986.

[17] G. Steiner, S. Tunc, M. Maitz, R. Salzer, Conformational changes during protein adsorption. FT-IR spectroscopic imaging of adsorbed fibrinogen layers, Analytical Chemistry. 79 (2007) 1311–1316. https://doi.org/10.1021/ac061341j.

[18] C.K. Kang, Y.S. Lee, The surface modification of stainless steel and the correlation between the surface properties and protein adsorption, Journal of Materials Science: Materials in Medicine. 18 (2007) 1389–1398. https://doi.org/10.1007/s10856-006-0079-9.

[19] M.L. Clarke, J. Wang, Z. Chen, Conformational changes of fibrinogen after adsorption, Journal of Physical Chemistry B. 109 (2005) 22027–22035. https://doi.org/10.1021/jp054456k.

[20] R. Tzoneva, M. Heuchel, T. Groth, G. Altankov, W. Albrecht, D. Paul, Fibrinogen adsorption and platelet interactions on polymer membranes, 2002.

[21] S. Höhn, S. Virtanen, A.R. Boccaccini, Protein adsorption on magnesium and its alloys: A review, Applied Surface Science. 464 (2019) 212–219. https://doi.org/10.1016/j.apsusc.2018.08.173.

[22] Y.L. Jeyachandran, E. Mielczarski, B. Rai, J.A. Mielczarski, Quantitative and qualitative evaluation of adsorption/desorption of bovine serum albumin on hydrophilic and hydrophobic surfaces, Langmuir. 25 (2009) 11614–11620. https://doi.org/10.1021/la901453a.

[23] T. Lenz-Habijan, P. Bhogal, M. Peters, A. Bufe, R. Martinez Moreno, C. Bannewitz, H. Monstadt, H. Henkes, Hydrophilic Stent Coating Inhibits Platelet Adhesion on Stent Surfaces: Initial Results In Vitro, CardioVascular and Interventional Radiology. 41 (2018) 1779–1785. https://doi.org/10.1007/s00270-018-2036-7.

[24] H. Liu, C. Pan, S. Zhou, J. Li, N. Huang, L. Dong, Improving hemocompatibility and accelerating endothelialization of vascular stents by a copper-titanium film, Materials Science and Engineering C. 69 (2016) 1175–1182. https://doi.org/10.1016/j.msec.2016.08.028.

[25] G.P. Lopez, D.G. Castner, B.D. Ratner, XPS 0 1s Binding Energies for Polymers Containing Hydroxyl, Ether, Ketone and Ester Groups, 1991.

[26] J.E. Barbato, E. Tzeng, Nitric oxide and arterial disease, Journal of Vascular Surgery. 40 (2004) 187–193. https://doi.org/10.1016/j.jvs.2004.03.043.

[27] Y. Yang, P.K. Qi, Z.L. Yang, N. Huang, Nitric oxide based strategies for applications of biomedical devices, Biosurface and Biotribology. 1 (2015) 177–201. https://doi.org/10.1016/j.bsbt.2015.08.003.

[28] J. Rao, H. Pan Bei, Y. Yang, Y. Liu, H. Lin, X. Zhao, Nitric Oxide-Producing Cardiovascular Stent Coatings for Prevention of Thrombosis and Restenosis, Frontiers in Bioengineering and Biotechnology. 8 (2020). https://doi.org/10.3389/fbioe.2020.00578.

[29] Z. Yang, Q. Tu, M.F. Maitz, S. Zhou, J. Wang, N. Huang, Direct thrombin inhibitor-bivalirudin functionalized plasma polymerized allylamine coating for improved biocompatibility of vascular devices, Biomaterials. 33 (2012) 7959–7971. https://doi.org/10.1016/j.biomaterials.2012.07.050.

[30] H. Qiu, P. Qi, J. Liu, Y. Yang, X. Tan, Y. Xiao, M.F. Maitz, N. Huang, Z. Yang, Biomimetic engineering endothelium-like coating on cardiovascular stent through heparin and nitric oxide-generating compound synergistic modification strategy, Biomaterials. 207 (2019) 10–22. https://doi.org/10.1016/j.biomaterials.2019.03.033.

[31] H.Z. Li, X. Zhao, J. Xu, MRI-compatible Nb-60Ta-2Zr alloy for vascular stents: Electrochemical corrosion behavior in simulated plasma solution, Materials Science and Engineering C. 56 (2015) 205–214. https://doi.org/10.1016/j.msec.2015.06.027.

[32] M.S. Ehrenberg, A.E. Friedman, J.N. Finkelstein, G. Oberdörster, J.L. McGrath, The influence of protein adsorption on nanoparticle association with cultured endothelial cells, Biomaterials. 30 (2009) 603–610. https://doi.org/10.1016/j.biomaterials.2008.09.050.

[33] L. Zhang, B. Casey, D.K. Galanakis, C. Marmorat, S. Skoog, K. Vorvolakos, M. Simon, M.H. Rafailovich, The influence of surface chemistry on adsorbed fibrinogen conformation, orientation, fiber formation and platelet adhesion, Acta Biomaterialia. 54 (2017) 164–174. https://doi.org/10.1016/j.actbio.2017.03.002.

[34] I. Firkowska-Boden, K.D. Jandt, C. Helbing, T.J. Dauben, M. Pieper, How nanotopography-induced conformational changes of fibrinogen affect platelet adhesion and activation, Langmuir. 36 (2020) 11573–11580. https://doi.org/10.1021/acs.langmuir.0c02094.

[35] M.I. Castellanos, J. Guillem-Marti, C. Mas-Moruno, M. Díaz-Ricart, G. Escolar, M.P. Ginebra, F.J. Gil, M. Pegueroles, J.M. Manero, Cell adhesive peptides functionalized on CoCr alloy stimulate endothelialization and prevent thrombogenesis and restenosis, Journal of Biomedical Materials Research - Part A. 105 (2017) 973–983. https://doi.org/10.1002/jbm.a.35988.

[36] N. Bricout, F. Chai, J. Sobocinski, A. Hertault, W. Laure, A. Ung, P. Woisel, J. Lyskawa, N. Blanchemain, Immobilisation of an anti-platelet adhesion and anti-thrombotic drug (EP224283) on polydopamine coated vascular stent promoting anti-thrombogenic properties, Materials Science and Engineering C. 113 (2020). https://doi.org/10.1016/j.msec.2020.110967.

[37] B. Sivaraman, R.A. Latour, The relationship between platelet adhesion on surfaces and the structure versus the amount of adsorbed fibrinogen, Biomaterials. 31 (2010) 832–839. https://doi.org/10.1016/j.biomaterials.2009.10.008.

[38] S. Sinn, T. Scheuermann, S. Deichelbohrer, G. Ziemer, H.P. Wendel, A novel in vitro model for preclinical testing of the hemocompatibility of intravascular stents according to ISO 10993-4, Journal of Materials Science: Materials in Medicine. 22 (2011) 1521–1528. https://doi.org/10.1007/s10856-011-4335-2.

[39] V. Milleret, A. Ziogas, S. Buzzi, R. Heuberger, A. Zucker, M. Ehrbar, Effect of oxide layer modification of CoCr stent alloys on blood activation and endothelial behavior, Journal of Biomedical Materials Research - Part B Applied Biomaterials. 103 (2015) 629–640. https://doi.org/10.1002/jbm.b.33232.

[40] S. Diaz-Rodriguez, P. Chevallier, C. Paternoster, V. Montaño-Machado, C. Noël, L. Houssiau, D. Mantovani, Surface modification and direct plasma amination of L605 CoCr alloys: on the optimization of the oxide layer for application in cardiovascular implants, RSC Advances. 9 (2019) 2292–2301. https://doi.org/10.1039/C8RA08541B.

[41] S. Bodhak, S. Bose, A. Bandyopadhyay, Role of surface charge and wettability on early stage mineralization and bone cell-materials interactions of polarized hydroxyapatite, Acta Biomaterialia. 5 (2009) 2178–2188. https://doi.org/10.1016/j.actbio.2009.02.023.

[42] M. Chen, P.O. Zamora, L. Peñ, P. Som, S. Osaki, NH 3 /O 2 mixed gas plasmas alter the interaction of blood components with stainless steel, 2003.

[43] P. van Wachem, T. Beugeling, J. Feijen, J. Detmers, W. van Aken, Interaction of cultured human endothelial cells with polymeric surfaces of different wettabilities, 1985.

[44] J.W. Shim, I.H. Bae, D.S. Park, K.S. Lim, S.Y. Lee, E.J. Jang, J.K. Park, J.H. Kim, M.H. Jeong, Evaluation of ion implantation for anti-thrombogenic coronary stent in vitro and in vivo, Journal of Industrial and Engineering Chemistry. 54 (2017) 290–297. https://doi.org/10.1016/j.jiec.2017.06.003.

[45] Y. Wu, F.I. Simonovsky, B.D. Ratner, T.A. Horbett, The role of adsorbed fibrinogen in platelet adhesion to polyurethane surfaces: A comparison of surface hydrophobicity, protein adsorption, monoclonal antibody binding, and platelet adhesion, Journal of Biomedical Materials Research - Part A. 74 (2005) 722–738. https://doi.org/10.1002/jbm.a.30381.

[46] L. Chen, G. Daum, R. Forough, M. Clowes, U. Walter, A.W. Clowes, Overexpression of Human Endothelial Nitric Oxide Synthase in Rat Vascular Smooth Muscle Cells and in Balloon-Injured Carotid Artery From the Departments of Surgery and Pathology (L, 1998. http://ahajournals.org.

[47] R. Khalifehzadeh, W. Ciridon, B.D. Ratner, Surface fluorination of polylactide as a path to improve platelet associated hemocompatibility, Acta Biomaterialia. 78 (2018) 23–35. https://doi.org/10.1016/j.actbio.2018.07.042.

[48] S. Marcondes, M.H.M. Cardoso, R.P. Morganti, S.M. Thomazzi, S. Lilla, F. Murad, G. de Nucci, E. Antunes, Cyclic GMP-independent mechanisms contribute to the inhibition of platelet adhesion by nitric oxide donor: A role for-actinin nitration, 2006. www.pnas.orgcgidoi10.1073pnas.0509397103.

[49] J.A. Carvajal, A.M. Germain, J.P. Huidobro-Toro, C.P. Weiner, Molecular Mechanism of cGMP-Mediated Smooth Muscle Relaxation, 2000.

Chapter 5

CORROSION BEHAVIORS AND TOXICITY ASSESSMENT OF PLASMA NANOCOATINGS

5.1. Abstract

Corrosion resistance is one of the most important characteristics to evaluate the biocompatibility of biomaterial devices. Corrosion causes inflammation in local tissues of biomaterials devices and decreases mechanical integrity, leading to decreasing effectiveness of the devices. Cobalt chromium L605 coronary artery stents and coupons were coated with trimethylsilane (TMS) plasma coatings of 20 ~ 30 nm in thickness followed by NH_3/O_2 plasma modification. The corrosion resistance, ion releasing resistance, and toxicity were assessed by immersion tests, electrochemical tests, ion releasing and cytotoxicity tests.

Immersion test (ASTM G31-72) was performed on L605 coupon and stent samples in simulated body fluid – Hank's solution – for 7 days and 45 days to evaluate both formation of corrosion products on sample surfaces and also material weight loss. Cyclic polarization tests were conducted to check pitting susceptibility, corrosion resistance and corrosion rates of samples. Ion releasing and cytotoxicity tests (ISO 10993) were carried out to determine the Ni, Cr, Co release and evaluate the toxicity to cell growth.

Results show that there was a calcium and phosphorous containing layer on uncoated L605 coupons and stents, while no product adsorption was found on plasma nanocoated coupons and stents. No pitting corrosion was detected on all samples. Cyclic polarization tests indicated that plasma nanocoated stents and coupons improved

corrosion resistance in PBS. Plasma nanocoated L605 samples gave corrosion current of one order of magnitude lower than that for uncoated L605 samples, implying that plasma nanocoatings reduce corrosion rates. Ion releasing test and cytotoxicity test (ISO 10993) revealed no cytotoxicity for all samples. Ni, Co, and Cr released from uncoated L605 were about 57% to 79% higher than those released from plasma nanocoated samples. These results suggest that TMS plasma nanocoatings with NH_3/O_2 plasma modification is suitable for stent applications.

5.2. Introduction

Cobalt chromium (CoCr) L605 stents have been widely used due to their excellent mechanical and radiopaque properties and acceptable biocompatibility [1,2]. Thin-strut stent design was claimed to reduce restenosis and thrombosis events in stenting implantation [3]. Despite containing thinner struts compared to stainless steel stents, CoCr L605 stents have minimal elastic recoil and also enhance X-ray visibility for implanting procedures [1].

Corrosion resistance is one method to evaluate the biocompatibility of biomaterial devices. Corrosion is an inevitable, deteriorating reaction when metallic materials come in contact with body fluid [4]. Corrosion has been recognized to cause inflammation in local tissues of biomaterials devices and decreases mechanical integrity, leading to decreasing effectiveness of the devices [5]. Restenosis occurs due to inflammation of the tissues in contact with the stent. Corrosion processes within the body are due to proteins and shearing stresses along the stent surface. In addition to inflammation, nickel particles have been implicated as potentially carcinogenic. The corrosion process starts within days of implantation and can potentially lead to loss of arterial structural integrity. Compared to other common vascular stent materials such as 316L stainless steel, Ti alloys, Mg alloys,

L605 is very highly corrosion resistant even in a hostile electrolytic environment of human body due to the development of passive oxide layer [6,7]. However, oxide layer of L605 alloys is not passive enough to avoid leakage of metal ions and electrochemical attack, resulting in adverse impacts to the human body [8,9]. CoCr-based implants are known to release chromium (Cr) and cobalt (Co) ions [7], which are responsible for allergic reactions. Additionally, the nickel (Ni) content in L605 is about 10% and its ability to induce allergic reactions and long-term complications such as restenosis are well documented [6,10]. A large amount of released metallic ions is generally harmful to human body [11].

Many surface techniques have been used to enhance corrosion resistance and ion-releasing resistance of metallic implants. Among various surface treatment methods, ion implantation and laser treatment are effective for improving corrosion resistance [13]. Those techniques, however, are costly and it is not easy to apply for complex shape implants such as cardiovascular coronary artery stents. Hard and rigid coatings containing bio-ceremics such as TiN, TiCN, Al_2O_3, SiC, BN, and Si_3N_4 showed cracks and delamination during stent expansion and implantation [14]. Other coatings including polymers, gold, diamond, and graphite have also been investigated. Studies on those coatings indicated the improved corrosion resistance for metallic implants, but inflammatory responses occurred evidently on the coatings [15,16].

To enhance the biocompatibility of stents by coatings, amorphous silicon carbide (a-SiC:H) coatings seem to be a better choice. Electron transfer reactions between fibrinogen and metallic implants can be halted by silicon carbide coatings, leading to reduce thrombogenicity. Stents coated with amorphous silicon carbide could inhibit thrombosis formation and thus feasibly enhance biocompatibility [17,18].

In early work, CoCr-based alloys are not susceptible to pitting corrosion. CoCr alloys with Ti-based coating by Ti plasma spray coating [19] or cathodic arc deposition method [20] indicated positive effects for corrosion behavior such as positive open circuit potential (OCP) values. Hryniewicz (2008) and his group focused on “magnetoelectropolishing” method to improve corrosion resistance. Corrosion current densities of the treated samples were increased, implying the corrosion resistant enhancement compared to untreated CoCr alloy [14]. Diaz (2014) has reported a method to increase corrosion resistance of L605 alloy due to reducing corrosion current by oxygen plasma ion immersion implantation. More positive corrosion potentials and partially decreasing corrosion current of treated L605 alloys were obtained [21,22].

In this chapter, corrosion behavior, ion releasing, and toxicity assessment were performed on uncoated L605 and plasma nanocoatings. While modified TMS+NH_3/O_2 plasma nanocoatings were shown to promote surface biocompatibility and hemo-compatibility in Chapter 3 and 4, they are expected to enhance corrosion and ion releasing resistance in comparison to uncoated L605.

5.3. Materials and Methods

5.3.1. Sample preparation

See Chapter 3 – section 3.3.1 in page 30.

5.3.2. Plasma nanocoating preparation

See Chapter 3 – section 3.3.2 in page 30.

5.3.3. Immersion test

In-vitro degradation immersion testing, was conducted in simulated body fluid (SBF) as described in [23]. SBF (1000 mL) contains NaCl (8.035 g), $NaHCO_3$ (0.355 g), KCl (0.225 g), K_2HPO_4. $3H_2O$ (0.231 g), $MgCl_2.6H_2O$ (0.311 g), 1M-HCl (39 mL), $CaCl_2$ (0.292 g), Na_2SO_4 (0.072 g), Tris (6.118 g) at 37°C and buffered to pH 7.4 exactly. The required test volume of the electrolyte was calculated based on a 30 mL/cm^2 volume-to-sample area ratio, according to ASTM-G31-72. During the immersion process, fresh SBF was replaced every 48 h. After 7 days and 45 days immersion, samples were ultrasonically cleaned in ethanol for 15 min and dried in room temperature air. The surface morphology was identified using SEM. Energy-dispersive X-ray spectroscopy (EDS) was used to determine elemental components of corrosion products. To determine pitting failures and corrosion rate after the immersion test, substrates were then cleaned with a 25% chromic acid for 5 min to remove the corrosion products. Samples were then quickly washed with distilled water and dried in room temperature air. SEM was used to detect pits. The sample weight was measured before and after immersion by a balance with accuracy of 0.1 mg, and corrosion rate was obtained based on the weight loss of samples by following formula: Corrosion rate = K*W/(A*T*D), where K = 8.76 x 10^4 (millimeter per year), W is mass loss (gram), A is exposure area (cm^2), T is exposure time (hours), and D is density (g/cm^3) [24].

The flowing model in 3.3.4. was used to perform immersion tests for stents. Three stents for each condition: uncoated L605, TMS, TMS+NH_3/O_2 were inserted in series in a Masterflex Puri-Flex tubing (Cole-Parmer Co., IL, USA) with the inner diameter of 3.1 mm. The tubing was placed within the head of a Masterflex peristaltic roller pump (Cole-Parmer Co., IL, USA). About 7 mL SBF was filled into the tube with two ends connected by an adapter. Temperature of water bath was set at 37°C and the pump speed of 36 rpm was performed for 7 days. After 7 days circulation, stents were removed, then ultrasonically

cleaned in ethanol in 15 min, rinsed with distilled water and dried in room temperature air. The morphologies of the stent surfaces were identified using SEM. Energy-dispersive X-ray spectroscopy (EDS) was used to determine elemental components of any corrosion products.

5.3.4. Electrochemical characterization

Cyclic polarization (CP) testing was performed for uncoated L605 and plasma nanocoated coupons to assess corrosion rates and pitting susceptibility. The corrosion protocol follows ASTM F2129-15. For metal coupons, an exposed area of 0.5 cm $\times$ 0.5 cm was created at one end of a strip (0.5 cm $\times$ 4 cm) by using epoxy and electric tape to cover the remaining area. A stainless-steel wire covered by electronic tapes was threaded through a borosilicate holder to collect signals from the working electrode (the sample). For stent sample, a stainless-steel wire (diameter: 0.006 in.) was threaded through the mesh at one end of stent and tied to form a taut knot contacting the stent. The tied knot and the stainless-steel wire were covered with epoxy. Sample was placed inside the corrosion cell containing phosphate buffered saline (PBS) (8.0 g/L NaCl, 0.2 g/L KCl, 1.15 g/L Na_2HPO_4-$7H_2O$, 0.2 g/L KH_2PO_4) at body temperature (37 $\pm$ 1°C) in stirring condition (60 rpm). The exposed area was kept submerged for 1.5 h for open circuit measurement prior to CP testing.

CP test was carried out with a PalmSens Emstat (Compact Electrochemical Interfaces- Randhoeve 221, 3995 GA Houten, The Netherlands) using the PSTrace 5.2 software package. Potentials were measured using a Luggin capillary and a saturated calomel electrode (SCE). All potentials given in this work were with respect to the SCE. A conventional 3-electrode arrangement was used with a coupon sample as the working electrode, a SCE as the reference electrode, and a graphite rod of 0.6 cm in diameter as

the counter electrode, and nitrogen gas inlet and outlet. The electrodes and the nitrogen bubbler were tightly inserted into the cell. Prior to the test, the medium in the electrochemical cell was purged with pure nitrogen gas for 30 min, then purged continuously during the test. The corrosion potential (E_{corr}) was monitored for 1.5 h in PBS prior to the CP testing, ensuring a stable open circuit potential (OCP). The CP curve was initiated at E_{corr} and scanned in the positive (more noble) direction. The scan was reversed after reaching the vertex potential E_v = 0.8 V. The reverse scan was stopped when potentials reached E_{corr}.

5.3.5. Ion releasing

To quantitatively determine the release of Co, Cr, and Ni from uncoated L605, TMS, TMS+NH_3/O_2 plasma nanocoatings, ion releasing test was performed according to ISO 10993-5 and ISO 10993-12. Square samples (10 mm × 10 mm × 0.4 mm) were utilized in this experiment. All edges of samples were smooth by using sand papers prior to extract preparation. Extracts were prepared by immersing uncoated L605 and plasma nanocoated coupons into extract medium (DI water) with surface area to medium ratio 6 cm^2/mL at 50°C for 72 h in shaking incubator. Extracts of uncoated L605, TMS, TMS+NH_3/O_2, and distilled water as control samples were utilized to determine ion concentrations with inductively coupled plasma mass spectrometry (ICP-MS) - NexION 300X (PerkinElmer, USA) operated in Kinetic Energy Discrimination mode (KED).

5.3.6. Cytotoxicity test

International standard ISO 10993-05 and ISO 10993-12 were adopted for cytotoxicity evaluation using porcine coronary artery endothelial cells (PCAECs). The cytotoxicity test was carried out by indirect contact. The cells were cultured in Dulbecco's

modified Eagle medium (DMEM, Gibco, USA) supplemented with 10% fetal bovine serum (FBS), 100 U/mL penicillin, and 100 μg/mL streptomycin. Extracts were prepared by immersing uncoated L605 and plasma nanocoated coupons into culture medium with surface area to medium ratio 6 cm^2/mL at 37°C for 24 h, according to ISO 10993-12. Extracts of natural latex rubber and high-density polyethylene (HDPE) were used as positive (+) inhibiting cells and (-) controls supporting cells, respectively.

Cells with density of 100,000 cells/well were seeded into a 96-well cell culture plates and incubated for 24 h at 37°C in a fully humidified air atmosphere containing 5% CO_2 to allow attachment. After being incubated for 24 h, the plates were then washed twice with phosphate-buffered saline (PBS), then the extracts were added to the 96-well plates with ratio of 100 μl/well. The cells were incubated in extracts at 37°C for 1 day. Cell morphology was observed by an inverted microscope after the test extracts and controls were removed from the 96-well plates. One hundred microliters MTT [3-(4,5-dimethylthiazol-2-yl)-2,5-diphenyl tetrazolium bromide] solution was added to each well and incubated for 4 h at 37°C. At the end, dimethyl sulfoxide (DMSO) was added to each well and shaken for 10 min. The spectrophotometric absorbance of the samples was measured by micro-plate reader at the wavelength of 570 nm. Extract medium (blank and non-test samples) without cells was used as control for absorbance reading. Viability reduction compared to the blank can be calculated by: $Viability\ \% = \frac{100\ x\ OD_{570e}}{OD_{570b}}$, where OD_{570e} is the density mean value of the 100% extracts of the test sample and OD_{570b} is the density mean value of the blanks. The lower the metabolic percentage value, the higher the cytotoxicity potential of the test sample. If the viability is lower than 70% of the blank, the test sample is potentially toxic.

5.3.7. Statistical analysis

Results were all expressed as mean ± standard deviation (SD) of the mean for each treatment group. Each experiment was repeated independently three times, if not indicated otherwise. Data were analyzed using one-way ANOVA. A *p*-value of 0.05 or less was considered significant.

5.4. Results and Discussion

5.4.1. Surface properties and morphologies after immersion test

Figure 5.1 shows surface morphologies for uncoated L605 and plasma nanocoated coupons before and after immersion test. There was a layer of adsorption products attached firmly on uncoated L605 surfaces. The 7-day immersion photos show some cracks and delamination occurring on the adsorption layer, but after 45-day immersion in SBF, the adsorption layer on uncoated L605 surface seems to be thicker and more firmly attached without cracking or delamination. EDS data in **Table 5.1** indicates the presence of mostly oxygen (O) – 39.06 wt.% and calcium (Ca) – 35.69 wt.%, followed by percentage concentrations of phosphorus (P), and a little amount of magnesium (Mg) within the adsorption layer. It is the fact that Ca is a big component of plaque which block the blood flow through stents, so the Ca containing mineral layer may need further assessments. However, in some other applications such as bone implants, Ca, P, Mg are considered biocompatible. Plasma nanocoated samples indicate no sign of corrosion products corrosion after ultrasonically cleaning with acetone as shown in **Figure 5.1**. No pitting corrosion was detected by SEM images on plasma nanocoated surfaces after 7-day and 45-day SBF immersion.

In order to evaluate corrosion rate and pitting corrosion for uncoated L605 surfaces, samples were submerged in chromic acid for 10 min, followed by soaking in DI water and rinsing by acetone. The mineral adsorption layer was all removed and it was shown that no pitting corrosion occurred on uncoated L605 surfaces. Corrosion rate was determined by the weight loss of samples before and after the immersion test. Corrosion rates for uncoated L605, TMS, TMS+NH_3/O_2 plasma nanocoatings were 4.98 $\times$ 10^{-5} [mm/year], 3.98 $\times$ 10^{-5} [mm/year], and 3.92 $\times$ 10^{-5} [mm/year], respectively. Acceptable corrosion rate of metallic implant systems is 2.5 $\times$ 10^{-4} mm/year [24,25], about one order higher than uncoated L605 and plasma nanocoated samples.

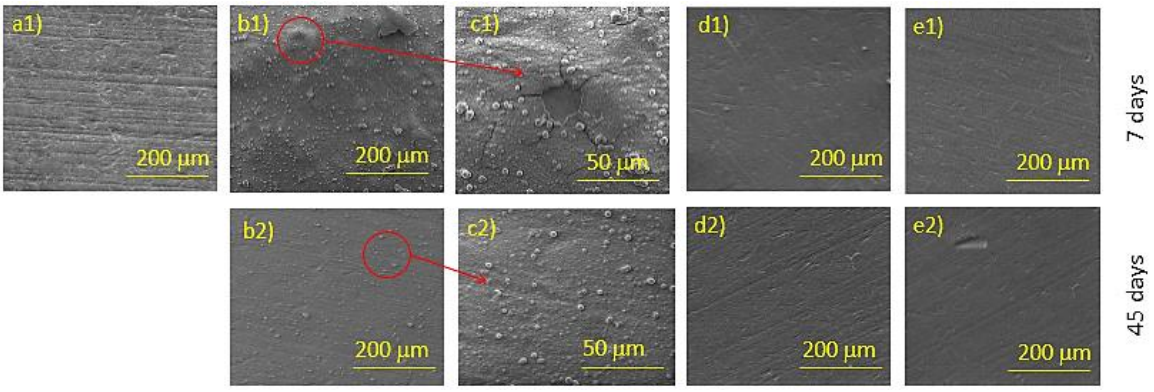

Figure 5.1: Surface morphology of uncoated L605 and plasma nanocoated coupons after immersion test: a1) Uncoated L605 before immersion test; b1) and c1) uncoated L605 after 7-day immersion; b2) and c2) uncoated L605 after 45-day immersion; d1) and e1) TMS and TMS+NH_3/O_2 plasma nanocoating, respectively, after 7-day immersion; d2) and e2) TMS and TMS+NH_3/O_2 plasma nanocoating, respectively, after 45-day immersion.

Table 5.1: Elemental concentration for uncoated L605 and TMS+NH_3/O_2 plasma nanocoatings determined by EDS spectra.

Elements	Uncoated L605 (wt.%)	Plasma nanocoatings (wt.%)
Ca	35.69	N/A

P	19.54	N/A
Mg	1.08	N/A
O	39.06	2.65

Results of immersion test in flow condition for stents are depicted in **Figure 5.2**. Similar to uncoated L605 coupons in static immersion test, uncoated L605 stents in flow condition setup presents adsorption products mostly on the abluminal surfaces, while on the luminal surfaces a few corrosion products were found due to the circulation model of the immersion test. EDS spectra shows similar components Ca, P, Mg, Na and O that were also detected on uncoated L605 coupon's surfaces. Plasma nanocoated stents were smooth and clean with no signs of pitting corrosion or adsorption products.

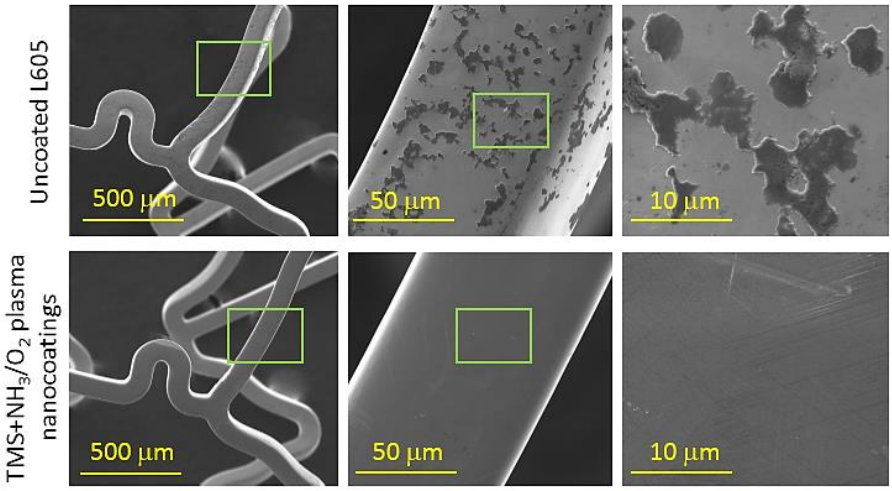

Figure 5.2: SEM images of uncoated L605 and plasma nanocoated stents after 7-day immersion: a) and b) uncoated L605; c) and d) TMS+NH_3/O_2; e) EDS spectra for uncoated L605 after 7-day immersion.

5.4.2. Electrochemical behavior

Open circuit potential (OCP) gives information about stability of sample surfaces in a particular corrosion environment. It shows time variation with changes in oxidation

tendency of surfaces. Corrosion potential (E_{corr}) is the electrical potential when no electrical current flows [26]. The OCP curves for uncoated L605, TMS plasma nanocoating, and TMS+NH_3/O_2 plasma nanocoating are presented in **Figure 5.3 a**. Each curve was repeated three times to ensure reproducibility. At the beginning of immersion, E_{corr} of the uncoated L605 dropped abruptly to -0.55 V (SCE) because PBS solution reached the substrate by diffusion and penetration through the oxide film that formed on the exposed surface [27]. However, as the immersion time increases, the formation of oxide film and corrosion product results in more noble E_{corr} [9]. E_{corr} reached equilibrium values of -0.26 V for uncoated samples within 1.5 h. During the same immersion time, more noble corrosion potentials (approximately -0.03 V) were obtained for plasma nanocoated surfaces, indicating an improved anodic protection of plasma nanocoated samples compared to the uncoated counterpart. The OCP measurements for plasma nanocoatings show a steady evolution during immersion time, pointing to stronger surface passivation [9] and homogeneous and pore-free nanocoatings [6]. In **Figure 5.3 b**, OCP for uncoated L605 and plasma nanocoated stents were shown. Compared to uncoated L605 coupons, the OCP for uncoated L605 stents in equilibrium is more noble (-0.03 V vs. 0.01 V) due to the post-manufacturing processes developed by stent companies. When those uncoated L605 stents were treated with modified NH_3/O_2 plasma coatings, its OCP increases to 0.18 V. The enhancement of open circuit potential is implied to better corrosion potential or greater corrosion resistance.

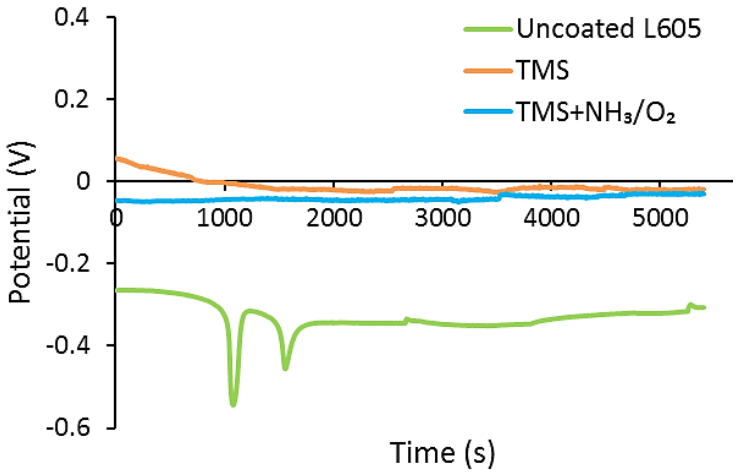

a)

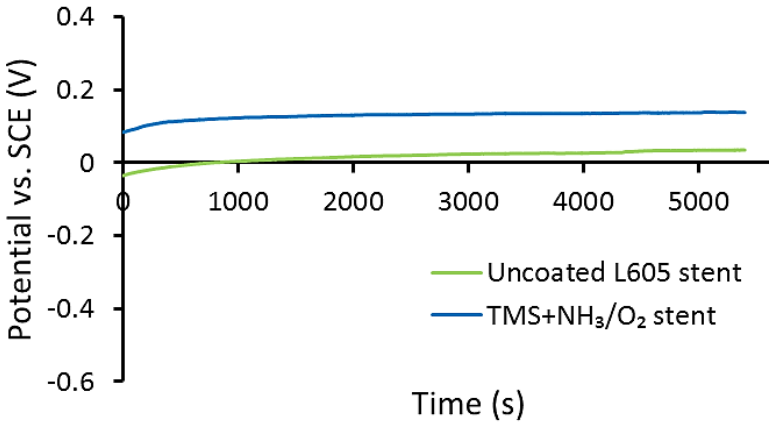

b)

Figure 5.3: Open circuit potentials for uncoated L605, TMS, and TMS+NH_3/O_2 plasma nanocoated substrates: a) Coupons, b) Stents.

Cyclic polarization (CP) curves generated on uncoated L605 and plasma nanocoated surfaces are shown in **Figure 5.4**. The curves are used to evaluate the susceptibility of samples to pitting corrosion and the corrosion rates. Curves for uncoated L605 and plasma nanocoatings are similar, but current density measured for plasma nanocoated surfaces is about one order of magnitude lower than that for uncoated L605

throughout CP scanning, implying that plasma nanocoated surfaces offer stronger corrosion protection due to lower corrosion rates than that of the uncoated L605 [28].

As shown in **Figure 5.4 a**, each curve consists of a forward scan starting at corrosion potential E_{corr} (point A) up to vertex potential E_v (point D), and a reverse scan starting from E_v and stop at E_{corr}. In CP curves, E_{corr} represents the potential of material in OCP after reaching steady state. In the forward scan, potentials increase with current density in active region (AB). This is due to the imperfection of substrate surfaces which may contain some defects to initiate corrosion propagation, resulting in an increase in current density [28]. In passive region (BC), the formation of passive layer on substrates leads to constant current density though the applied potential keeps rising. A protective oxide layer was formed in passive region to prevent metal dissolution from the surface [29].

Followed by the passive region (BC), if current density starts increasing rapidly, point C becomes pitting potential. In **Figure 5.4 a**, however the current density starts decreasing with the increase of potentials, implying that no pitting corrosion occurs for uncoated L605 as well as plasma nanocoated coupons. When potentials reach vertex potential (point D), reverse scan starts. The reverse scan comes above the forward scan, indicating materials are resistant to pitting and crevice corrosion [30]. In other words, the existence of negative hysteresis loop (counter-clockwise loop) points out that localized corrosion did not occur for those materials. In the absence of pitting, the reverse scan fails to intersect the forward scan to identify re-passivation potential. The intersection of reverse and forward scan at low potentials of 0.2V for plasma nanocoating and 0.05V for uncoated L605 was not considered as re-passivation potential because under these low intersection values reverse current density was higher than forward current density. The CP corrosion test data verify that both uncoated L605 and plasma nanocoating show no pitting

corrosion, confirming high pitting corrosion resistance for uncoated L605 in literature reviews [30,31]. The high pitting corrosion resistance would be expected by the top most oxide layer of cobalt oxide followed by chromium oxide (Cr_2O_3) [31]. Plasma nanocoated coupons contain Si-O bonding as indicated in **Figure 3.3** resulting in good corrosion resistance because the lower dissolution rate of Si-O bonding compared to other metal oxides [32]. Also, the presence of Si (**Figure 3.4**) can be explained for an improved anodic protection of plasma nanocoatings in OCP curves [9] as shown in **Figure 5.3 a**.

In **Figure 5.4 b,** cyclic polarization curves for uncoated L605 stents and TMS+NH_3/O_2 plasma nanocoated stents with different coating thickness were shown. It can be seen that, compared to uncoated L605 ($V_{corrosion}$ = -1.7 V), all plasma nanocoated stents show more noble corrosion potentials (about -0.05 V). The corrosion rate in all plasma nanocoated stents is about one order of magnitude lower in comparison to uncoated L605. There is no clear effect of plasma nanocoating thickness on corrosion behavior and thinner coatings could be advantageous since less stress cracking is possible.

In **Figure 5.4 c**, cyclic polarization for uncoated L605 and TMS+NH_3/O_2 plasma nanocoated stents were depicted. Compared to cyclic polarization curves on coupon samples, those on stents show similar trends and aspects, such as no pitting corrosion in all stents and the corrosion rate in plasma nanocoated stents was about one order lower than uncoated L605. It can be implied that coupon surfaces are good representatives for stents in term of corrosion behavior.

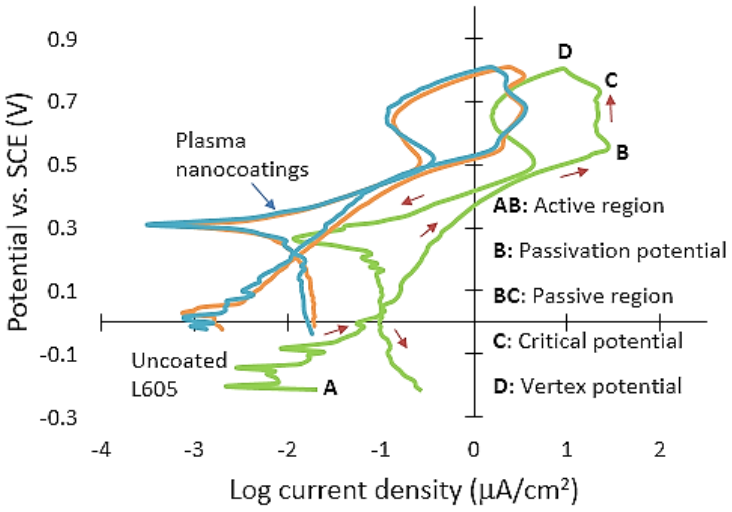
Potential vs. SCE (V)
Log current density (µA/cm²)
Plasma nanocoatings
Uncoated L605
A
B
C
D
AB: Active region
B: Passivation potential
BC: Passive region
C: Critical potential
D: Vertex potential

a)

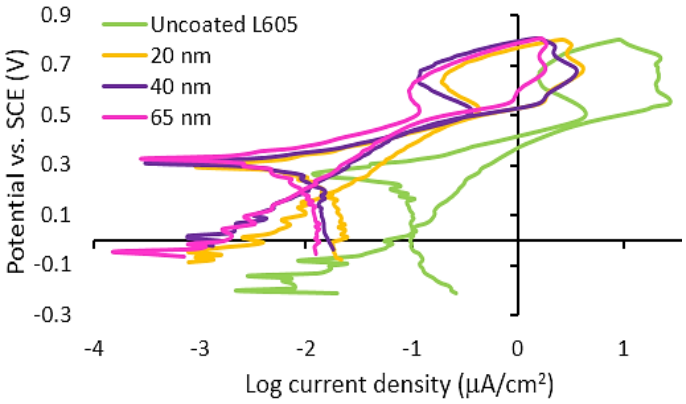
Potential vs. SCE (V)
Log current density (µA/cm²)
Uncoated L605
20 nm
40 nm
65 nm

b)

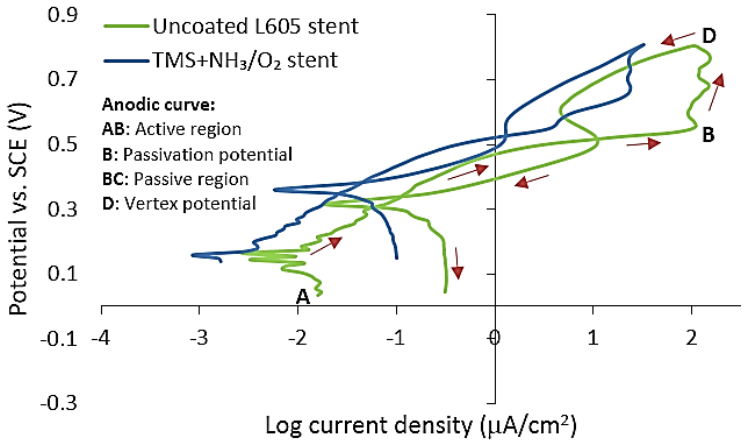
Potential vs. SCE (V)
Log current density (µA/cm²)
Uncoated L605 stent
TMS+NH₃/O₂ stent
Anodic curve:
AB: Active region
B: Passivation potential
BC: Passive region
D: Vertex potential
A
B
D

c)

Figure 5.4: Electrochemical curves of uncoated L605 and plasma nanocoatings: a) on coupons, b) TMS+ NH_3/O_2 plasma nanocoated coupons with different coating thickness, and c) on stents.

5.4.3. Ion releasing

Table 5.2 and **Figure 5.5** show metal ion releasing concentration for uncoated L605 and plasma nanocoated samples into DI water after an ion releasing test. The Cr, Co, Ni ion concentrations are similar for plasma nanocoating extracts with and without TMS+NH_3/O_2 modification; however, ion amount detected in uncoated L605 extracts is considerably higher ($p < 0.05$). The Cr, Co, and Ni concentrations in plasma nanocoatings decreased 64%-79%, 67%-69%, and 57%-72%, respectively, compared to those in uncoated L605 extracts, indicating plasma nanocoatings are able to minimize ion releasing from surfaces. The higher levels of Co and Cr ion releasing in all samples compared to Ni can be attributed to Co and Cr oxides that form on the top surface of uncoated L605 [11]. Ni is not commonly found on the very top surface of uncoated L605, but Ni can be exposed at the cutting surfaces of samples.

Table 5.2: Metal ion releasing concentration into DI water after ion releasing test

Samples	Cr (μg/kg)	Co (μg/kg)	Ni (μg/kg)
DI water	5.62	< 0.014	< 0.080
Uncoated L605	761.5 ± 5.3	956 ± 9.2	256.8 ± 12.7
TMS	273.5 ± 7.4	312.4 ± 8.8	109.5 ± 5.5
TMS+NH_3/O_2	162 ± 7.1	289.3 ± 11.3	72 ± 4.7

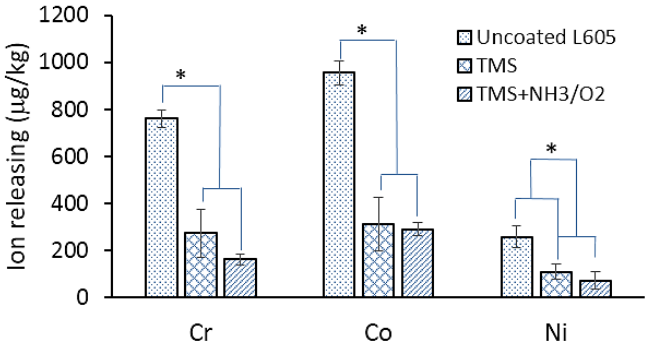

Figure 5.5: Metal ion releasing amount detected from extracts of uncoated L605, TMS, and TMS+NH_3/O_2 plasma nanocoatings. Plotted values are means ±SD (n=3), *p < 0.05.

5.4.4. Cytotoxic potential of plasma nanocoatings

Cytotoxicity is one of the most basic tests of biocompatibility of stent materials. In the cytotoxicity test, sample extracts were used for cell culture to verify if extracts from samples could have negative effect on cell viability. The cytotoxicity results using PCAECs on uncoated L605, TMS, TMS+NH_3/O_2, negative control (HDPE), and positive control (rubber latex) were shown in **Table 5.3** and **Figure 5.6**. The average absorbance measured from plasma nanocoating extracts is comparable to that collected from negative control (HDPE). Compared to positive control – rubber latex, the average absorbance measured from plasma nanocoating extracts is 10 times stronger, suggesting that plasma nanocoating has no negative effect on cell viability. There is no significant difference between absorbance detected from plasma nanocoated extracts and uncoated L605 extracts. According to ISO 10993-5, if viability is reduced to less than 70 % of the blank, it is a sign of cytotoxicity. All viability percentages for uncoated L605, TMS, TMS+NH_3/O_2 plasma nanocoatings are higher than 70%, indicating that no cytotoxic potential for uncoated L605 and plasma nanocoatings. **Figure 5.7** presents cells growth after 3 days. There are no obvious differences in the cell growth between PCAECs cultured in plasma

nanocoating extracts and negative control extracts, but most cells cultured in the extracts of positive controls are dead, implying the support of plasma nanocoating extract medium to PCAEC proliferation. This indicates degradation products of uncoated L605 and plasma nanocoating did not have significant impact on PCAECs cell viability, thus plasma nanocoating could be considered as nontoxic and biocompatible materials.

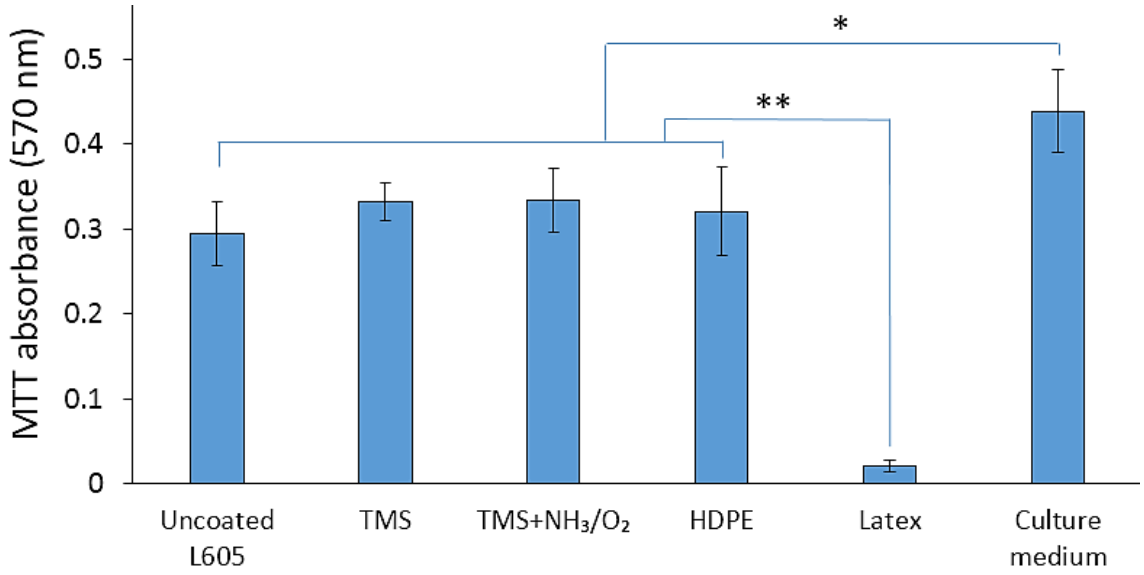

Figure 5.6: Metabolic activity of ECs proliferation in cytotoxicity test evaluated by MTT assay

Table 5.3: Average absorbance, viability percentage and assigned ranks in cytotoxicity test

	Uncoated L605	TMS	TMS+ NH_3/O_2	HDPE (+)	Latex (-)	Culture medium
Average absorbance	0.312	0.332	0.334	0.321	0.02	0.439
% Viability	71.12	75.84	76.14	73.10	4.63	100

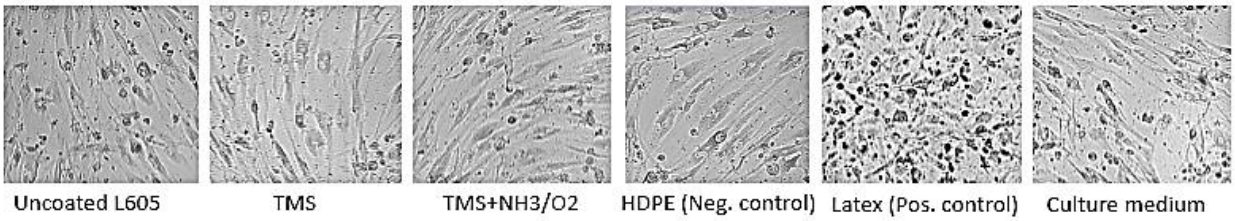

Figure 5.7: Cell morphology in cytotoxicity test after 3 days

5.5. Conclusions

In summary, TMS plasma nanocoatings showed improved corrosion resistance for cobalt chromium L605 coronary artery stents with low ion releasing, and no cytotoxicity. Therefore, TMS plasma nanocoatings with NH_3/O_2 plasma modification were speculated to minimize inflammation and thrombosis events, and potentially suitable candidates for cardiovascular stent applications.

5.6. References

[1] R.I.M. Asri, W.S.W. Harun, M. Samykano, N.A.C. Lah, S.A.C. Ghani, F. Tarlochan, M.R. Raza, Corrosion and surface modification on biocompatible metals: A review, Materials Science and Engineering C. 77 (2017) 1261–1274. https://doi.org/10.1016/j.msec.2017.04.102.

[2] Y. Zhang, X. Wang, Z. Ma, B. Bai, J. Liu, L. Yang, G. Qin, E. Zhang, A potential strategy for in-stent restenosis: Inhibition of migration and proliferation of vascular smooth muscle cells by Cu ion, Materials Science and Engineering C. 115 (2020). https://doi.org/10.1016/j.msec.2020.111090.

[3] T. Hu, C. Yang, S. Lin, Q. Yu, G. Wang, Biodegradable stents for coronary artery disease treatment: Recent advances and future perspectives, Materials Science and Engineering C. 91 (2018) 163–178. https://doi.org/10.1016/j.msec.2018.04.100.

[4] Y. Wu, F.I. Simonovsky, B.D. Ratner, T.A. Horbett, The role of adsorbed fibrinogen in platelet adhesion to polyurethane surfaces: A comparison of surface hydrophobicity, protein adsorption, monoclonal antibody binding, and platelet adhesion, Journal of Biomedical Materials Research - Part A. 74 (2005) 722–738. https://doi.org/10.1002/jbm.a.30381.

[5] B. Clarke, P. Kingshott, X. Hou, Y. Rochev, A. Gorelov, W. Carroll, Effect of nitinol wire surface properties on albumin adsorption, Acta Biomaterialia. 3 (2007) 103–111. https://doi.org/10.1016/j.actbio.2006.07.006.

[6] S. Diaz-Rodriguez, P. Chevallier, C. Paternoster, V. Montaño-Machado, C. Noël, L. Houssiau, D. Mantovani, Surface modification and direct plasma amination of L605 CoCr alloys: on the optimization of the oxide layer for application in cardiovascular implants, RSC Advances. 9 (2019) 2292–2301. https://doi.org/10.1039/C8RA08541B.

[7] C. Díaz, J.W. Gerlach, S. Mändl, J.A. García, Reduction of corrosion current of CoCr alloys by post-PIII oxidation, Surface and Coatings Technology. 256 (2014) 59–63. https://doi.org/10.1016/j.surfcoat.2014.03.027.

[8] T. Hryniewicz, R. Rokicki, K. Rokosz, Co-Cr alloy corrosion behaviour after electropolishing and “magnetoelectropolishing” treatments, Materials Letters. 62 (2008) 3073–3076. https://doi.org/10.1016/j.matlet.2008.01.130.

[9] D. Starosvetsky, I. Gotman, TiN coating improves the corrosion behavior of superelastic NiTi surgical alloy, Surface and Coatings Technology, Volume 148, Issues 2–3, 3 December 2001, Pages 268-276.

[10] B.G. Pound, Electrochemical behavior of cobalt - Chromium alloys in a simulated physiological solution, Journal of Biomedical Materials Research - Part A. 94 (2010) 93–102. https://doi.org/10.1002/jbm.a.32684.

[11] A. Ornberg, J. Pan, M. Herstedt, C. Leygraf, Corrosion Resistance, Chemical Passivation, and Metal Release of 35N LT and MP35N for Biomedical Material Application, Journal of The Electrochemical Society. 154 (2007) C546. https://doi.org/10.1149/1.2754073.

[12] A. Ornberg, J. Pan, M. Herstedt, C. Leygraf, Corrosion Resistance, Chemical Passivation, and Metal Release of 35N LT and MP35N for Biomedical Material Application, Journal of The Electrochemical Society. 154 (2007) C546. https://doi.org/10.1149/1.2754073.

[13] R. Tzoneva, M. Heuchel, T. Groth, G. Altankov, W. Albrecht, D. Paul, Fibrinogen adsorption and platelet interactions on polymer membranes, Journal of Biomaterials Science, Polymer Edition, Volume 13, 2002 - Issue 9 2002.

[14] Y. Zang, K.C. Popat, M.M. Reynolds, Nitric oxide-mediated fibrinogen deposition prevents platelet adhesion and activation, Biointerphases. 13 (2018) 06E403. https://doi.org/10.1116/1.5042752.

[15] S. Höhn, S. Virtanen, A.R. Boccaccini, Protein adsorption on magnesium and its alloys: A review, Applied Surface Science. 464 (2019) 212–219. https://doi.org/10.1016/j.apsusc.2018.08.173.

[16] Y.L. Jeyachandran, E. Mielczarski, B. Rai, J.A. Mielczarski, Quantitative and qualitative evaluation of adsorption/desorption of bovine serum albumin on

hydrophilic and hydrophobic surfaces, Langmuir. 25 (2009) 11614–11620. https://doi.org/10.1021/la901453a.

[17] T. Lenz-Habijan, P. Bhogal, M. Peters, A. Bufe, R. Martinez Moreno, C. Bannewitz, H. Monstadt, H. Henkes, Hydrophilic Stent Coating Inhibits Platelet Adhesion on Stent Surfaces: Initial Results In Vitro, CardioVascular and Interventional Radiology. 41 (2018) 1779–1785. https://doi.org/10.1007/s00270-018-2036-7.

[18] H. Liu, C. Pan, S. Zhou, J. Li, N. Huang, L. Dong, Improving hemocompatibility and accelerating endothelialization of vascular stents by a copper-titanium film, Materials Science and Engineering C. 69 (2016) 1175–1182. https://doi.org/10.1016/j.msec.2016.08.028.

[19] G.P. Lopez, D.G. Castner, B.D. Ratner, XPS 0 1s Binding Energies for Polymers Containing Hydroxyl, Ether, Ketone and Ester Groups, 1991.

[20] H.Z. Li, X. Zhao, J. Xu, MRI-compatible Nb-60Ta-2Zr alloy for vascular stents: Electrochemical corrosion behavior in simulated plasma solution, Materials Science and Engineering C. 56 (2015) 205–214. https://doi.org/10.1016/j.msec.2015.06.027.

[21] B. Sivaraman, R.A. Latour, The Adherence of platelets to adsorbed albumin by receptor-mediated recognition of binding sites exposed by adsorption-induced unfolding, Biomaterials. 31 (2010) 1036–1044. https://doi.org/10.1016/j.biomaterials.2009.10.017.

[22] M.S. Ehrenberg, A.E. Friedman, J.N. Finkelstein, G. Oberdörster, J.L. McGrath, The influence of protein adsorption on nanoparticle association with cultured endothelial cells, Biomaterials. 30 (2009) 603–610. https://doi.org/10.1016/j.biomaterials.2008.09.050.

[23] T. Kokubo, H. Takadama, How useful is SBF in predicting in vivo bone bioactivity?, Biomaterials. 27 (2006) 2907–2915. https://doi.org/10.1016/j.biomaterials.2006.01.017.

[24] B.J. O'Brien, J.S. Stinson, S.R. Larsen, M.J. Eppihimer, W.M. Carroll, A platinum-chromium steel for cardiovascular stents, Biomaterials. 31 (2010) 3755–3761. https://doi.org/10.1016/j.biomaterials.2010.01.146.

[25] L. Chen, G. Daum, R. Forough, M. Clowes, U. Walter, A.W. Clowes, Overexpression of Human Endothelial Nitric Oxide Synthase in Rat Vascular Smooth Muscle Cells and in Balloon-Injured Carotid Artery From the Departments of Surgery and Pathology (L, 1998. http://ahajournals.org.

[26] Z. ur Rahman, K.M. Deen, L. Cano, W. Haider, The effects of parametric changes in electropolishing process on surface properties of 316L stainless steel, Applied Surface Science. 410 (2017) 432–444. https://doi.org/10.1016/j.apsusc.2017.03.081.

[27] X. Li, H. Qiu, P. Gao, Y. Yang, Z. Yang, N. Huang, Synergetic coordination and catecholamine chemistry for catalytic generation of nitric oxide on vascular stents, NPG Asia Materials. 10 (2018) 482–496. https://doi.org/10.1038/s41427-018-0052-3.

[28] H. Qiu, P. Qi, J. Liu, Y. Yang, X. Tan, Y. Xiao, M.F. Maitz, N. Huang, Z. Yang, Biomimetic engineering endothelium-like coating on cardiovascular stent through heparin and nitric oxide-generating compound synergistic modification strategy, Biomaterials. 207 (2019) 10–22. https://doi.org/10.1016/j.biomaterials.2019.03.033.

[29] C. Bayram, A.K. Mizrak, S. Aktürk, H. Kurşaklioğlu, A. Iyisoy, A. Ifran, E.B. Denkbaş, In vitro biocompatibility of plasma-aided surface-modified 316L stainless steel for intracoronary stents, Biomedical Materials. 5 (2010). https://doi.org/10.1088/1748-6041/5/5/055007.

[30] S. Esmailzadeh, M. Aliofkhazraei, H. Sarlak, Interpretation of Cyclic Potentiodynamic Polarization Test Results for Study of Corrosion Behavior of Metals: A Review, Protection of Metals and Physical Chemistry of Surfaces. 54 (2018) 976–989. https://doi.org/10.1134/S207020511805026X.

[31] M. Dinu, I. Pana, P. Scripca, I.G. Sandu, C. Vitelaru, A. Vladescu, Improvement of CoCr alloy characteristics by Ti-based carbonitride coatings used in orthopedic applications, Coatings. 10 (2020). https://doi.org/10.3390/COATINGS10050495.

[32] R.A. Pareta, A.B. Reising, T. Miller, D. Storey, T.J. Webster, Increased endothelial cell adhesion on plasma modified nanostructured polymeric and metallic surfaces for vascular stent applications, Biotechnology and Bioengineering. 103 (2009) 459–471. https://doi.org/10.1002/bit.22276.

Chapter 6

CONCLUSIONS AND FUTURE WORK

6.1. Conclusions

Cobalt chromium (CoCr) L605 is known as a biocompatible material due to its cell supporting surface, good corrosion resistance, and low toxicity potential. However, L605 stents have limitations in in-stent restenosis and thrombosis. This study has investigated the surface chemistry and properties of TMS plasma nanocoating with or without NH_3/O_2 plasam modification by DC glow discharge and their effects on cell proliferation and corrosion resistance. TMS plasma nanocoatings deposited onto L605 coupon substrates and stents with and without NH_3/O_2 post treatment/modification were smooth, highly conformal, pin hole free, and highly adhesive to substrates. TMS plasma nanocoatings post-treated with NH_3/O_2 plasma provided improvement on L605 coupons with increased corrosion resistance, low ion releasing, and no cytotoxicity, which could be speculated to minimize inflammation and thrombosis events. In comparison with TMS plasma nanocoating onlhy, TMS plasma nanocoatings with NH_3/O_2 post-treatment whoed enhanced wettability due to introduction of nitrogen and oxygen polar groups on the coating surfaces. The moderate surface hydrophilicity from NH_3/O_2 plasma post-treatment retained PCAECs on the plasma nanocoatings as comparable to those of uncoated L605. The N and O containing plasma nanocoatings introduced from NH3/O2 plasma post-treatment prevented PCASMC proliferation and may subsequently inhibit restenosis. In the mean time, the TMS plasma nanocoatings with NH_3/O_2 plasma post-treatment could inhibit the survivability of PCASMCs, reduce the number of adhered platelets, minimize platelet activation, and does not adversely impact the proliferation of PCAECs. Therefore,

TMS plasma nanocoatings with NH_3/O_2 plasma post-treatment are good candidate materials for preventing restenosis and thrombosis in stent applications.

6.2. Future work

Future work on plasma nanocoated stents will be focus on optimizing plasma parameters to get better biological responses which promote more endothelial cell attachment and proliferation. Quantitative data for the platelet and fibrin adhesion is needed to reinforce assessment by imaging. A study on fibrinogen and albumin conformation will be addressed to explain why adsorbed fibrinogen amount on TMS plasma nanocoatings with NH_3/O_2 plasma post-treatment was higher than that on uncoated L605, but the platelet and fibrin adhesion on the plasma nanocoatings was much lower compared to uncoated L605. Ethylene oxide (EO) sterilization study might be addressed to assure that the behavior of endothelial and smooth muscle cells unchanged with and without sterilization process. EO can change the surface chemistry and leave residues behind. An exhaustive validation study is only feasible for stent, but coupons might give good preliminary data.

VITA

ThiThuHa Phan was born in Thai Nguyen, Vietnam. She finished her undergraduate studies in 2007 at ThaiNguyen University of Technology, Thai Nguyen, Vietnam, obtaining a Bachelor of Science in Mechanical Engineering. From August 2007 to July 2010, she worked mainly at Division of Undergraduate and Graduate Studies at ThaiNguyen University of Technology, Vietnam. In 2010, she started her graduate studies at University of Missouri – Columbia, where she earned her Master of Science in Mechanical Engineering in 2012. She went back to Vietnam to work as an instructor in Mechanical Engineering Department before she started pursuing her PhD degree in August 2018 under the advisement of Dr. Qingsong Yu. It was here that ThiThuHa furthered her knowledge of plasma physics and applications of plasma nanocoatings on cardiovascular coronary artery stents. After the defense of this dissertation, she expects to receive a PhD in Mechanical Engineering in July 2022.